Tissue-Material Interactions: Bioadhesion and Tissue Response

by

Tarek Shazly

B.S. Mechanical Engineering
Georgia Institute of Technology, Atlanta, GA 2001

M.S. Bioengineering
Georgia Institute of Technology, Atlanta, GA 2004

M.S. Materials Science and Engineering
Massachusetts Institute of Technology, Cambridge, MA 2007

SUBMITTED TO THE DEPARTMENT OF MATERIALS SCIENCE AND ENGINEERING
IN PARTIAL FULFILLMENT OF THE REQUIREMENTS FOR THE DEGREE OF

DOCTOR OF PHILOSOPHY IN MATERIALS SCIENCE AND ENGINEERING
AT THE
MASSACHUSETTS INSTITUTE OF TECHNOLOGY

September 2009

Signature of Author:_____
Department of Materials Science and Engineering
August 5, 2009

Certified by:_____
Elazer R. Edelman
Thomas D. and Virginia W. Cabot Professor of Health Sciences and Technology
Thesis Supervisor

Read by:_____
David Roylance
Professor of Materials Science and Engineering
Thesis Reader

Accepted by:_____
Christine Ortiz
Chair, Departmental Committee for Graduate Students

Tissue-Material Interactions: Bioadhesion and Tissue Response

by

Tarek Shazly

Submitted to the Department of Materials Science and Engineering on
August 5, 2009 in Partial Fulfillment of the Requirements for the
Degree of Doctor of Philosophy in Materials Science and Engineering

Abstract

Diverse interactions between soft tissues and implanted biomaterials directly influence the success or failure of therapeutic interventions. The nature and extent of these interactions strongly depend on both the tissue and material in question and can presumably be characterized for any given clinical application. Nevertheless, optimizing biomaterial performance remains a challenge in many implant scenarios due to complex relationships between intrinsic material properties and tissue response. Soft tissue sealants are clinically-relevant biomaterials which impart therapeutic benefit through adhesion to tissue, thus exhibiting a direct functional dependence on tissue-material reactivity. Because adhesion can be rigorously quantified and correlated to the local tissue response, sealants provide an informative platform for studying material properties, soft tissues, and their interplay. We developed a model hydrogel sealant composed of aminated polyethylene glycol and dextran aldehyde (PEG:dextran) that can possess a wide range of bulk and adhesive properties by virtue of constituent polymer modifications. Through comparison to traditional sealants, we established that highly viscoelastic adhesion promotes tissue-sealant interfacial failure resistance without compromising underlying tissue morphology. We analyzed multiple soft tissues to substantiate the notion that natural biochemical variability facilitates the design of tissue-specific sealants which have distinct advantages over more general alternatives. We confirmed that hydrogel-based materials are an attractive material class for ensuring sealant biocompatibility, but found that a marked reduction in adhesive strength following characteristic swell can potentially limit clinical efficacy. To mitigate the swell-induced loss of hydrogel-based sealant functionality, a biomimetic conjugation strategy derived from marine mussel adhesion was applied to PEG:dextran and shown to favorably modulate adhesion. In all phases of this research, we defined material design principles that extend beyond the immediate development of PEG:dextran with potential to enhance the clinical performance of a range of biomaterials.

Table of Contents

Acknowledgements

The work embodied in this thesis was made possible only with the help of my peers and mentors. I was extremely fortunate to join a lab consisting of remarkable people with scientific abilities matched only by their willingness and desire to help each other succeed. In the time I spent in the Edelman Lab, there was not even a single instance where I had to look beyond my immediate surroundings for sincere assistance with either academic or research challenges. Our lab has a pervasive communal culture that is rare within the often competitive scientific environment, and originates from an unmistakable source, Dr. Elazer Edelman.

Elazer is himself a unique man who operates on so many levels, means so much to so many, and selflessly strives to extend the great success in his life to all those around him. Elazer's professional accomplishments are too vast and varied for meaningful summary, but I've always had a distinct feeling that he considers them secondary to the positive impact he has on others well-being. Elazer leads by example, and those privileged by his leadership always benefit – to him I am forever grateful, and I am proud that he is both a mentor and a friend.

Of the Edelman Lab members, I am especially indebted to Dr. Aaron Baker, who taught me numerous experimental techniques and constantly provided crucial scientific insight into my research. I am also particularly grateful to Dr. Vijaya Kolachalama who was a guiding force underlying my work and who provided valuable feedback on a number of aspects related to my work. Aaron and Vijaya are talented scientist that I look up to from a professional standpoint in addition to being great friends that I am lucky to have made. All of the Edelman Lab members heavily depend on assistance in various matters from Laurie May-in this I am no exception. Laurie works extraordinarily hard on our behalf in lab- and institute-related matters and does so with a level of professionalism that is truly remarkable.

I am so thankful for my family, for without them I would not have been in position to even attend graduate school. My parents Hassan and Mona have always stressed the importance of education in my life and gave me all the resources I needed to complete my studies. My sister Dina and brother-in-law Mark gave their support and encouragement throughout my studies, while my grandmother Oma, although half-a-world away, always thinks of me and wishes for success. I have a distinct memory of my late grandmother Connie, i.e. Granny, calmly guaranteeing that I would one day graduate from MIT- this memory always gave me assurance when things got tough. Finally, to my wife Lindsay, who has always provided my with support, encouragement, perspective, and most importantly love that makes even life's challenges enjoyable In my case getting a degree from a place like MIT is more of a family rather than personal achievement.

Dedication

To my family...

List of Figures

List of Tables

1. Introduction

1.1 Project Overview

Interactions between tissues and materials are of paramount importance in determining the overall efficacy of implanted medical devices [1-3]. These interactions happen on various timescales, with both local tissues and implanted materials often undergoing significant property changes throughout the course of therapeutic treatment. The nature of relevant property changes differs among clinical applications, and can range from an instant instigation of blood clotting to the chronic evolution of a stiff fibrotic capsule around an initially flexible implant [4, 5]. In all cases, the dynamic interplay between tissues and materials will determine both the duration and extent of therapeutic benefit to the patient. In this thesis, focus is directed towards the study of tissue-material interactions operative with application of soft tissue sealants. These degradable implants are characterized by a functional dependence on material bioreactivity, motivating an in-depth analysis of soft tissue-adhesive material interactions.

Soft tissue sealants are used in surgery as a means to attain homeostasis, prevent anastomotic leakage, and provide mechanical support to healing tissues [6-8]. Particular sealant applications include repair of internal lacerations, filling of void spaces after tissue resection, and suture-line reinforcement to prevent tissue dehiscence [9-12]. Although clinical outcomes following the use of current sealants are generally acceptable, available materials are classically limited by a lack of adhesion strength and/or tissue insult upon adherence [13-15]. Commercial fibrin sealants lose adhesion

to tissue shortly after implantation and exhibit a dangerous tendency to pool bacteria and biologic debris at a wound site [16, 17]. More chemically reactive sealants, such as polycyanoacrylate derivatives, are also available and provide superior adhesion strength. However, *in vivo* data suggest that the cost of prolonged adhesion with these materials includes tissue ischemia, inflammation, and undesirable peritoneal adhesion formation. Previous studies have even reported a significant inhibition of cellular proliferation when fibroblasts are indirectly exposed to polycyanoacrylates in an elution test system [18, 19].

In this work we seek methods of controlling tissue-material interactions to yield high strength adhesion without excessive tissue insult. We employ a canonical class of biochemistry to direct tissue-material adhesion, namely aldehyde-amine covalent bonding. We analyze tissue-material interactions in experimental frameworks which consider practical issues such as adhesive mechanics, tissue inflammation, tissue-specific adhesion, and functionally deterministic property changes following implantation. The goal of this work is to better understand tissue-material interactions in the context of bioadhesive sealants, and to generalize the resulting concepts to the design and development of other implanted biomaterials.

Basic sealant properties

Multiple properties are required to qualify a material as a potential soft tissue sealant [20]. Primarily, the material must be capable of adhesion to soft tissues under physiologic conditions. In order to justify clinical use, a sealant must remain at the application surface for a given period of time throughout which some therapeutic benefit (i.e. mechanical support, leakage prevention, or localized drug delivery) is conferred to underlying tissue. The material must be biodegradable or bioeliminable, such that upon implant clearance local tissues can complete regeneration or repair processes. The material must be usable in the surgical setting, generally requiring a phase transition from a low viscosity liquid during administration into a solid or gel-like material *in situ*. A material which satisfies the above properties may well function as a clinically effective sealant, although attempts with a wide range of candidate adhesives have yielded limited success.

State of the art

Materials which adhere to soft tissues typically exhibit a limiting tradeoff between adhesion strength and biocompatibility (Figure 1). Canonical soft tissue sealants represent opposite ends of this property spectrum, as fibrin glues (FG) and cyanoacrylate derivatives (CA) are functionally bounded by insufficient adhesion strength or poor biocompatibility, respectively [13-15]. FG achieve adherence via Factor XIIIa-mediated covalent bond formation between constituent fibrin polymer and tissue collagen in a process analogous to natural blood coagulation (Figure 2). CA derivatives achieve adherence via on-site anionic polymerization in response to tissue-present

hydroxyl ions or weak-base proteins (Figure 3). Highly reactive CA-based materials densely crosslink tissue and as a result display high strength adhesion, but in doing so deform native morphology, incite tissue inflammation, and induce cytotoxicity upon degradation and release of typically small crosslinking molecules (such as formaldehyde). Less reactive FG achieve comparatively sparse tissue crosslinking and as a result adhere weakly, but generally cause minimal tissue inflammation or deformation. Despite significant compositional variance between available soft tissue sealants, no adhesive material fully meets clinical demands.

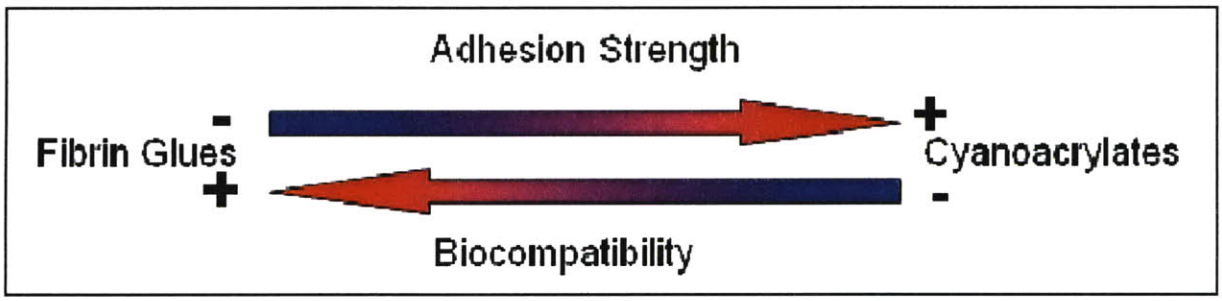

Figure 1 Schematic representation of the tradeoffs associated with use of currently available soft tissue sealants. Canonical materials generally are limited by suboptimal adhesion strength or biocompatibility.

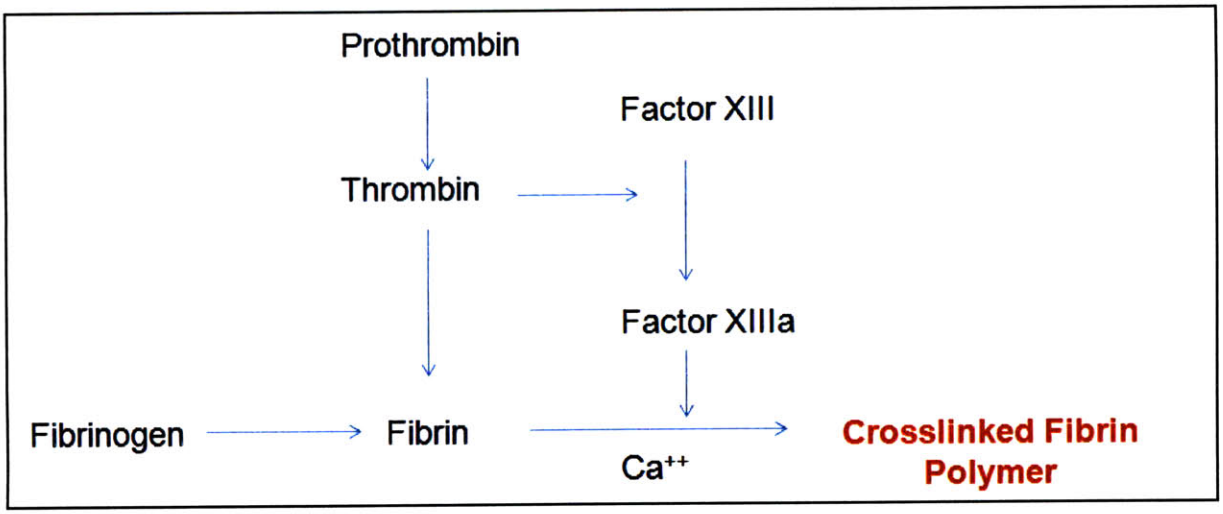

Figure 2 Schematic representation of the crosslinking mechanism employed by fibrin glues.

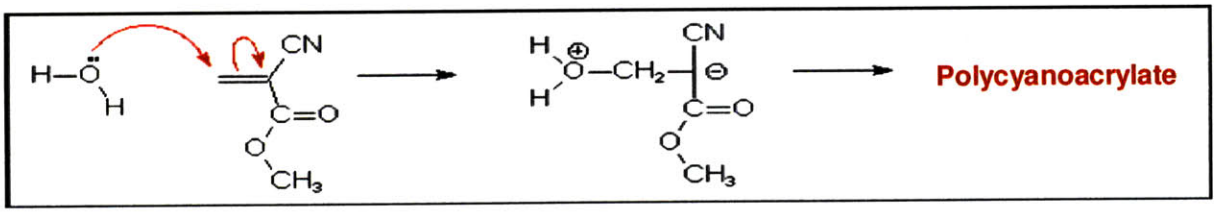

Figure 3 Schematic representation of the crosslinking mechanism employed by cyanoacrylate-based sealants.

It is clear that functional material adherence to tissue requires rapid, on-site sealant polymerization and integrative bond formation with tissue-present moieties. Ultimate sealant efficacy is understood as a function of adhesion strength, bulk material properties, material degradation kinetics, local tissue response, and the biocompatibility of by-products evolved throughout material clearance. These deterministic properties are likely correlated due to a common dependence on the extent and nature of tissue-material interactions.

1.2 CLINICAL MOTIVATION

Small bowel resection (Figure 4) is a common medical procedure for treating numerous diseases of the gastrointestinal tract [21-24]. Clinical instances of intestinal obstruction or inflammation requiring resection can stem from a variety of conditions, including scar tissue formation, trauma, tissue deformities, gastrointestinal stromal tumors (GIST), and Crohn's Disease (Figure 5). Following tissue excision, the created ends of the small intestine are typically reconnected via staples or sutures. Such methodology is generally successful, but post-operative complications are reported in approximately 15% of procedures [25-27]. Risk factors of resection procedures include bleeding, infection, and leakage from the anastomotic site, all which arise primarily from incomplete closure or healing of the surrounding tissue. Modification of the anastomotic site to enhance integrity and promote healing is a logical approach to reduce the occurrence of intestinal dehiscence and associated risk factors. Adhesive sealants could improve intestinal healing if used in conjunction with standard closure techniques. The potential benefits of anastomotic augmentation justify small bowel resection as a clinical model for study of adhesive sealants.

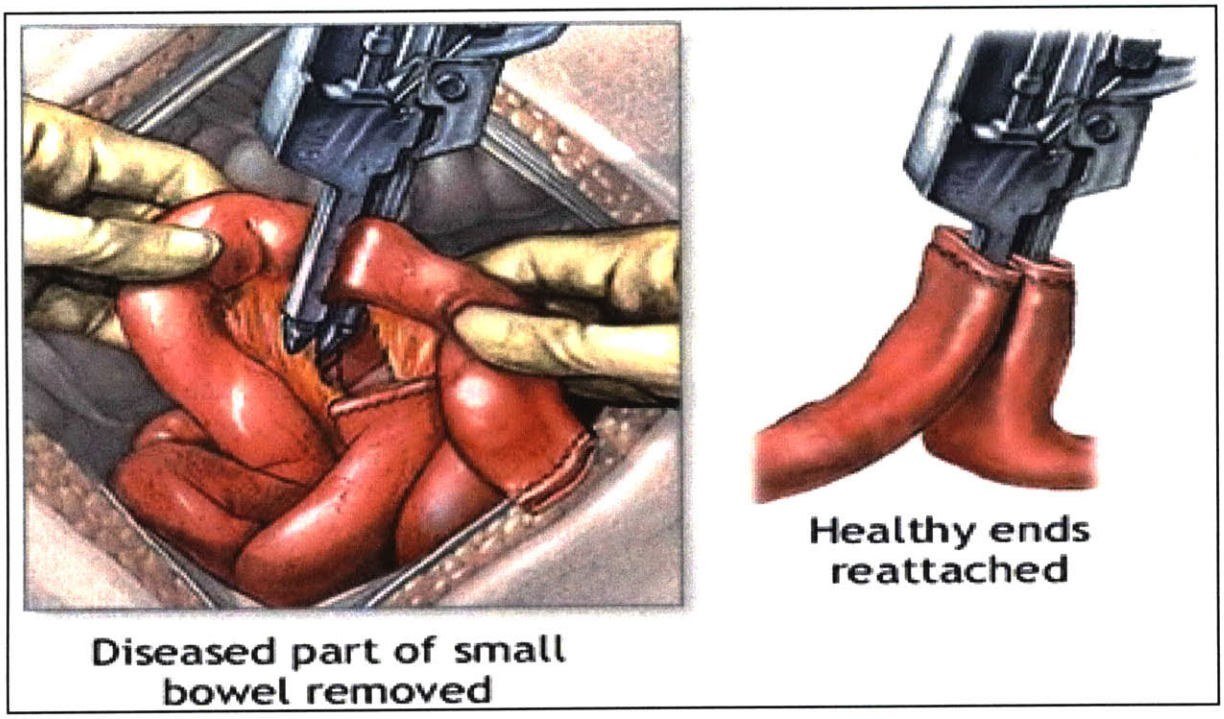

Figure 4 Pictorial description of small bowel resection. Following resection, healthy tissue is reattached with sutures or staples [28].

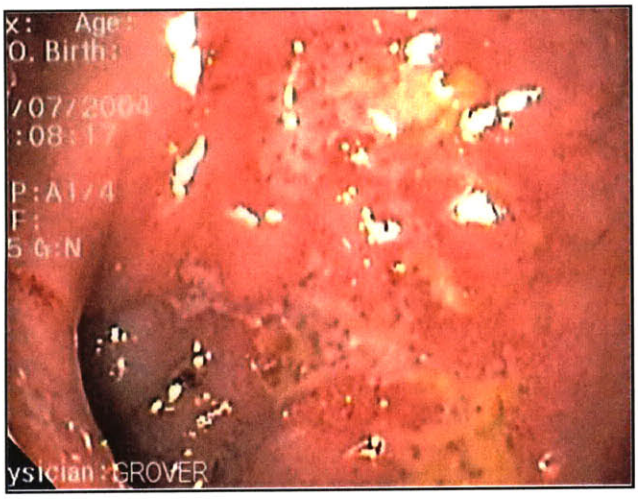

Figure 5 Endoscopic image of ulcer prevalent in Crohn's disease. In some cases, recurrent or numerous ulcers must be surgically removed via tissue resection [29].

Additional clinical sealant applications motivate the examination of interactions between adhesive materials and various soft tissues. Resection procedures are routinely conducted to remove diseased or dysfunctional soft tissue, including pulmonary, hepatic, and cardiac tissues [30-33]. In these and other similar operations, tissue sealants can provide a means of quickly attaining hemostasis and further provide a temporary scaffold to enhance surgical wound healing. Despite such an array of applications, differences between tissue propensities for adherence have not been explicitly considered in sealant design. Because the adhesive strength of a surgical sealant is derived from bonding to apposed tissue, interfacial properties and ultimately sealant performance are expected to depend on the chemistries of both the tissue and material. We expect that consideration of target tissue bed reactivity in application-specific adhesive design can lead to increasingly biocompatible and efficacious clinical sealants.

1.3 SCOPE

The use of biomaterial implants has been noted throughout ancient history, with documented examples occurring an astonishing 32,000 years ago [34]. Today, countless clinical applications feature biomaterials integrated into medical devices or implants, and many others use such materials in isolation. About 60 years ago it was recognized that the interactions between biomaterials and surrounding tissues largely determine the ultimate success or failure of a particular intervention, spurring a movement to design increasingly biocompatible materials [1, 34].

A major challenge of biomaterials engineering is first defining and second fulfilling the emergent requirement of biocompatibility for a given clinical application. A material cannot be accurately designated as 'biocompatible' in any general sense. Instead, biocompatibility must be based on "the ability of a material to perform with an appropriate host response in a specific situation [1]." Biocompatibility and biomaterial efficacy can only be assessed with a unified understanding of material properties, tissue response, and therapeutic intent.

As stated above, this thesis is a study of tissue-material interactions in the context of soft tissue adhesive sealants. The universal challenge of engineering material biocompatibility underlies this work, while limitations of soft tissue sealants focus the scope of study. We pose following questions, which if answered will further the understanding of tissue-material interactions and potentially lead to the design of a superior soft tissue sealant.

1. Can aldehyde-mediated chemistry provide a platform for attaining rapid and directed adhesion between tissue and material?

2. Is there a relationship between constitutive descriptors of adhesive interfacial mechanics and metrics of sealant performance?

3. Can viscoelastic relaxation of interfacial stress be exploited as design strategy for minimally reactive yet efficacious soft tissue sealants?

4. Do all soft tissues interact similarly with adhesive materials, or does biochemical variation facilitate tissue-specific sealant design for optimal clinical performance?

5. Do the adhesive properties of a hydrogel sealant significantly diminish with hydration state? If so, can a hydrogel adhesive be chemically modified to prevent property loss upon swell?

2. Outline

2.1 Thesis Statement

Tissue-material interactions are influenced by the chemical and physical properties of the tissue as well as the material. Biomaterial adhesion to soft tissues should therefore be sensitive to tissue type, enabling rational design, choice and evaluation of therapeutic sealants. Bioadhesive materials provide a clinically-relevant and informative platform to study tissue-material interactions. In particular, these implants have a functional dependence on reaction with tissue, are formulated reproducibly with a full spectrum of physical and chemical properties, and can be assessed in a quantifiable and rigorous fashion. Bioadhesion is amenable to study via a variety of techniques, including mechanical testing, mechanical modeling, quantitative microscopy, *ex vivo* tissue experiments, and subcutaneous implantation studies. Employing a diverse set of methodology and correlating resultant data should shed mechanistic insight into tissue-material interactions and ultimately provide guidelines for design, evaluation and use of advanced surgical sealants and other implantable biomaterials which interact with soft tissue.

2.2 HYPOTHESES

1. Aldehyde-amine chemistry can provide a means by which to control material cohesion and tissue-material adhesion as amines within the materials control the former and amines within the tissues determine the latter.
    a. Soft tissue beds present different densities of target reactive sites for aldehyde-mediated adhesion (amines) enabling tissue-specific formulations of an optimal sealant.

2. High molecular weight hydrogel adhesives can preserve native tissue mechanics and as a consequence induce minimal disturbance to local tissue structure under physiologic loading conditions if their tissue crosslinking is controlled and molecular mobility maintained.
    a. The density of tissue-material crosslinks as well as the bulk material mechanics together will determine the extent to which underlying tissue mechanics are altered with sealant application.
    b. High molecular weight hydrogel polymers in the hydrated state will retain significant molecular mobility and better approximate tissue composition (as compared to stiff, hydrophobic, high strength adhesives with low molecular weight crosslinking) such that destructive interfacial stress concentrations are minimized.

3. Sealant swelling, although desirable for harmonizing tissue-material properties, will notably diminish sealant performance as a consequence of passive interfacial deformation.
    a. Sealant swell occurring subsequent to the formation of a thin adhesive interface will displace the material from tissue due to an asymmetric expansion of the highly hydrophilic material with respect to stable tissue geometry. This displacement represents an important form of intrinsic stress which will amplify physiologic forces opposing tissue-material adhesion.
    b. If deemed excessive, the adhesive loss of a hydrogel sealant upon swell can be mitigated through a biomimetic approach based on the wet adhesion mechanisms exhibited by marine animals.

2.3 SPECIFIC AIMS

The specific aims of this thesis fall into two main categories, specifically controlling biomaterial-tissue adhesion and understanding the effects of hydration on hydrogel-mediated bioadhesion. The following specific aims are designated to test the stated hypotheses.

Control of adhesion

1. Formulate and characterize an adhesive material system which features high molecular weight aldehydes as the primary reactive constituent for interaction with soft tissues.
2. Characterize the surface chemistry of various soft tissues with respect to susceptibility for aldehyde-mediated adhesion. Rate tissue-bed modulation of adhesive interactions.
3. Model the resultant mechanics following material adhesion to soft tissue and correlate mechanical properties to metrics of sealant performance.
4. Relate adhesive mechanics to material and tissue properties.

Effects of hydration

5. Determine the extent of adhesive property loss of a hydrogel sealant as a function of hydration.
6. Conjugate a biomimetic constituent to the hydrogel network in an effort to recapitulate the wet adhesion exhibited by marine animals.

3. Experimental Studies

3.1 Study 1 Characterization of a Model Soft Tissue Sealant

Publication disclosure
The following presentation of Study 1 is based on:
Characterization of star adhesive sealants based on PEG/Dextran hydrogels.
Artzi N, Shazly T, Crespo C, Ramos AB, Chenault HK, Edelman ER.
Macromol Biosci. 2009 Apr 21.
AND
Property Determinants of Dextran:Polyethylene Glycol Adhesive Sealants.
Shazly T., MS Thesis, MIT, Department of Material Science and Engineering, 2007

3.1.1 Abstract

A novel class of bioreactive hydrogels composed of aminated polyethylene glycol (PEG) and dextran aldehyde polymers (PEG:dextran) are proposed as candidate soft tissue sealants with potential to improve upon the performance of currently used materials. Multiple compositional variations are available for both the PEG and dextran constituent polymers, thus providing a family of PEG:dextran that is ideal for selectively probing tissue-material interactions and informing iterative sealant design. Key material properties determining sealant efficacy include swelling and degradation kinetics, elastic modulus, bioadhesion strength, and biocompatibility. Relationships between these pertinent properties and available compositional variations are determined for PEG:dextran. A series of complementary studies reveal the following determinants of material properties in PEG:dextran: constituent PEG amine molecular complexity dictates hydrogel swell and stability in aqueous medium, PEG amine solid content dictates hydrogel stiffness, available dextran aldehyde groups dictate adhesion strength, and total material solid content and reactive group ratio dictate the cellular response. Knowledge of functional property determinants facilitates design of PEG:dextran for high strength, biocompatible adhesion to soft tissue, and enables the

use of these materials to selectively study various aspects of tissue-material interactions.

3.1.2 Introduction

Internal surgical intervention necessitates the intentional wounding of soft tissue. In many clinical procedures, soft tissue healing is dependent on established wound closure techniques, such as suturing or stapling of disjoined tissues. Risk factors associated with these techniques are largely attributed to the discrete nature of interfacing with tissue, often inducing deleterious stress concentrations in healing tissues and compromising wound site integrity [35, 36]. Clinical adhesive sealants are biomaterials which can mitigate these risks by forming a continuous layer to stabilize tissues and provide a temporary scaffold to support healing processes [6, 9, 37, 38]. However, available sealants present additional risk factors, are restricted in surgical use, and have a clinical failure rate of approximately 15 % [25-27].

Commercially available sealants are generally limited by inadequate adhesion strength or unacceptable local tissue response [13, 39-41]. Although fibrin glues are considered biocompatible for most internal applications, they exhibit low strength bioadhesion and quickly lose sealant functionality under physiologic loads. Alternatively, cyanoacrylate-based polymers are high strength bioadhesives, but are cytotoxic, induce inflammation, and can deform native soft tissue morphology; due to their lack of biocompatibility, these materials are now primarily reserved for dermal applications. A clear need exists for a high strength, biocompatible adhesive materials for application to the full range of soft tissues.

Aldehydes are classic reactive groups for tissue fixation and have been proposed as primary bioreactive constituents in experimental adhesive sealants [42-44]. When imbedded within a polymer network, aldehyde groups presented on short carbon backbones (glutaraldehyde and formaldehyde) highly crosslink tissue, but upon material degradation are cytotoxic, penetrate deep within tissues, and incite a significant inflammatory response. Here we integrate a high molecular weight aldehyde (10 – 60 kDa) as the primary bioreactive constituent in an adhesive hydrogel. We intuit that the toxicity following aldehyde-tissue interactions will be minimal if the aldehydes are mounted on higher molecular weight materials such as dextran, a natural polymer of glucose residues.

We demonstrate that when dextran aldehydes are crosslinked with an aminated polyethylene glycol, spontaneous formation of a bioadhesive gel (PEG:dextran) occurs via Schiff base reaction between constituent polymers. We synthesized and characterized a family of PEG:dextran materials and found that network properties are most responsive to variations in the PEG component (molecular structure and solid content), while tissue-material adhesion and cellular response are aldehyde-mediated. The established property determinants for PEG:dextran enables the design high strength yet biocompatible materials and hints at a potential for tissue- and application-specific formulations.

3.1.3 Materials and Methods

PEG:dextran hydrogels

A novel material system is developed and utilized throughout this work to investigate soft tissue-adhesive material interactions. The material under study is a bioadhesive hydrogel which was pioneered by DuPont and has since emerged as a candidate sealant with potential to address clinical needs [45, 46]. The Edelman Lab has collaborated with DuPont on a number of research initiatives within the context of the DuPont-MIT Alliance (DMA). DMA endeavors have resulted in both the elucidation of scientific principles underlying clinically-relevant tissue-material interactions and the advancement of a range of biotechnologies.

The novel adhesive hydrogel system features polyethylene glycol (PEG) and dextran polymers which are functionalized to promote both cohesive network formation and adhesive bonding to tissue. Solutions of an amine-modified PEG are prepared with either linear or star-shaped polymers with molecular weights of 2 or 10 kDa. The linear PEG has two amine groups per molecule which are tethered to each end, while the star PEG consists of eight PEG chains joined at the center of a complex macromolecule with an amine end group on each arm (Figure 6). The second hydrogel component is oxidized dextran with reactive aldehyde side-groups present throughout the entire polymer chain (Figure 7). The extent of oxidation is determined by the dextran molecular weight (10 – 60 kDa) and the relative amount of sodium periodate with which it is reacted. A calculable number of aldehyde groups will be available after the dextran oxidation step and will spontaneously react with the amines of PEG when the two components are mixed [47].

Aldehyde groups which remain free following network formation will potentially facilitate bioadhesion, as previous studies have indicated that oxidized dextran readily reacts with soft tissues [48, 49].

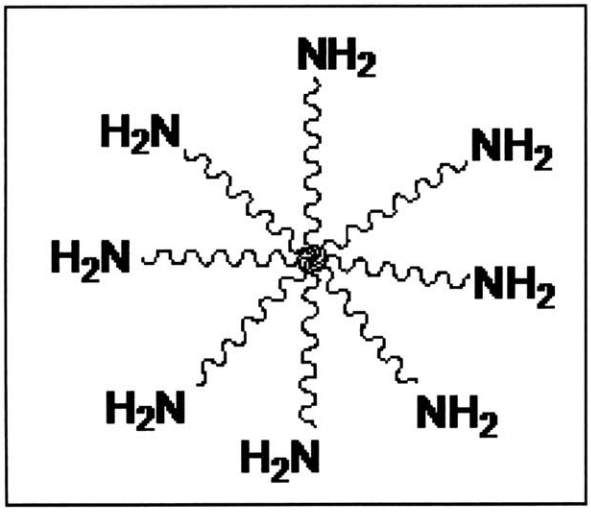

Figure 6 Molecular structure of eight arm PEG amine.

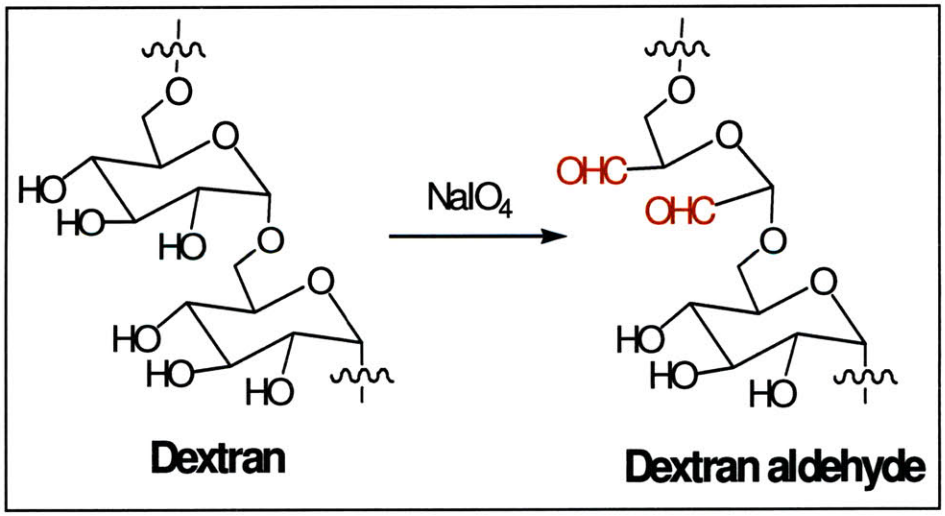

Figure 7 Oxidation of dextran polymer with sodium periodate yields dextran aldehyde.

PEG and dextran constituents are separately prepared as aqueous solutions with low viscosities to ensure practical sealant delivery. The highest solid content formulated for either component (60 wt.%) has low enough viscosity to allow for easy injection through a 5 ml syringe and a 20-gauge needle at room temperature. Prior to polymerization, equal volumes of material components are loaded into separate chambers of a dual-chamber syringe. A 12-step mixing tip is attached to the syringe as a means to promote repeatable and extensive mixing of the two components (Figure 8). Following mixed injection, the dextran aldehyde and aminated PEG form a covalently crosslinked copolymer network (PEG:dextran) within seconds to minutes through Schiff base intermediates (Figure 9).

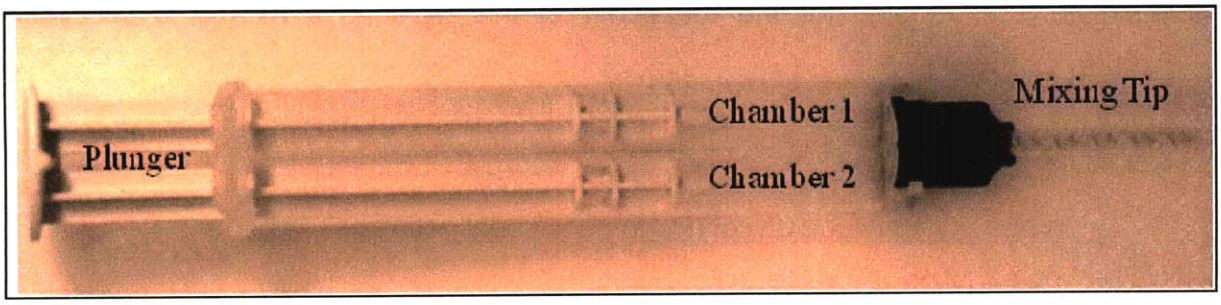

Figure 8 A dual-chambered syringe equipped with a 12-step mixing tip is used to uniformly mix PEG amine and dextran aldehyde polymers to yield crosslinked PEG:dextran hydrogels.

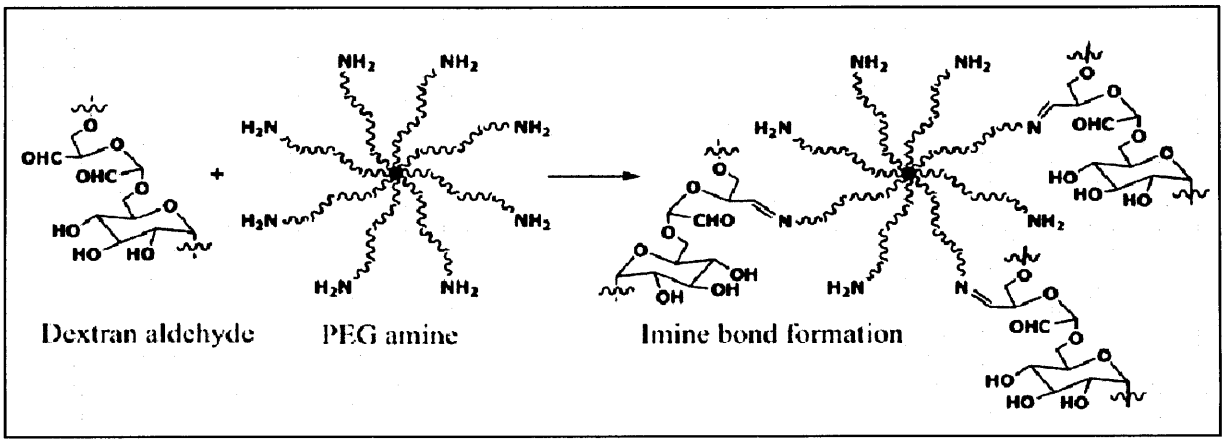

Figure 9 Schematic representation of network formation between star PEG amine and dextran aldehyde. Constituent polymers are crosslinked by imine bonds formed between aldehyde and amine groups.

The synthesis and preparation of constituent polymers allows for flexibility in a number of compositional variables in the PEG:dextran system. The following nomenclature is adopted for the remainder of this work as a means to succinctly describe a particular material formulation.

Aminated polyethylene glycol (**P**) compositional variables

a. Number of arms per molecule (2 or 8)

b. Molecular weight of PEG molecule (kDa)

c. Solid content (%)

Dextran aldehyde (**D**) compositional variables

d. Molecular weight (kDa)

e. Oxidative conversion (%)

f. Solid content (%)

The shorthand notation used to quickly identify the composition of these materials reads:

P a-b-c **D** d-e-f

For example, if a 60 kDa, 20% converted, and 50% solid content dextran aldehyde is polymerized with an 8-arm, 10 kDa, 60% solid content polyethylene glycol, then the resultant hydrogel is denoted as:

P 8-10-60 **D** 60-20-50

In addition to the above description, the ratio between aldehyde and amine concentrations ($CHO:NH_2$) in a given PEG:dextran formulation is calculated and provided to reflect the relative reactive group densities of constituent polymers.

Gravimetric analysis of PEG:dextran swell response

The hydration and hydrolytic degradation properties of PEG:dextran hydrogels were assessed by the swell response of material sample submerged in aqueous media. Gravimetric data of disk-shaped material samples (Table 1) were collected throughout a suspension period and used to calculate swelling ratios as follows,

$$\text{Swelling Ratio } (\%) = \left[\frac{W_\infty - W_D}{W_D}\right] \times 100$$

where W_∞ is the maximal disk mass measured throughout the suspension period and W_D is the initial disk mass prior to suspension (dry sample). The time point at which the disk mass peaked and subsequently declined is defined as onset of material degradation, although it is recognized that this does not strictly reflect degradation kinetics which proceed at some finite rate immediately upon contact with water. The present assessment of material swell response is valuable for comparing among various PEG:dextran formulations but does not provide a rigorous measurement of network degradation kinetics. *Please see appendix for additional detail* (A1 Swelling and Degradation).

Table 1 Compositional description of PEG:dextran variants prepared for assessment of material swelling and degradation in an aqueous medium.

Sample description	CHO:NH_2
P 2-2-50 **D** 10-50-7	0.96
P 2-2-30 **D** 60-20-25	2.14
P 2-2-50 **D** 10-50-20	2.74
P 2-2-50 **D** 10-50-25	3.42
P 2-2-30 **D** 10-50-45	10.27
P 8-10-40 **D** 10-50-5	1.07
P 8-10-38 **D** 10-50-5	1.13
P 8-10-38 **D** 60-20-15	1.27
P 8-10-40 **D** 10-50-14	3.00
P 8-10-20 **D** 40-25-15	3.04
P 8-10-21 **D** 60-20-20	3.06
P 8-10-21 **D** 10-50-14	5.71
P 8-10-10 **D** 40-25-25	10.15
P 8-10-21 **D** 10-50-25	10.19

Uniaxial tensile testing

**Based on the swelling and degradation data (shown below), present and subsequent experiments are limited to PEG:dextran formulations featuring constituent star PEG only (as opposed to linear PEG).*

Moderate uniaxial extensions (stretch ratio < 1.15) of dog bone-shaped material specimens were used to capture the linear elastic deformation regime of PEG:dextran hydrogels. An ElectroForce® 3450 mechanical tester (22 N load cell, 5 mm displacement stroke) was used for uniaxial tensile testing. Uniform testing regions (dog bone shape with rectangular cross section) of cast material samples were extended at constant displacement rate of 0.05 mm per second with the Electroforce® system (Figure 10). The force response was recorded by the system load cell and converted to true stress. The elastic modulus of each PEG:dextran sample is the slope of the generated true stress versus stretch ratio plot.

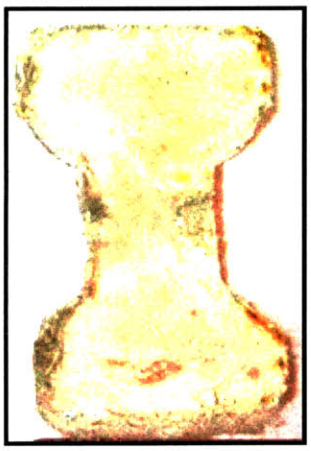

Figure 10 Dog bone-shaped sample of PEG:dextran used for uniaxial tensile testing.

The dog bone-shaped samples of PEG:dextran materials produced for uniaxial tensile testing do not conform to ASTM standards. The samples used are thicker in the test region than prescribed by ASTM. Efforts made to cast samples within the geometrical guidelines were thwarted by an inability to remove polymerized specimens from the molds without inducing damage. Even when specimens were extracted from molds in the hydrated state to reduce friability, tears at the material-mold interface damaged the samples. Nevertheless, the utilized dog bone-shaped geometry was sufficient to yield repeatable measurements of sample elastic moduli and prevent material failure at the sample-grip interface.

The PEG:dextran design space (**Table 2**) chosen for uniaxial tensile testing facilitates comparison of material moduli at low and high compositional variable levels in otherwise identical material pairs (**Figure 11**). Three such low versus high comparisons were made for each compositional variable to indicate the relative influence of available constituent alterations on PEG:dextran modulus. The average change in elastic moduli with each isolated compositional variation is reported as the main effect. The relative magnitudes of the variable main effects are used to discern the compositional determinants of material properties. The benefits and limitations of the utilized main effect analyses have been previously discussed [50]. *Please see appendix for additional detail (***A2 Uniaxial Tensile Testing***).*

Table 2 Compositional description of PEG:dextran variants prepared for uniaxial tensile testing. The materials are selected to facilitate calculation of compositional variable main effects on PEG:dextran stiffness.

Sample description	$CHO:NH_2$
P 8-2-20 **D** 10-20-20	0.64
P 8-2-20 **D** 60-20-20	0.64
P 8-10-60 **D** 10-20-20	1.07
P 8-10-60 **D** 60-20-20	1.07
P 8-2-20 **D** 10-20-40	1.29
P 8-2-20 **D** 10-50-20	1.71
P 8-10-60 **D** 10-20-40	2.14
P 8-10-60 **D** 10-50-20	2.85
P 8-10-20 **D** 10-20-20	3.21
P 8-10-20 **D** 60-20-20	3.21
P 8-10-20 **D** 10-20-40	6.43
P 8-10-20 **D** 10-50-20	8.56

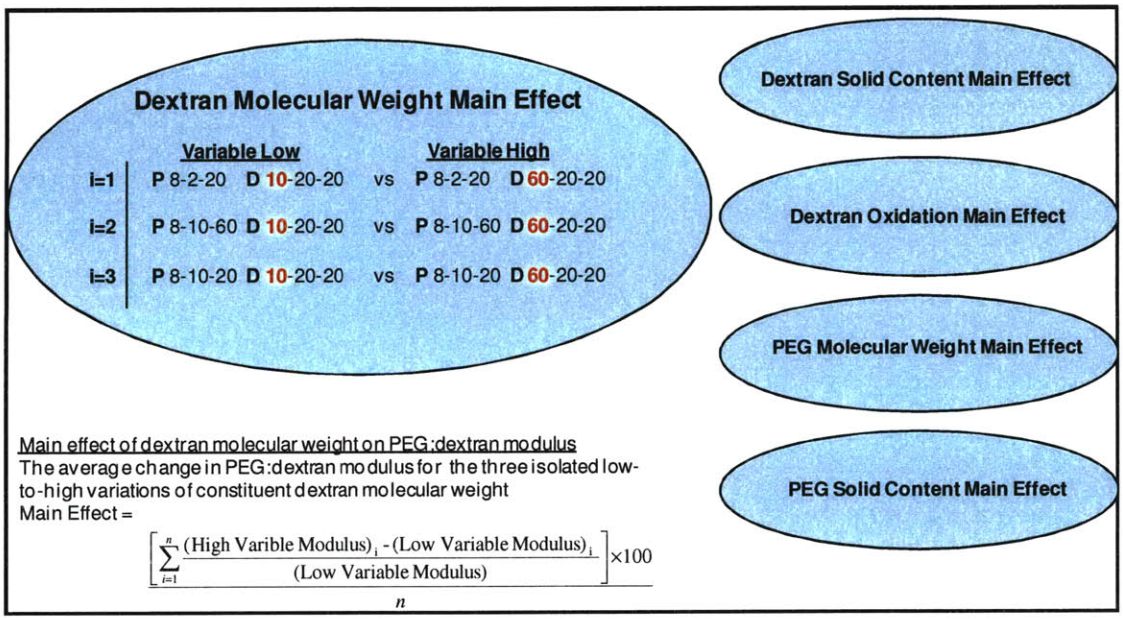

Figure 11 Schematic of material design space selected to facilitate main effect analyses. The effect of dextran molecular weight on PEG:dextran modulus is highlighted, although analogous methodology is applied for all analyzed compositional variables.

Adhesion strength testing

The adhesive strength of PEG:dextran to the serosal surface of rat small intestine was measured through application of a tensile force to a tissue-material-tissue interface (Figure 12). As with uniaxial tensile testing, the material design space for adhesion strength testing facilitates estimation of compositional variable main effects on the property of interest (Table 3). Two serosal surfaces are joined with a PEG:dextran polymer, with subsequent application of a tensile force. The maximal force detected prior to interface failure reflects the bioadhesive strength of the material formulation. Please see appendix for additional detail (A3 Adhesion Strength Testing I).

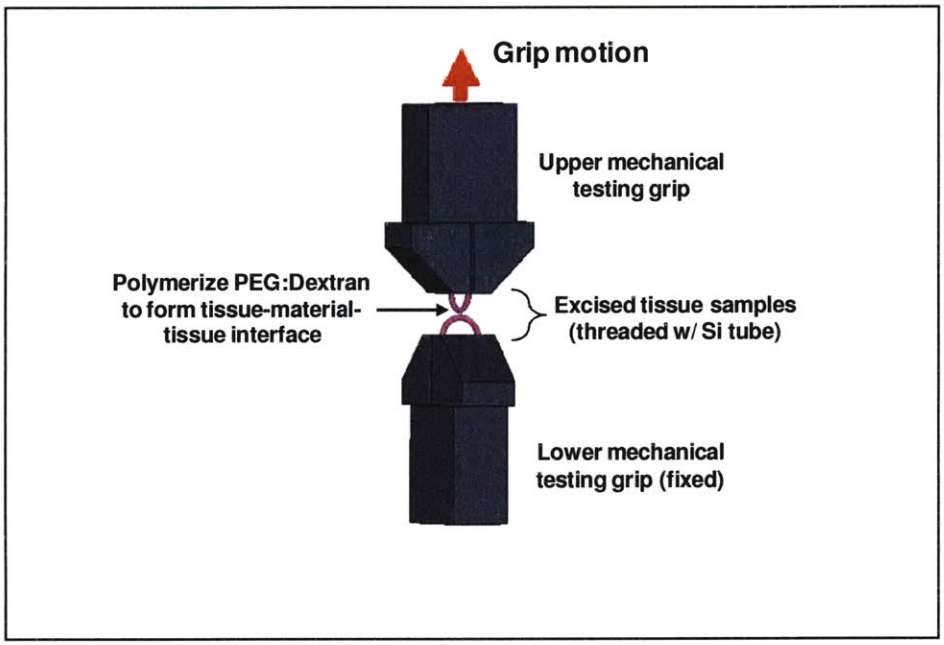

Figure 12 Schematic of adhesion strength testing procedure. Tissue-material-tissues interfaces are displaced at a constant rate while the force response is recorded. The maximum force prior to interfacial failure indicates material adhesion strength.

Table 3 Compositional description of PEG:dextran variants prepared for adhesion strength testing. The materials are selected to facilitate calculation of compositional variable main effects on PEG:dextran adhesion strength.

Sample description	$CHO:NH_2$
P 8-2-20 **D** 10-20-20	0.64
P 8-2-20 **D** 60-20-20	0.64
P 8-10-60 **D** 10-20-20	1.07
P 8-10-60 **D** 60-20-20	1.07
P 8-2-20 **D** 10-20-40	1.29
P 8-2-20 **D** 10-50-20	1.71
P 8-10-60 **D** 10-20-40	2.14
P 8-10-60 **D** 10-50-20	2.85
P 8-10-20 **D** 10-20-20	3.21
P 8-10-20 **D** 60-20-20	3.21
P 8-10-20 **D** 10-20-40	6.43
P 8-10-20 **D** 10-50-20	8.56

Cytotoxic effect of PEG:dextran degradation products

The response of vascular smooth muscle cells (bovine vSMC) to pooled PEG:dextran degradation products was quantified with cytotoxicity assays. Comparisons were made between the degradation products of materials with various total solid contents and reactive group ratios. The selected materials allow for comparison of the effects of either material solid content or reactive group ratio at four levels (Table 4). The first four tabulated samples span a range of wide solid contents (12.5 %– 42.5 %) with limited variance in reactive group ratio (2.11-2.96), while the second four samples span a wide range of reactive group ratios (0.42-10.7) with limited variance in solid content (21.5 %-22.5 %). *Please see appendix for additional detail (*A4 Cytotoxicity Studies*).*

Table 4 PEG:dextran variants prepared for assessment of material cytotoxicity. The first four materials have a range of solid contents and similar reactive group ratios, while the second four materials have similar solid contents and a range of reactive group ratios.

Sample description	Total solid content (%)	CHO:NH_2
P 8-10-20 **D** 10-50-5	12.5	2.14
P 8-10-38 **D** 60-20-25	31.5	2.11
P 8-10-38 **D** 60-20-35	36.5	2.96
P 8-10-50 **D** 60-20-35	42.5	2.25
P 8-10-38 **D** 60-20-5	21.5	0.42
P 8-10-38 **D** 10-50-5	21.5	1.13
P 8-10-20 **D** 60-20-25	22.5	4.02
P 8-10-20 **D** 10-50-25	22.5	10.7

Cytotoxicity assay description

A cytotoxicity assay kit (Vybrant) was used to quantify the concentration of the cytosolic enzyme glucose 6-phosphate dehydrogenase (G6PD) in cell culture supernatant. The release of this enzyme by cells is indicative of cell damage or death. The cytotoxic levels (G6PD concentrations) of cell populations subject to various treatments were converted to a relative cytotoxicity by means of comparison to a lysis control, which gave the G6PD level for a totally dead cell population of known size. A Multisizer 3 Coulter Counter (Beckman) was used to count cells populations in 12-well plates following various culture treatments. The counts provide a basis for adjusting the relative cytotoxicity measurements to account for well cell density which is subject to a slight but measurable variance.

The adjusted relative cytotoxicity considers both the size (cell density) and the health (relative cytotoxicity) of cell cultures after exposure to PEG:dextran degradation products. The adjusted relative cytotoxicity is a metric for cell culture health, and is calculated as follows:

Adjusted Relative Cytotoxicity = (Relative Cytotoxicity) / (Cell Density)

Proliferative effect of polymerized PEG:dextran materials

Fibroblast migration and proliferation are key cellular processes in wound healing [51-54]. Limitations in the performance of cyanoacrylate polymers have been attributed to interference with fibroblast activity, resulting in incomplete tissue healing and increased risk of surgical complications [19, 55]. An ideal tissue sealant would promote regular fibroblast activity at a wound site, motivating examination of the effect of PEG:dextran on fibroblast proliferation *in vitro*. Controlled volumes of PEG:dextran variants with increasing aldehyde content (Table 5) were applied to sub-confluent 3T3 fibroblasts in culture , which were then allowed to proliferate for an additional 24 hours. A colorimetric assay was then conducted on the cell cultures to determine the effect of material exposure on fibroblast proliferation. *Please see appendix for additional detail* (A5 Proliferation Studies).

Table 5 PEG:dextran variants prepared for assessment of material effect on fibroblast proliferation.

Sample description	Total solid content (%)	CHO:NH_2
P 8-10-50 **D**10-20-20	35	1.29
P 8-10-40 **D**10-20-20	30	1.61
P 8-10-32 **D**10-20-20	26	2.01
P 8-10-40 **D**10-50-14	27	3.00
P 8-10-32 **D**10-50-18	25	4.82
P 8-10-40 **D**10-50-27	29	5.78
P 8-10-32 **D**10-50-27	29.5	7.22

Proliferation assay description

A MTT colorimetric assay (Chemicon) was used to quantify the proliferation of 3T3 fibroblast cells following various culture treatments. The assay is based on absorbance

measurements designed to detect the cleavage of 3-(4, 5-dimethylthiazol-2-yl)-2,5-diphenyl tetrasodium bromide, a process which requires mitochondrial activity. The MTT assay provides precise measurements of live cell populations, as mitochondrial activity ceases rapidly following cell death.

3.1.4 Results

Swelling ratio and onset of degradation

The swell response of PEG:dextran was gravimetrically monitored over a period of sustained sample submersion in aqueous medium. The analyses were conducted until disk fragmentation due to extensive hydrolytic degradation prevented sample handling. Two descriptors of the swell response were extracted from gravimetric analyses as described above, specifically the maximal swelling ratio and the onset of material degradation.

A representative plot of the gravimetric data acquired for PEG:dextran disk suspensions (**P** 8-10-40 **D** 10-50-14, initial mass = 0.34 ± 0.03 g) shows an initial mass gain due to swell followed by a mass loss due to crosslink degradation and material erosion (Figure 13). The sample suspension was maintained for 96 hours, with a maximal mass of 3.26 g measured at the 54 hour time point. The maximal swelling ratio for this sample is 853.2 % and the onset of degradation occurs after 54 hours of submersion. At times exceeding 96 hours the sample disk has visibly fragmented and is no longer appropriate for gravimetric analysis.

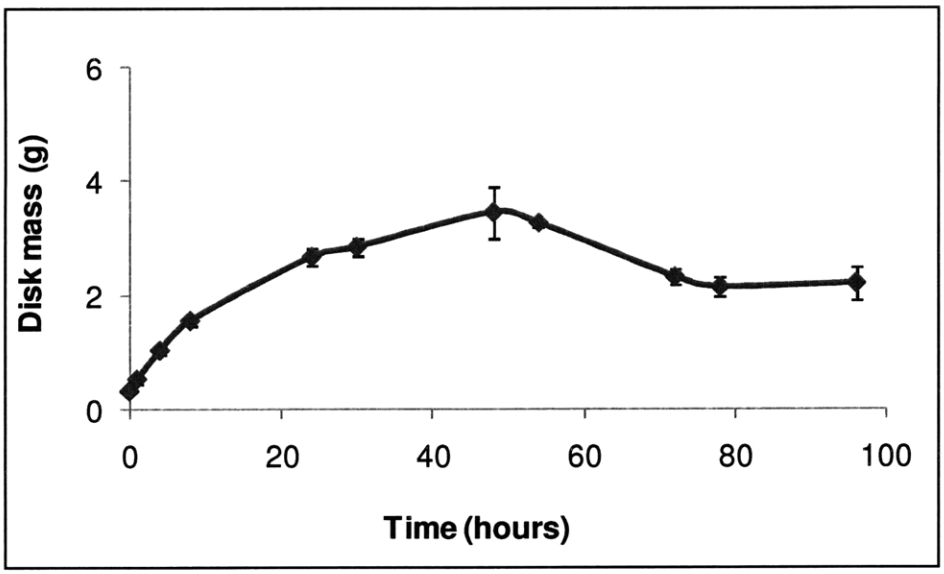

Figure 13 A representative plot of PEG:dextran disk mass as a function of swell time. Measurements were taken until sample disk fragmentation prevented handling.

The gravimetric data of PEG:dextran hydrogels portray a wide variance of material swell response among examined formulations (Table 6). The swelling ratios and degradation times for the analyzed materials range from -37.3 % to 926.7 % and 0.6 hours to 54 hours, respectively, with a negative swelling ratio indicating a net loss of mass prior to the first measurement (1 hour). When grouped to reflect the dependence on the constituent PEG, swelling ratios (Figure 14) and degradation times (Figure 15) are generally greater with star and opposed to linear polymers, suggesting multiple reactive arms facilitate polymer network formation and material stability after swell. Furthermore, the swelling ratio and degradation time across material formulations correlate well with each other, with a Pearson's correlation coefficient of 0.88 (Figure 16). PEG:dextran materials featuring star rather than linear PEG constituent are more amenable to clinical soft tissue sealant applications which generally require material stability for days to weeks [20].

Table 6 Summary of the swelling and degradation data for PEG:dextran hydrogels. Both swelling ratio and onset of degradation dramatically vary among selected material formulations.

Gravimetric analyses	Swelling ratio (%)		Onset of degradation (hours)	
Sample description	Average	Standard deviation	Average	Standard deviation
P 2-2-50 D 10-50-7	-37.3	6.0	0.6	0.0
P 2-2-50 D 10-50-20	80.2	9.1	4.7	1.7
P 2-2-30 D 10-50-45	89.0	7.8	6.7	2.3
P 2-2-50 D 10-50-25	95.8	24.1	4.0	0.0
P 2-2-30 D 60-20-25	10.0	2.3	2.0	0.0
P 8-10-10 D 40-25-25	182.1	16.3	8.0	0.0
P 8-10-21 D 10-50-25	621.7	49.8	50.0	3.5
P 8-10-40 D 10-50-5	231.7	76.9	32.3	11.6
P 8-10-38 D 60-20-15	492.6	126.2	46.0	13.9
P 8-10-40 D 10-50-14	926.7	178.1	44.0	10.4
P 8-10-20 D 40-25-15	293.0	44.2	23.8	5.5
P 8-10-21 D 60-20-20	401.0	76.8	44.7	8.0
P 8-10-38 D 10-50-5	217.7	18.0	24.0	0.0
P 8-10-21 D 10-50-14	631.0	83.3	54.0	0.0

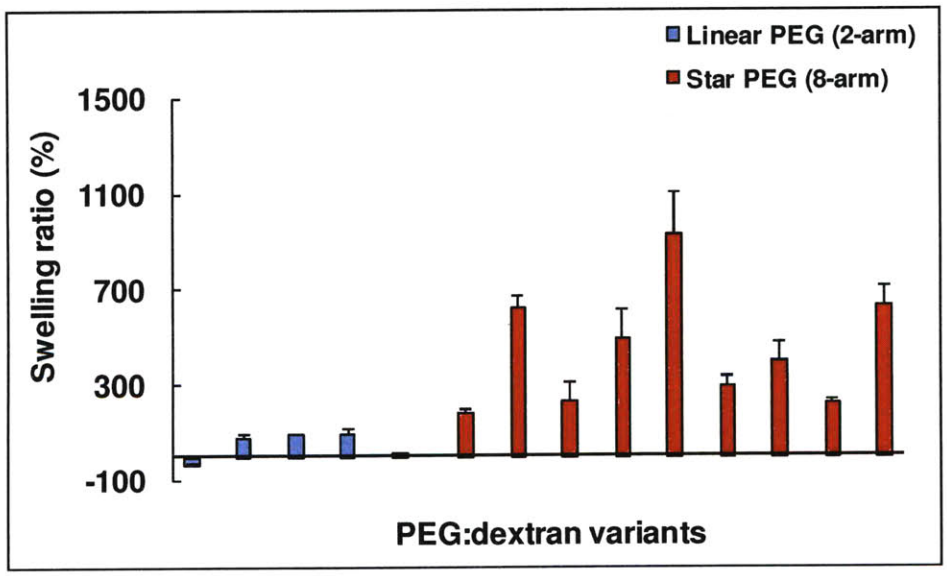

Figure 14 Swelling ratios of PEG:dextran variants, with samples differentiated only by PEG amine arm number. Formulations with star PEG exhibited an increased swell response as compared to the linear PEG alternative.

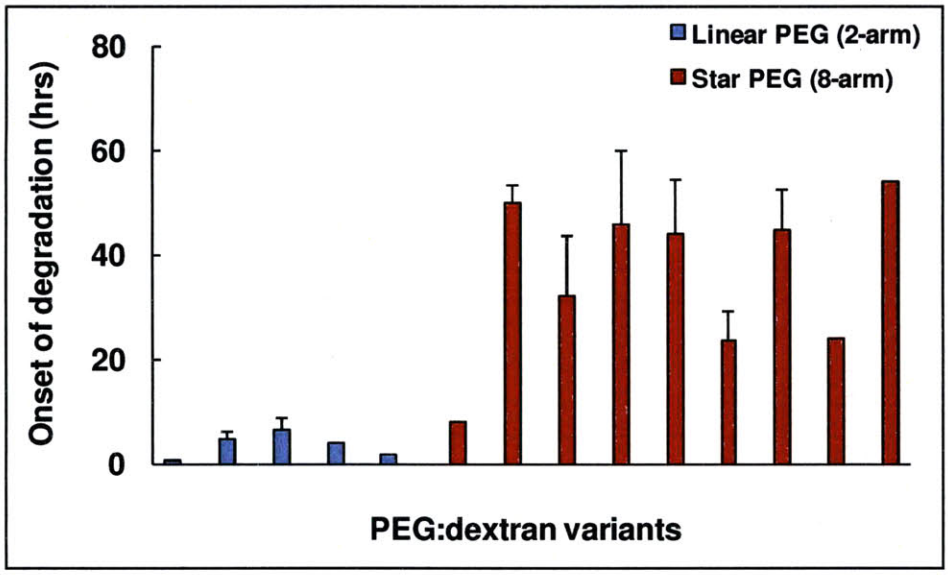

Figure 15 Onset of degradation times of PEG:dextran variants, with samples differentiated only by PEG amine arm number. Formulations with star PEG exhibited protracted degradation kinetics as compared to the linear PEG alternative.

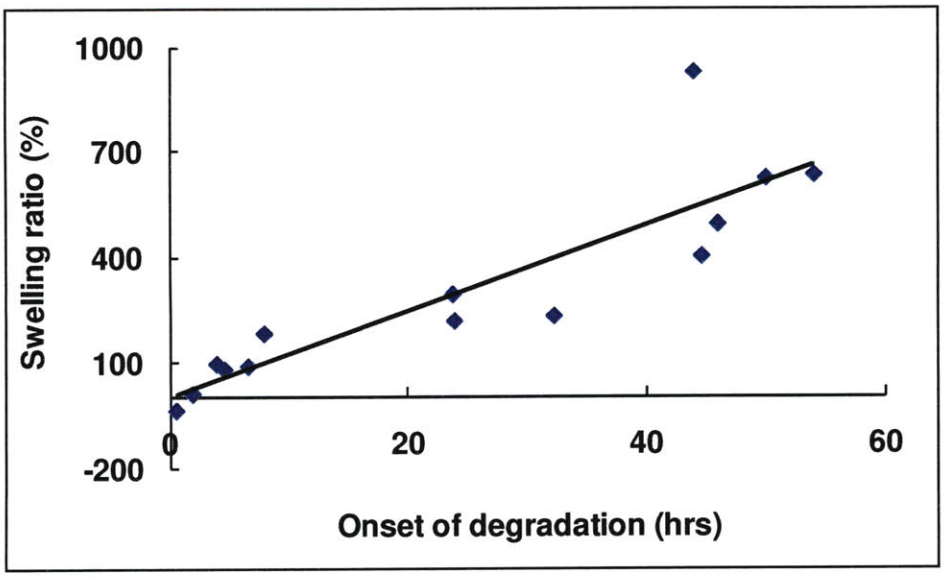

Figure 16 The swelling ratio and onset of degradation of PEG:dextran variants exhibit a linear correlation, with a Pearson's correlation coefficient of 0.88 across examined material variants.

Elastic modulus

Uniaxial tensile testing data of PEG:dextran samples were processed to compute the elastic moduli of selected material formulations. The direct outputs of a uniaxial tensile test (force versus displacement) were readily transformed into true stress versus stretch ratio with the appropriate normalizations. A representative plot of PEG:dextran deformation shows a linear elastic mechanical response (Figure 17). The sample was elongated to a stretch ratio of 1.12, which corresponds to a 12 % increase in length. The stress arising in the sample linearly increases in this deformation regime with a slope indicative of the sample elastic modulus, which was 211 kPa in the representative plot.

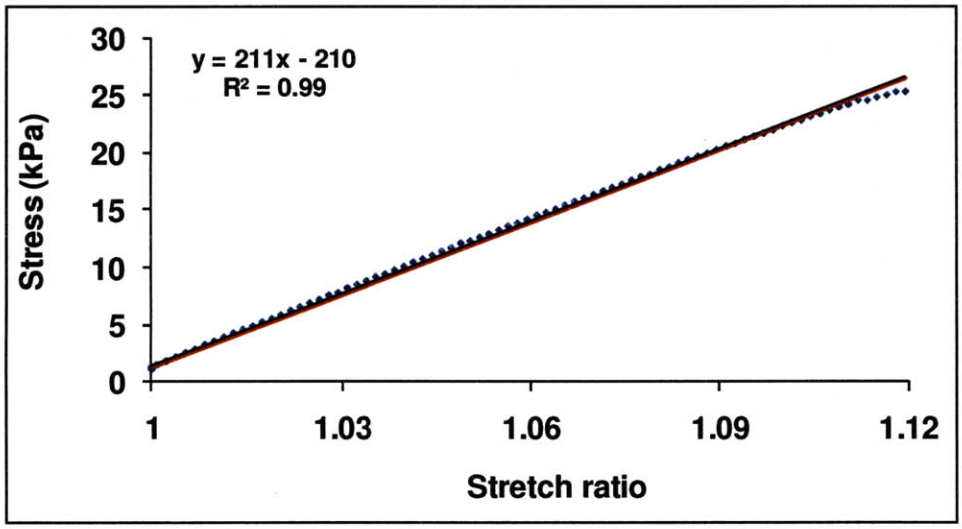

Figure 17 A representative plot of PEG:dextran stress response under applied uniaxial extension. The slope of stress response indicates the material elastic modulus.

The measured elastic moduli of all tested PEG:dextran materials span an order of magnitude, ranging from approximately 30 – 300 kPa (Table 7). A main effect analysis is conducted to characterize a PEG:dextran property dependence on available compositional variation. Main effects provide a rough indication of the influence of each compositional variable in determining the elastic modulus of PEG:dextran materials. A positive main effect indicates that increasing the compositional variable value will increase modulus, while a negative main effect indicates the opposite. Although design space limitations require careful interpretation of main effect analyses, compositional determinants of material properties can be confidently inferred in some cases.

Table 7 Summary of the elastic moduli of PEG:dextran hydrogels as assessed by uniaxial extension of dog bone-shaped material samples. PEG:dextran elastic modulus varied by an order-of-magnitude among examined formulations.

Uniaxial tensile testing	Elastic modulus (kPa)	
Sample description	Average	Standard deviation
P 8-2-20 **D** 10-20-20	202.4	16.7
P 8-2-20 **D** 60-20-20	62.9	0.6
P 8-2-20 **D** 10-20-20	86.2	0.4
P 8-10-20 **D** 60-20-20	31.9	0.3
P 8-10-20 **D** 10-20-40	61.5	4.0
P 8-10-20 **D** 10-50-20	66.0	3.6
P 8-2-20 **D** 10-20-40	258.1	6.7
P 8-10-20 **D** 10-50-20	63.9	1.6
P 8-10-60 **D** 10-20-20	195.3	3.1
P 8-10-60 **D** 60-20-20	207.9	13.1
P 8-10-60 **D** 10-20-40	316.4	24.6
P 8-10-60 **D** 10-50-20	258.2	8.5

The solid content of constituent PEG had an overwhelmingly large positive main effect (+466.7 %) on PEG:dextran elastic moduli when compared to the other compositional variables (Table 8). Dextran solid content and oxidation state also have positive main effects on material modulus, as expected with increased material and crosslinking density, respectively. The main effects of constituent molecular weights are relatively slight, but in the case of PEG may reflect a steric inhibition of network formation for large constituent polymers (a dextran aldehyde polymer may often react with only a single star PEG amine rather than join two PEG molecules as required in a network). In any case, molecular weight is a weak determinant of network properties and offers little control over PEG:dextran modulus.

Table 8 Main effect analysis reflecting the dependence of PEG:dextran modulus on compositional variables. PEG solid content exhibited the strongest influence over material modulus.

Compositional variable	Modulus main effect (%)
Dextran molecular weight	12.8
Dextran oxidation	71.4
Dextran solid content	82.1
PEG molecular weight	-55.6
PEG solid content	**466.7**

Adhesion strength

Interfaces between excised rat intestinal tissues and PEG:dextran materials were mechanically tested to rate hydrogel bioadhesive strength. Tissue-material test elements were subjected to a normal displacement at a constant rate as described above. The force required to disjoin the interface indicates the adhesive strength of the material. The force measurements in the developed protocol were invariably small due to the limited polymer volume applied to the interface (0.25 ml) and to the small interface contact area (< 1 mm^2). The use of a high fidelity load cell and mechanical testing system allows for detection of mN forces and facilitates differentiation of PEG:dextran adhesive strengths with the described testing protocol.

A representative plot of an interfacial displacement shows an initially increasing force that peaks around 0.16 N (**Figure 18**). The maximum force response throughout the applied interfacial displacement was recorded as the material sample adhesion strength. After peaking, there is a rapid drop in force which corresponds to interfacial failure. The adhesion strengths measured for PEG:dextran materials show a large relative variance, with an absolute span from near 0 to about 0.2 N (**Table 9**). The relative adhesion strength of tested compositional variants promotes selection and design of PEG:dextran for tissue sealant applications.

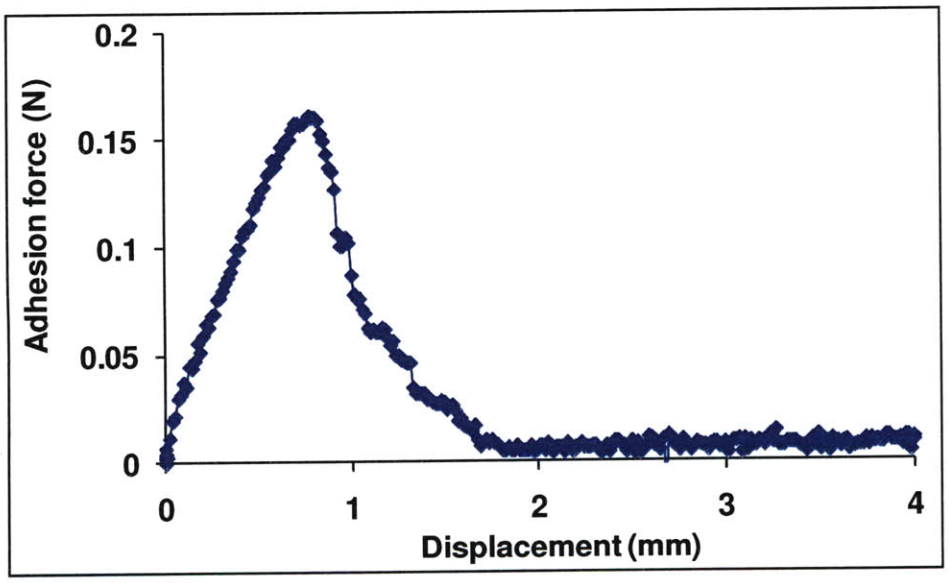

Figure 18 A representative plot of a tissue-material-tissue interface force response to uniaxial displacement. The peak force corresponds to interfacial failure and is indicative of the material adhesion strength.

Table 9 Summary of the adhesion strength of PEG:dextran hydrogels as assessed by uniaxial displacement of tissue-material-tissue interfaces.

Adhesion strength testing	Adhesion strength (N)	
Sample description	Average	Standard deviation
P 8-2-20 **D** 10-20-20	0.056	0.022
P 8-2-20 **D** 60-20-20	0.112	0.041
P 8-10-20 **D** 10-20-20	0.008	0.002
P 8-10-20 **D** 60-20-20	0.021	0.001
P 8-10-60 **D** 10-20-20	0.057	0.007
P 8-10-60 **D** 60-20-20	0.020	0.007
P 8-2-20 **D** 10-50-20	0.110	0.049
P 8-10-20 **D** 10-50-20	0.124	0.009
P 8-10-60 **D** 10-50-20	0.145	0.036
P 8-10-20 **D** 10-20-40	0.190	0.053
P 8-2-20 **D** 10-20-40	0.125	0.035
P 8-10-60 **D** 10-20-40	0.108	0.032

A main effect analysis of the PEG:dextran adhesion strength with compositional variation is conducted as above (Table 10). The most deterministic variables of adhesion strength are the constituent dextran oxidation and solid content. The positive main effects of these compositional variables on adhesion strength are relatively large in magnitude, and are both related to the number of aldehyde groups in PEG:dextran. Increasing either the dextran oxidation or solid content in a given material formulation will result in an increase of free aldehyde content after network formation, provided all other compositional variables remain unaltered. Based on the main effect analyses, aldehyde reactivity with tissue is identified as the primary compositional determinant of PEG:dextran adhesion strength.

Table 10 Main effect analysis reflecting the dependence of PEG:dextran adhesion strength on compositional variables. Dextran oxidation state and solid content exhibited the strongest influence over material adhesion strength, suggesting that PEG:dextran bioadhesion is achieved via free material aldehyde binding to soft tissue surfaces.

Compositional variable	Adhesion strength main effect (%)
Dextran molecular weight	26
Dextran oxidation	**220**
Dextran solid content	**170.1**
PEG molecular weight	13.9
PEG solid content	-4.2

The small negative main effect (-4.2 %) of constituent PEG solid content on adhesion strength suggests that PEG amine reactivity with tissue is minimal, and is at most a secondary mechanism for tissue-material interactions. Additionally, studies of PEG:dextran polymerization rates show that increasing PEG solid content dramatically reduces the gel time of the tested materials. Accelerated gelling rates will limit the material spreading (and thus contact area) when polymerized on tissues. The associated decrease in gelling time and consequentially tissue-material contact area may explain the negative main effect of PEG solid content observed for PEG:dextran adhesion strength.

Cytotoxicity of PEG:dextran degradation products

The adjusted relative cytotoxicity following smooth muscle cell exposure to PEG:dextran degradation products varies with both formulation reactive group ratio and total solid content (Table 11). In all co-cultures, cellular exposure to pooled PEG:dextran degradation products results in elevated levels of adjusted relative cytotoxicity. The general increase in adjusted relative cytotoxicity between early and late degradation

products of the same material suggests that extensive material degradation is required to instigate a cellular response.

Table 11 Summary of PEG:dextran degradation product cytotoxicity as indicated by the *in vitro* response of bSMC. Degradation products were pooled and applied to cell cultures after one (early) or three (late) weeks of PEG:dextran suspension in aqueous media.

Cytotoxicity testing	Early degradation cytotoxicity (G6PD release/cell x 10^6)		Late degradation cytotoxicity (G6PD release/cell x 10^6)	
Sample description	Average	Standard deviation	Average	Standard deviation
DMEM Control	0.236	0.113	0.199	0.085
P 8-10-20 **D** 10-50-5	0.661	0.113	1.233	0.286
P 8-10-38 **D** 60-20-25	0.444	0.113	0.644	0.051
P 8-10-38 **D** 60-20-35	0.417	0.103	1.419	0.509
P 8-10-50 **D** 60-20-35	0.641	0.205	3.355	0.445
P 8-10-38 **D** 60-20-5	0.734	0.073	3.614	1.294
P 8-10-38 **D** 10-50-5	0.868	0.122	0.659	0.142
P 8-10-20 **D** 60-20-25	0.265	0.038	0.255	0.106
P 8-10-20 **D** 10-50-25	0.325	0.096	0.888	0.301

A subset of the adjusted relative cytotoxicity data highlights the effect of total material solid content variation on the cellular response (Figure 19). A positive correlation expected between adjusted relative cytotoxicity and material solid content is intuitive and largely supported by the data, with the exception of the cytotoxic effect of the low solid content PEG:dextran formulation. The unexpected level of adjusted relative cytotoxicity with a low solid content PEG:dextran is understood through the degradation rates operative in these materials. Through visual inspection of material samples, it appeared that the low solid content formulation had completely dissolved following the 21 day suspension period, while other materials persisted to some extent proportional to the initial solid content. In other words, the supernatant of 12.5% solid content material suspension was likely more concentrated with by-product than expected when considering only initial solid content and ignoring degradation rates. The high level of cytotoxicity for the low solid content material variant is likely an artifact of increased by-

product pooling. Positive correlation between solid content and adjusted relative cytotoxicity is still expected to persist, without exception, once materials have all undergone complete degradation.

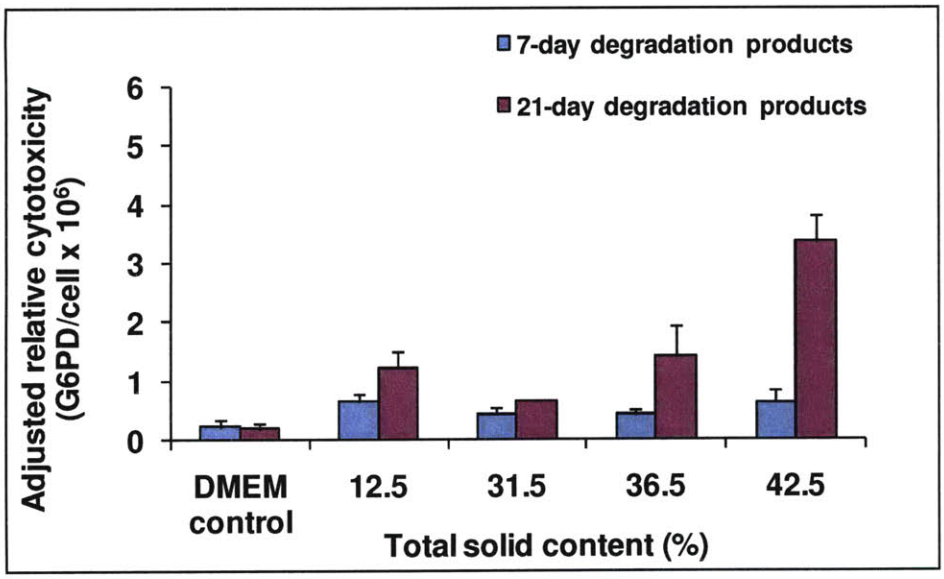

Figure 19 Cytotoxicity of PEG:dextran degradation products as a function of total material solid content.

A second subset of the adjusted relative cytotoxicity data shows a more complex dependence on PEG:dextran reactive group ratio (Figure 20). Material compositions with exceedingly high or low levels of CHO:NH_2 are relatively cytotoxic upon degradation. An intermediate reactive group ratio PEG:dextran material (**P** 8-10-20 **D** 60-20-25, CHO:NH_2=4.02) showed no statistically significant difference in cytotoxicity as compared to DMEM controls. Possible explanations for the exhibited dependence are discussed below.

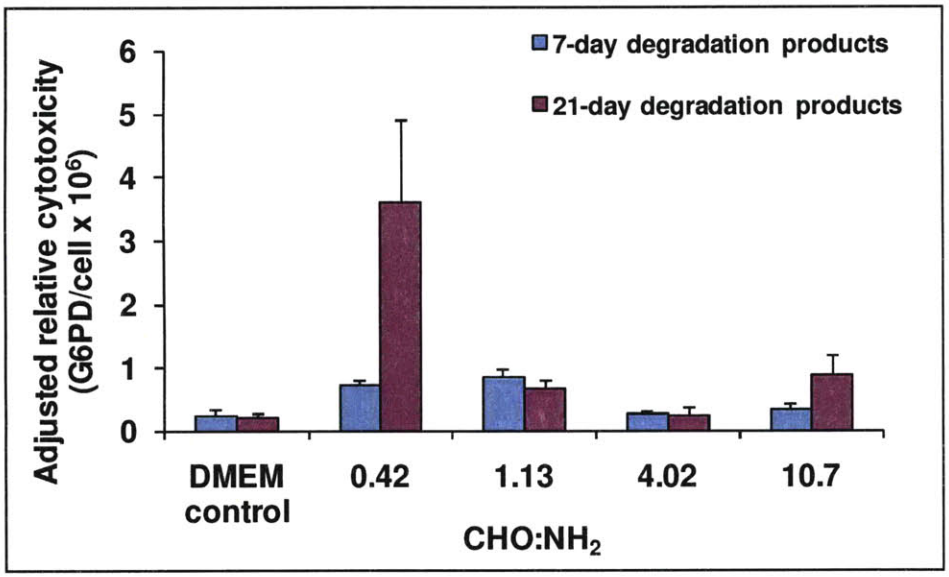

Figure 20 Cytotoxicity of PEG:dextran degradation products as a function of material reactive group ratio.

Proliferative effect of PEG:dextran copolymers

The cellular response to direct applications of PEG:dextran polymers was studied with a colorimetric proliferation assay. Small volumes of various PEG:dextran materials were applied to 3T3 fibroblast cultures, which were subsequently incubated for 24 hours as described above. The cell numbers following incubation with the polymers indicates the material effects on cell proliferation.

The proliferation data for all tested PEG:dextran materials are represented as a percent of control samples to which no materials were applied (Table 12). The cellular response to PEG:dextran polymers ranges from inhibition to stimulation of proliferation. The significant range in cellular response to PEG:dextran can be expressed as a function of the material reactive group ratio, and suggests that aldehyde-mediated reactivity influences proliferation in a dose-dependent manner (Figure 21). As with the cytotoxicity studies, the *in vitro* data indicates that PEG:dextran material formulations with intermediate reactive group ratios (2 - 3) are minimally reactive with cells

Table 12 Summary of the effect of PEG:dextran on fibroblast proliferation *in vitro*. Data are presented as a percentage of control wells maintained at standard culture conditions.

Proliferation testing	3T3 proliferation (% positive control)	
Sample description	Average	Standard deviation
P 8-10-50 **D**10-20-20	46.6	16.8
P 8-10-40 **D**10-20-20	72.4	12.2
P 8-10-32 **D**10-20-20	68.6	9.8
P 8-10-40 **D**10-50-14	116.2	11.3
P 8-10-32 **D**10-50-18	169.8	28.5
P 8-10-40 **D**10-50-27	159.9	14.3
P 8-10-32 **D**10-50-27	183.8	13.2

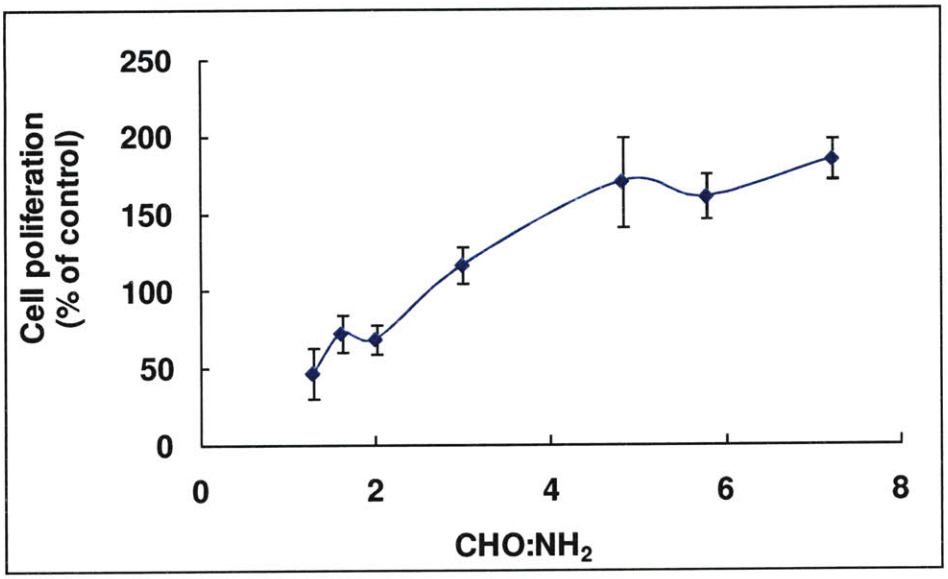

Figure 21 The cellular response to PEG:dextran as a function of material reactive group ratio. Fibroblast proliferation exhibits a positive dependence on material aldehyde content.

3.1.5 Discussion

Soft tissue sealants are a clinically-significant class of biomaterials that provide an ideal framework for study of tissue-material interactions. Despite extended efforts toward sealant development, the need for high strength and biocompatible materials persists within the medical community. We intuit that the challenges in sealant design fundamentally stem from conflicting dependencies of both tissue response and bioadhesion on tissue-material interactions. Because these phenomena are readily quantifiable from an experimental standpoint, tissue sealants facilitate evaluations of material modifications both in terms of a functional biomaterial gain (i.e. adhesion strength to soft tissue, leakage prevention at anastomotic junction, adhesive interface stability) and a prohibitive biological response (i.e. cytotoxicity, tissue inflammation, immune response).

Through collaboration with industry, we have developed the bioadhesive hydrogel PEG:dextran which spans a significant property space by virtue of compositional manipulation. Constituent aminated PEG and dextran aldehyde polymers were synthesized with a range of molecular weights, solid contents, reactive group densities, and molecular structures to probe material property response to compositional variations. Order-of-magnitude differences in multiple material properties were observed among compositional variants, suggesting that this material system can be optimized with respect to sealant performance. Here we synthesized a collection of PEG:dextran materials and compared their swell response, elastic modulus, adhesion strength and cellular compatibility to determine which compositional variables elicit the greatest

relative influence over key sealant properties. The results of these initial characterizations provide guidelines for subsequent use of the PEG:dextran system to examine tissue-material interactions and further impetus for continued development of these materials for sealant applications.

When applied to soft tissues in the surgical setting, adhesive materials will be subjected to biological fluids such as blood, interstitial fluid, and tissue exudates, all of which have high water content. Accordingly, PEG:dextran hydrogels are expected to swell *in situ*, resulting in both a mass gain due to fluid uptake and hydrolytic degradation of network bonds. Ideal clinical sealants would approximate tissue composition to promote biocompatibility and would persist as a continuous solid at the application site for days-to-weeks to provide the desired therapeutic benefit. We found that the eight-arm star form of constituent PEG amine favors PEG:dextran water uptake and stability in aqueous suspension, in essence achieving more tissue-like composition for longer times as compared to the linear alternative. Presumably the multi-functional nature of star PEG is more conducive to stable network formation due to multiple, near nodes for aldehyde-amine crosslinking. Future experimentation with PEG:dextran variants will focus on the star as opposed to linear PEG amine based on the preferred swell response.

In addition to compositional similitude, mechanical compliance matching between adhesive materials and soft tissues should be sought to minimize interfacial stress concentrations. A compliance-matched sealant would likely impart interfacial failure

resistant under dynamic loading conditions (i.e. a peristaltic wave) and induce less compression in underlying tissues (as observed with overly stiff cyanoacrylate materials). In these studies, we found that the stiffness of PEG:dextran is highly responsive to variations in the solid content of the star PEG amine. Interestingly, the stiffness dependence on dextran aldehyde solid content is substantially less dramatic, suggesting that star PEG is the limiting polymer in achieving PEG:dextran network formation. The observed limitation may stem from a lesser molecular mobility of the complex macromolecule and a steric hindrance to bond formation introduced by the presence of multiple arms. Due to the exhibited dependencies, manipulation of PEG amine solid content will be the employed design strategy for controlling bulk mechanical properties in the PEG:dextran system.

The primary functional property of soft tissue sealants is clearly bioadhesion. Main effect analyses of PEG:dextran variants strongly suggest that these materials interact with soft tissues via aldehyde-mediated bond formation. The total aldehyde density of PEG:dextran can be readily controlled through the oxidation state and/or solid content of the dextran aldehyde polymers. Prior to PEG:dextran formation, material aldehyde groups face four conceivable fates: bonding to amine groups presented by the PEG constituent (cohesive bond formation), bonding to amine groups on the tissue surface (adhesive bond formation), chemical conversion (reduction into a primary alcohol or oxidation into a carboxylic acid), or remaining free. Consequently, aldehyde-mediated adhesion between PEG:dextran and soft tissue can be directly controlled by the initial aldehyde density in a particular formulation, but is influenced by the relative amine

density presented by the PEG component and the target tissue surface. The identification of the mechanism by which PEG:dextran adheres to tissue enables rational design for sealant application and facilitates the development of tailored formulations based on the propensity of target tissue beds for aldehyde-mediated adhesion.

Excessive bioreactivity can potentially elicit an undesirable biological response and limit material biocompatibility. In the PEG:dextran system, we demonstrated that material density (total solid content) and bioreactivity (aldehyde content) interfere with cellular activities in a complex fashion. Degradation products released from formulations with extreme levels (low or high) of total solid content or low aldehyde content induced elevated cytotoxicity *in vitro*. We attribute these phenomena to the actual amount of degradation products that accumulate in the culture well plates throughout the duration of the experiment, which is relatively high in these cases due to either fast degradation (low solid or low aldehyde content) or more initial material (high solid content). The highest aldehyde content variant (**P** 8-10-20 **D** 10-50-25), although comparatively stable, also induced increased cytotoxicity upon degradation. In this case, we conclude that the high concentration of bioreactive aldehyde groups is the cause of by-product cytotoxicity. This, along with the observed monotonic increase in cellular proliferation with $CHO:NH_2$, suggest that arbitrarily increasing the aldehyde content in PEG:dextran will reduce material biocompatibility throughout the implantation period.

Preliminary characterizations of PEG:dextran demonstrate the property span possible with this material system. Key properties, including material swell response, stiffness, bioadhesion strength, and cellular compatibility, all vary among material formulations in a predicable manner. Future studies will exploit the identified material-property relationships in order to better understand tissue-material interactions and appropriate PEG:dextran for clinical sealant applications.

3.1.6 Conclusion

PEG:dextran hydrogels constitute a family of bioadhesive materials with potential for medical use as soft tissue sealants. In this preliminary work we identified compositional variables which have the strongest relative influence on central material properties, thus providing a basis for future rational design of PEG:dextran sealants. The following property determinants have been identified for the PEG:dextran material system.

1. Network complexity (constituent PEG arm number) determines material hydration and stability in an aqueous environment
2. Constituent PEG solid content determines elastic modulus
3. Aldehyde reactivity determines adhesion strength to tissue
4. Reactive group ratio determines material biocompatibility

Identification of these compositional determinants not only guides PEG:dextran development for bioadhesive applications but additionally suggests underlying mechanisms of tissue-material interaction between these complex polymers and soft tissue. Future work will focus on additional characterization of PEG:dextran property response to compositional variation, constitutive modeling of adhesive mechanics, analyses of *in vivo* tissue response to PEG:dextran, *in vitro-in vivo* data correlation, and ultimately the integration of experimental data to gain mechanistic understanding of adhesive tissue-material interactions and overall sealant performance.

3.1.7 Study Transition

The characterizations of PEG:dextran presented in Study 1 demonstrate that hydrogel cohesion and adhesion are highly responsive to compositional variations. More importantly, the identified property determinants provide rationale for designing families of PEG:dextran most appropriate for probing particular tissue-material interactions and advancing the potential of these materials as clinical sealants. The primary functional property of sealants is tissue-material adhesion, which we are now poised to strategically analyze with the PEG:dextran system. We anticipate that alteration in PEG:dextran aldehyde content will elicit control of adhesion to duodenal tissue, and that a series of materials with increasing aldehyde content can be used to correlate between adhesive properties and tissue response. To this end, we next synthesize the proposed material series, construct a constitutive model of adhesion, and apply model predictions to understand better the relationships between adhesion and tissue response which govern overall sealant performance.

3.2 STUDY 2 VISCOELASTIC MODEL OF ADHESIVE MECHANICS

Publication disclosure
The following presentation of Study 2 is based on:
Viscoelastic adhesive mechanics of aldehyde-mediated soft tissue sealants.
Shazly T, Artzi N, Boehning F, Edelman ER.
Biomaterials. 2008 Dec;29(35):4584-91.

3.2.1 Abstract

Soft tissue sealants generally sacrifice adhesive strength for biocompatibility, motivating the development of materials which interact with tissue to a predictable and controllable extent. Crosslinked hydrogels comprising aminated star polyethylene glycol and high molecular weight dextran aldehyde polymers (PEG:dextran) display aldehyde-mediated adhesion and readily tunable reactivity with soft tissue *ex vivo*. Evaluation of PEG:dextran compositional variants revealed that the burst pressure of repaired intestinal wounds and the extent of material-induced tissue deformation both increase nonlinearly with formulation aldehyde content and are consistently within the desired range established by traditional sealants. Adhesive test elements featuring PEG:dextran and intestinal tissue exhibited considerable viscoelasticity, prompting use of a standard linear solid (SLS) model to describe adhesive mechanics. Model elements were accurately represented as continuous functions of PEG:dextran chemistry, facilitating prediction of adhesive mechanics across the examined range of compositional formulations. SLS models of traditional sealants were also constructed to allow general correlative analyses between viscoelastic adhesive mechanics and metrics of sealant performance. Linear correlation of equilibrium SLS stiffness to sealant-induced tissue deformation indicates dense adhesive crosslinking restricts tissue expansion, while correlation of instantaneous SLS stiffness to burst pressure suggests the adhesive

stress relaxation capacity of PEG:dextran enhances their overall performance relative to traditional sealants.

3.2.2 Introduction

Adhesive sealants assist tissue repair and reduce operative risk through anastomotic stabilization, promotion of wound healing between disjoined tissues, and induction of rapid hemostasis [6-8]. Bioadhesive properties are largely a consequence of material reactivity with tissue, and as a result controlling unintended and deleterious reactivity is a major challenge of sealant design [56]. Tradeoffs between various adhesive properties dependent on bioreactivity are exemplified by common cyanoacrylate- and fibrin-based sealants [13-15]. Cyanoacrylate derivatives are highly bioreactive and adhere strongly to tissue, but are clinically limited due to excessive inflammation upon application and the release of cytotoxic by-products [18, 19]. Fibrin sealants are generally more biocompatible, but weakly adhere to tissue and introduce a risk of infectious transmission given their biological origin [7, 16, 17, 57]. A clear need persists for a soft tissue sealant capable of high strength and prolonged adhesion with minimal immune or inflammatory response.

Limitations of existing sealants could in part reflect a disturbance in underlying tissue mechanics following adhesive bond formation. Many soft tissues are viscoelastic and entropically dissipate significant amounts of mechanical stress under physiologic loading [58-61]. Highly reactive cyanoacrylate derivatives achieve high strength bioadhesion but in doing so may reduce native viscoelasticity as a consequence of low molecular weight tissue crosslinking. Conversely, less adherent fibrin sealants will likely maintain tissue viscoelasticity but cannot provide the mechanical strength necessary for wound stabilization and other clinical applications [62]. A viscoelastic model of adhesive

mechanics could meaningfully describe tissue-material interactions and facilitate correlation of mechanical properties with ultimate function.

Biomaterial applications of both star polyethylene glycol (PEG) and various polysaccharides have been extensively studied [49, 63-67]. Clinical interest in these materials has emerged because of their excellent biocompatibility, readily modifiable chemistries, and capability to form tissue-like hydrogel matrices. Here, crosslinked hydrogels composed of various ratios of aminated star PEG and dextran aldehyde polymers (PEG:dextran) were evaluated as potential soft tissue sealants with tunable adhesive properties [45, 46]. We hypothesized that the aldehyde content of PEG:dextran hydrogels will heavily influence their adhesion, and that the large reactive polymer constituent (10 kDa dextran aldehyde) will allow viscoelastic adhesive crosslinking. Adhesion of PEG:dextran to soft tissue should contrast the effect of small aldehyde-based fixatives, such as formaldehyde and glutaraldehyde, which tightly crosslink tissues and radically alter their physical and mechanical properties [68].

A series of PEG:dextran formulations with increasing aldehyde content were synthesized to examine the impact of aldehyde-mediated interactions on functional adhesive properties. Burst pressure of repaired intestinal wounds and the extent of material-induced tissue deformation served as *ex vivo* metrics of sealant performance. Tensile testing of adhesive constructs was used to probe the viscoelastic properties of PEG:dextran-tissue interactions and allow development of a standard linear solid (SLS) model relating adhesive mechanics to material chemistry. Additional mechanical testing

and SLS modeling of traditional fibrin and octyl-cyanoacrylate sealants promoted general relation of viscoelastic adhesive mechanics to *ex vivo* performance metrics. Correlative analyses revealed that adhesive bond density is a primary determinant of sealant functionality, and further suggested that overall performance is enhanced through operational stress relaxation mechanisms following PEG:dextran adhesion to soft tissue.

3.2.3 Materials and Methods

Synthesis and network formation of PEG:dextran

The synthesis of star PEG amine and dextran aldehyde as well as the network formation of PEG:dextran have been previously described [45, 46]. Briefly, eight-arm, 10 kDa star PEG polymer with amine end groups was dissolved in water to form a 25 wt % aqueous solution. Linear dextran (10 kDa) was oxidized with sodium periodate to yield dextran aldehyde polymer (50 % oxidation of glucose rings, 2 aldehyde groups per oxidized glucose ring), which was also prepared as an aqueous solution (2.95 – 20.65 wt %). The two homogeneous polymer solutions were loaded into a dual-chamber syringe equipped with a 12-step mixing tip. PEG:dextran network formation occurs within seconds to minutes following the injection and controlled mixing of PEG amine and dextran aldehyde via a Schiff's base reaction between the constituent reactive groups (aldehydes and amines).

Selection and designation of PEG:dextran variants

Compositional variables of both star PEG amine and dextran aldehyde are easily manipulated in the synthesis of PEG:dextran. The solid contents, molecular weights, and reactive group content of polymer constituents are readily altered to achieve crosslinked networks with distinct material properties [45, 46]. The present study focused on examining the effects of relative aldehyde concentration on adhesive mechanics, motivating the synthesis of a series of material formulations with isolated variation in dextran aldehyde solid content. As star PEG amine compositional variables (and consequently amine group concentrations) are held constant, the formulations

under study are meaningfully differentiated by the ratio of aldehyde to amine reactive group concentrations, designated as $CHO:NH_2$ (Table 13).

Table 13 Compositional description of the examined five-material series of PEG:dextran

PEG amine				Dextran aldehyde				PEG:dextran
Arm Number	Molecular Weight	Solid Content	Amine Content	Molecular Weight	Percent Oxidation	Solid Content	Aldehyde Content	Reactive Group Ratio
(#)	(kDa)	(%)	(# per ml)	(kDa)	(%)	(%)	(# per ml)	($CHO:NH_2$)
8	10	25	1.2×10^{20}	10	50	**2.95**	$\mathbf{1.2 \times 10^{20}}$	**1**
8	10	25	1.2×10^{20}	10	50	**5.90**	$\mathbf{2.4 \times 10^{20}}$	**2**
8	10	25	1.2×10^{20}	10	50	**8.85**	$\mathbf{3.6 \times 10^{20}}$	**3**
8	10	25	1.2×10^{20}	10	50	**14.75**	$\mathbf{6.0 \times 10^{20}}$	**5**
8	10	25	1.2×10^{20}	10	50	**20.65**	$\mathbf{8.4 \times 10^{20}}$	**7**

Wounding, repair, and dynamic loading of intestinal tissue

Adult Sprague-Dawley rats (250 - 300 g, Charles River Laboratories, MA) were sacrificed via carbon dioxide asphyxiation under university IACUC protocol and federal guidelines for animal care. Following sacrifice, the duodenum was immediately excised and immersed in 10 ml Krebs-Henseleit buffer at room temperature. Longitudinal duodenal segments were cut and inserted into a mechanical testing apparatus configured for luminal perfusion (Bose® Biodynamic Test Instrument, Minnetonka, MN). A wound was introduced by full-thickness puncturing of the intestinal wall with an 18 gauge needle. Wounds were then repaired with a 200 µl application of PEG:dextran, octyl-cyanoacrylate (Dermabond, Ethicon Inc.), or fibrin sealant (Calbiochem) to the outer intestinal surface. A five minute sealant curing time was allowed, after which pulsatile loads were applied through controlled perfusion of the intestine lumen with phosphate buffered saline (PBS). All repair sites featuring PEG:dextran variants

remained intact throughout loading, substantiating clinical potential of these materials as a soft tissue sealing agent (Figure 22).

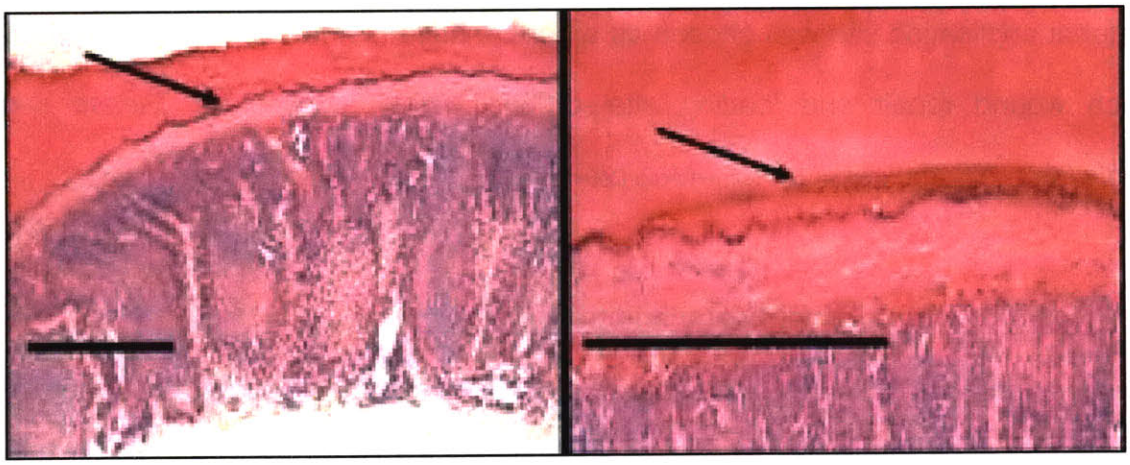

Figure 22 The tissue-material interface formed between the serosal surface of excised rat duodenum and PEG:dextran appeared continuous after histological processing (cryo-sectioning, hematoxylin and eosin stain) and microscopic analysis (left). Following sinusoidal loading (frequency =1 Hz, amplitude = 25 mmHg, cycle number = 1000) the interface remained well intact with no indication of material detachment (right). Scale bars are 1 mm and arrows indicate the location of tissue-material interface.

Measurement of burst pressure and tissue deformation

The burst pressure of repaired intestinal wounds (prepared and treated as above) was measured through gradual increase of lumen pressure. A slow development of pressure was achieved through restriction of flow distal to the sample lumen and monitored at the inlet of the intestine. The burst pressure was easily detected in this manner, as failure of the repair site resulted in an immediate loss of developed inlet pressure and visible PBS leakage. The maximum luminal pressure prior to interface failure was recorded as the wound burst pressure. *Please see appendix for additional detail* (A6 Burst Pressure Testing).

The tissue response to wound repair and loading was assessed through histological processing (hematoxylin and eosin stain) and numerical image analyses (Matlab, Mathworks Inc.) of intestinal samples. The reduction of lumen area directly adjacent to the material application site was chosen as a performance metric to indicate the extent to which wound repair and loading altered local tissue architecture. *Please see appendix for additional detail (*A7 Lumen Area Determination*).*

Stress relaxation of intestinal tissue and bulk PEG:dextran

Intestinal ring samples were prepared by transversely sectioning rat duodenum immediately after sacrifice and tissue excision. Ring samples of approximately 3 mm width were inserted into a mechanical testing apparatus configured for tensile testing (Bose® Biodynamic Test Instrument, Minnetonka, MN). Tissue samples were fixed in the mechanical tester such that the displacement axis was coincident with the ring radial direction. A programmed step displacement was used to impart a 0.2 tensile strain for six minutes, with continuous acquisition (scan rate of 50/sec) of the resultant force via the system load cell and software package (WinTest® Software, Minnetonka, MN). Mechanical data were processed to yield a tissue stress relaxation curve.

The viscoelastic response of a representative PEG:dextran material was also analyzed under constant applied displacement. Test samples were prepared by polymerization of PEG:dextran in Lexan strip molds with oversized ends, allowing secure attachment to soft-sample clamps of the mechanical testing apparatus. Following a cure time of five minutes, strip samples were moderately hydrated with a 10

ml PBS rinse over surfaces within the test region. As before, a tensile strain of 0.2 was applied for six minutes through a programmed step displacement. The resultant load data were acquired and processed to yield a bulk PEG:dextran stress relaxation curve.

Bulk PEG:dextran stiffness

Ramped uniaxial displacements (displacement rate of .05 mm/sec) were applied to bulk strip samples of PEG:dextran materials (prepared and treated as above) with a mechanical testing apparatus configured for tensile testing (Bose® Biodynamic Test Instrument, Minnetonka, MN). Resultant force and displacement data were continuously recorded (scan rate 200/sec) throughout mechanical testing by the system load cell and software package (WinTest® Software, Minnetonka, MN). Force versus displacement data were transformed into true stress versus strain for each test sample, facilitating calculation of bulk elastic moduli.

PEG:dextran gelation time

The gelation times of PEG:dextran formulations were determined through constant agitation and visual monitoring of material components undergoing network formation. Material samples were injected into glass plates through dual-chamber syringes equipped with mixing tips. A magnetic stir rod was used to agitate samples immediately following the mixed injection. The gelation time of each material sample was designated as the elapsed time after injection at which the stir rod rotation was hindered due to the progression of PEG:dextran network formation.

Stress relaxation of adhesive test elements

The small intestines of adult Sprague-Dawley rats were excised and immersed in buffer as above. Approximately two cm-long segments were cut from the duodenum and bisected along the mesenteric line, creating intestinal sheets. Surface samples were constructed by securing an intestinal sheet over a tubular fitting, consistently providing a flat and stable presentation of the outer serosal surface. Samples were inserted into the upper and lower arms of a mechanical testing apparatus configured for tensile testing (Bose® Biodynamic Test Instrument, Minnetonka, MN). A 50 µl volume of test sealant was then applied directly to the lower intestinal surface. The upper and lower intestinal surfaces were immediately brought into contact, and the adhesive material allowed to cure between the tissues for five minutes under a 0.3 N setting force. The tissues and adhesive were subsequently rinsed with two ml PBS, with particular focus on the interfacial region. The described tissue-material configuration provided convenient adhesive test elements for analysis under constant tensile displacement. *Please see appendix for additional detail (*A8 Adhesion Strength Testing II*)*

Stress relaxation of adhesive test elements featuring PEG:dextran, octyl-cyanoacrylate, or fibrin sealant was measured following application of a 0.2 mm step displacement for a five minute period. Load data were converted to engineering stress and plotted as a function of time, providing a measure of the test element viscoelasticity following tissue-material interaction.

3.2.4 Results

Burst pressure and tissue response following dynamic loading

Excised intestinal tissues were puncture wounded and repaired with PEG:dextran, octyl-cyanoacrylate (CA), or fibrin sealant (FG). Following repair, pulsatile loads were applied to tissue samples through programmed luminal perfusion with PBS. No leakages were detected and all tissue-material interfaces consistently appeared intact and continuous throughout loading. Adhesive failure resistance was quantified through gradual pressurization of sample lumens and reported as the burst pressure of the tissue-material interface. PEG:dextran application burst pressure ranged from 62.2 ± 4.8 to 112.0 ± 9.5 mmHg and rose nonlinearly with $CHO:NH_2$ (Figure 23). The CA-tissue interface had a comparatively higher burst pressure of 132.5 ± 5.8 mmHg, while the FG-tissue interface burst at a lower pressure of 52.0 ± 6.1 mmHg.

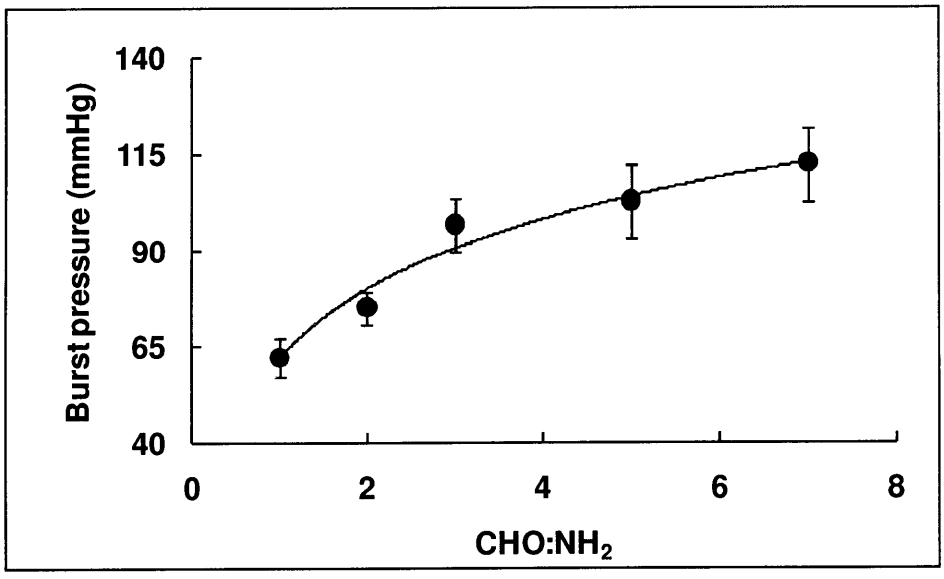

Figure 23 Burst pressure of wounded intestinal tissue (length = 4 cm) repaired with PEG:dextran nonlinearly rose with $CHO:NH_2$ across the examined range. Data points represent averages ± SEM (n = 4 – 5).

Wound repair and cyclical loading consistently induced compressive tissue deformation local to sealant applications. Specifically, the retained intestinal lumen area after PEG:dextran treatment ranged from 57.5 ± 5.74 to 74.2 ± 9.4 % of native dimensions, with increased CHO:NH_2 initially causing more compression but reaching a threshold value (Figure 24). CA and FG elicited comparatively more or less deformation, with retained lumen area of 24.2 ± 0.9 % and 84.8 ± 8.7 %, respectively.

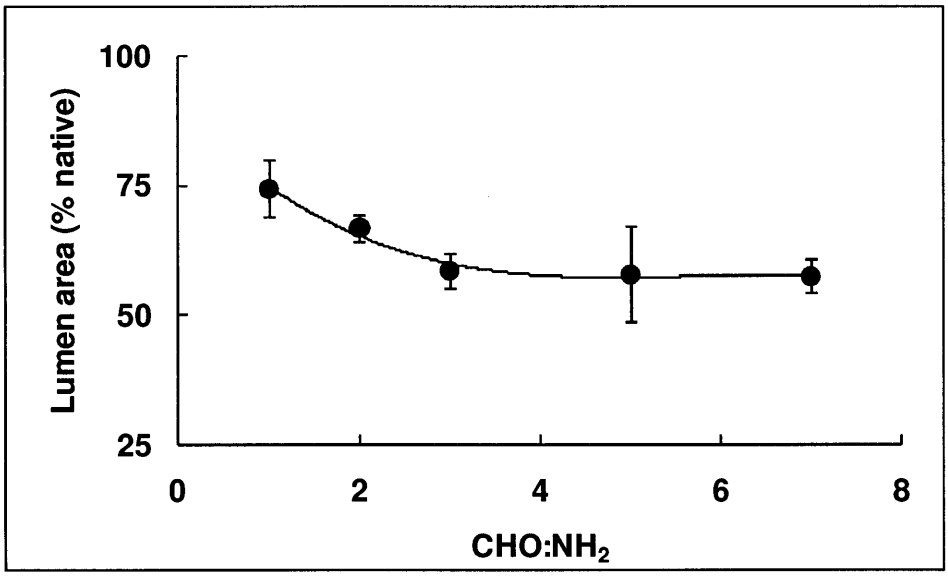

Figure 24 The percent retention of native lumen area following PEG:dextran wound repair and cyclical loading initially decreased with CHO:NH_2 but approached a threshold value. Data points represent averages ± SEM (n = 4 – 5)

Properties of interfacial components in isolation

PEG:dextran materials were studied in isolation to elucidate the dependence of network formation on constituent reactive chemistry. CHO:NH_2 variation imparted order of magnitude ranges of bulk elastic moduli (16.1 ± 0.8 to 161.0 ± 10.8 kPa) and gelation times (6.7 ± 2.5 to 69.2 ± 7.5 sec), demonstrating a significant network response to

aldehyde density (Figure 25 and Figure 26). Trends in elastic moduli and gelation time illustrate that CHO:NH_2 increase yields stiffer networks which form in less time. However, both bulk properties have a reduced sensitivity to CHO:NH_2 at higher aldehyde content (CHO:NH_2 > 3), suggesting that the extent and kinetics of network formation approach saturation at critical concentrations of constituent dextran aldehyde.

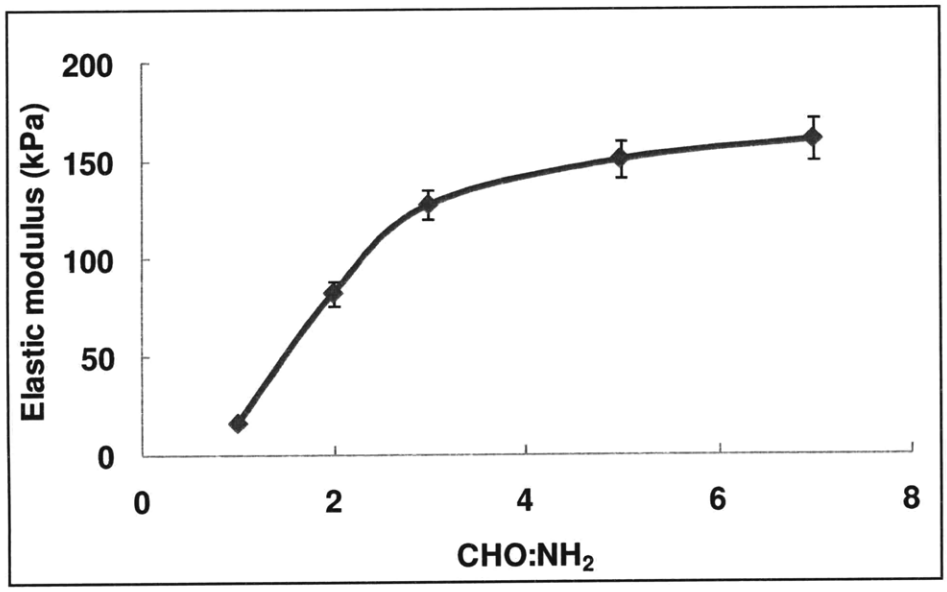

Figure 25 The elastic moduli (uniaxial tensile test parameters of strain rate = 0.005/sec, final strain = 0.1) of PEG:dextran are highly responsive to CHO:NH_2, with order of magnitude variances across material formulations. Data points represent averages ± SEM (n = 4 – 5)

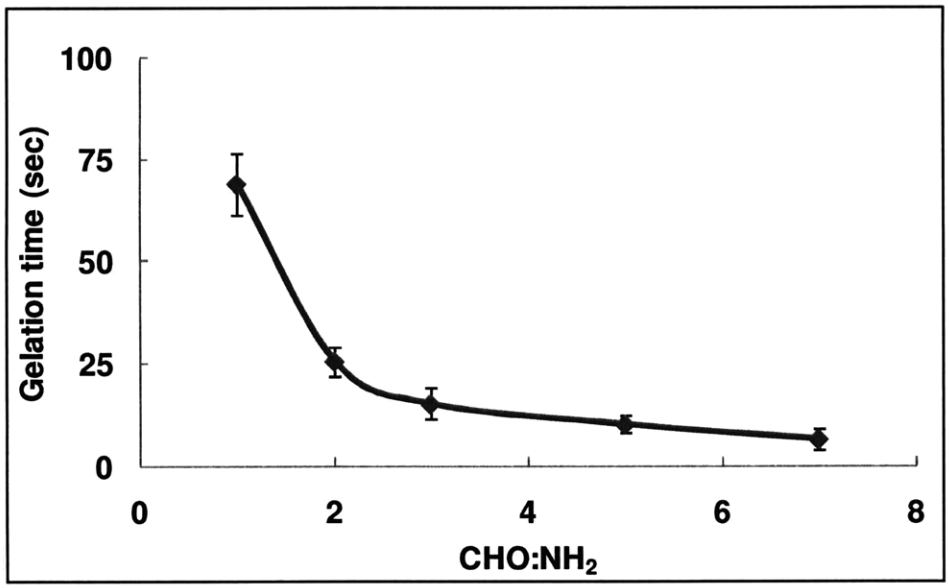

Figure 26 The gelation times (1 ml total material volume) of PEG:dextran are highly responsive to CHO:NH_2, with order of magnitude variances across material formulations. Material properties have reduced sensitivity to aldehyde content when CHO:NH_2 > 3, indicating approach to a threshold value. Data points represent averages ± SEM (n = 4 – 5)

An intermediate PEG:dextran formulation (CHO:NH_2 of 3) and excised intestinal tissue were individually examined under constant strain (Figure 27). PEG:dextran exhibited notable viscoelasticity, as the instantaneous stress of 28.0 ± 4.3 kPa relaxed to 19.6 ± 2.9 kPa throughout the observation time, while intestinal tissue relaxed more extensively from an instantaneous stress of 20.1 ± 1.3 kPa to 4.9 ± 0.3 kPa. Viscoelastic relaxation mechanisms have presumably evolved in many soft tissues to passively dissipate wall stress under low frequency loading, as particularly characteristic of the digestive process. Both bulk PEG:dextran and tissue relax stress, suggesting that tissue-material adhesive constructs composed of the two may also behave as viscoelastic solids.

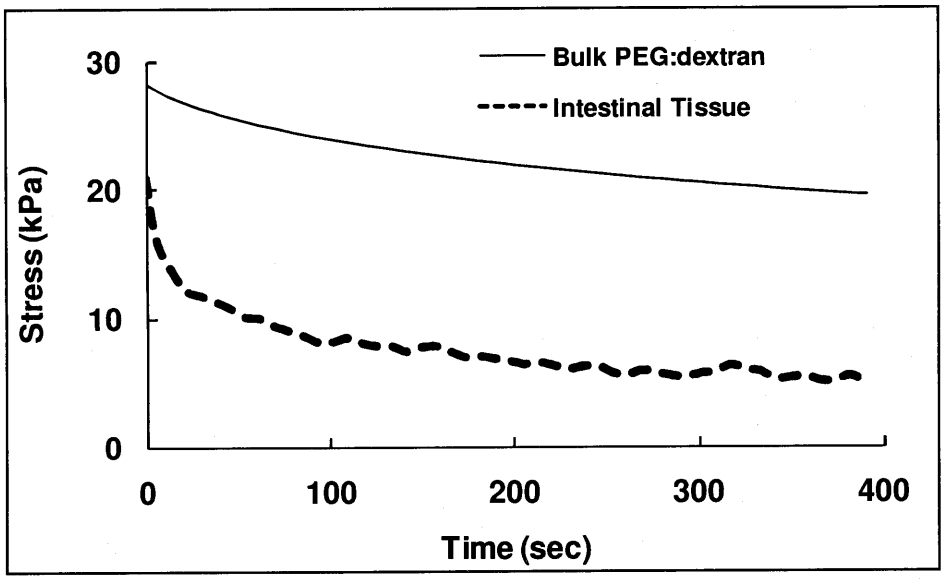

Figure 27 Bulk PEG:dextran (CHO:NH2 = 3, sample dimensions of length = 10 mm, width = 8 mm, thickness = 4 mm, n = 3) and rat intestine ring samples (ring width = 3 mm, n = 3) exhibited stress relaxation in response to a maintained 0.2 strain. The instantaneous tissue stress was approximately 20 kPa, and relaxed to an equilibrium value of 5 kPa over the 400 sec observation time. The bulk PEG:dextran was notably stiffer, with an instantaneous stress of approximately 33 kPa partially relaxing to 22 kPa over the same time period.

Stress relaxation of adhesive test elements

The viscoelastic behavior of soft tissue adhesion was assessed through the stress relaxation exhibited by tissue-material constructs. Adhesive test elements comprising sealants and intestinal tissue were held at a 0.2 strain, with constant monitoring of resultant loads. All PEG:dextran test elements instantaneously experience a maximal adhesive stress followed by relaxation to an equilibrium value within 300 seconds (Figure 28). PEG:dextran adhesive mechanics were responsive to CHO:NH_2 variation, with instantaneous and equilibrium stress ranges of 2.0 ± 0.2 to 7.1 ± 0.5 kPa and 1.4 ± 0.1 to 3.2 ± 0.5 kPa, respectively. The vertical shift of relaxation curves with increasing CHO:NH_2 parenthetically supports the notion of aldehyde-mediated reactivity with soft tissue. The viscoelastic adhesive mechanics of tissue-material test elements comprising

CA and FG bracketed those of PEG:dextran variants, as the former displayed elevated and the latter reduced stresses.

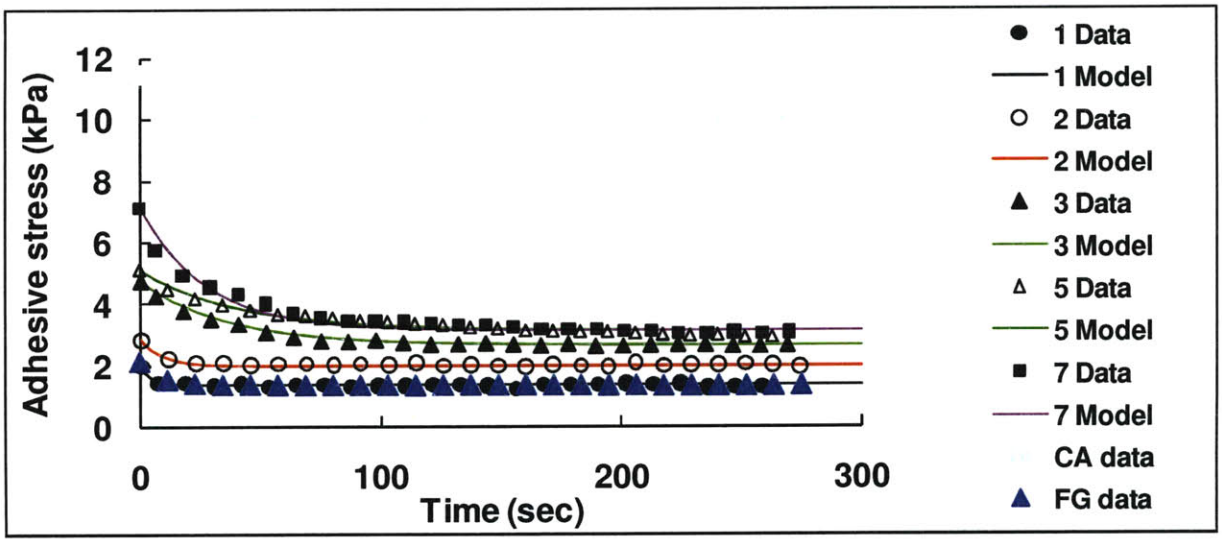

Figure 28 Adhesive test element composed of traditional (CA=cyanoacrylate, FG=Fibrin glue) and PEG:dextran (number denotes formulation CHO:NH_2) exhibited substantial stress relaxation over five minutes of maintained displacement. PEG:dextran stress relaxation closely follows curves (colored lines) generated with mechanical modeling.

Stress relaxation is derived from the capacity of materials or composite structures to reduce conformational entropy through stress-oriented molecular extensions [69]. Comparison of the instantaneous, equilibrium, and relaxed stress demonstrated that PEG:dextran adhesive constructs relaxed significant fractions of instantaneous stress, with the total amount of relaxed stress generally rising with CHO:NH_2. CA-tissue adhesion achieved high instantaneous stress but underwent minor relative relaxation to reach the equilibrium state, while FG-tissue constructs underwent a substantial relative relaxation but dissipated little overall stress due to a diminished instantaneous response (Table 14).

Table 14 Comparison between the instantaneous, equilibrium, and relaxed stress exhibit by adhesive test elements featuring PEG:dextran, octyl-cyanoacrylate (CA), and fibrin (FG) sealants. Table entries represents average ± SEM (n =3-5).

	PEG:dextran Variants ($CHO:NH_2$)					Traditional Sealants	
	1	2	3	5	7	FG	OC
Instantaneous Stress (kPa)	2.0 ± 0.2	2.9 ± 0.1	4.7± 0.3	5.1± 0.4	7.1 ± 0.5	2.2 ± 0.2	11.4 ± 0.6
Equilibrium Stress (kPa)	1.4 ± 0.1	2.0 ± 0.1	2.7 ± 0.3	3.2 ± 0.2	3.2 ± 0.5	1.4 ± 0.3	10.3 ± 0.2
Relaxed Stress (kPa)	0.6 ± 0.2	0.9 ± 0.1	2.0 ± 0.4	1.9 ± 0.4	3.9 ± 0.7	0.8 ± 0.3	1.1 ± 0.5
Relative Relaxation (%)	30 ± 10	31 ± 3.6	43 ± 8.9	37 ± 8.4	55 ± 10	36 ± 14	10 ± 4.3

The stress relaxations of adhesive test elements mimic the response of viscoelastic solids, motivating the use of a standard linear solid (SLS) model to describe adhesive mechanics (Figure 29). Model elements consist of a spring (equilibrium arm) arranged in parallel with a series spring and dashpot (Maxwell arm). Although this SLS modeling approach does not inform on the mechanics of individual interfacial components (two tissue layers, two tissue-material interfaces, and the material layer), it instead lumps together elemental contributions and represents the cumulative mechanical environment following tissue-material interaction. In the following section, stress relaxation data are used to develop, functionalize, and verify a SLS model of PEG:dextran adhesive mechanics.

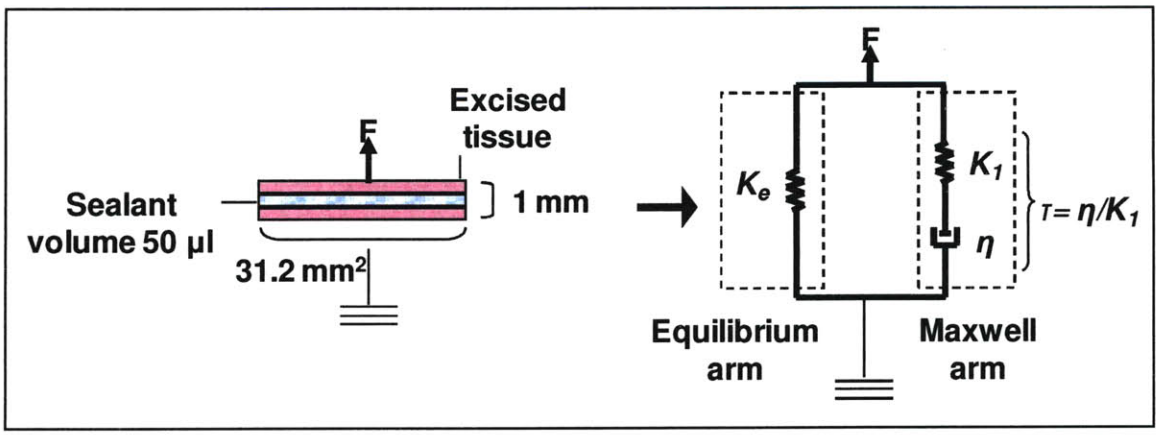

Figure 29 The viscoelasticity of adhesive test elements (left) was modeled with a standard linear solid (right). The equilibrium arm features a single spring of stiffness Ke and models time-invariant adhesive mechanics. The Maxwell arm is composed of a spring of stiffness K1 in series with a dashpot of viscosity η and models dynamic adhesive mechanics.

Application of the standard linear solid model to adhesive mechanics

SLS model development

The governing SLS differential equation is displayed in Eq. 1, where σ is the adhesive stress and ε is the tensile strain. The model elements and descriptors of SLS mechanics are the equilibrium spring with stiffness K_e [kPa], Maxwell spring with stiffness K_1 [kPa], and Maxwell dashpot with viscosity η [kPa-sec]. The relaxation time constant τ [sec] characterizes the kinetics of viscoelastic adhesive mechanics and is calculated from Maxwell arm components as $\tau = \eta / K_1$. In the following treatment, SLS element descriptors are represented as functions of $CHO:NH_2$, providing a means of incorporating PEG:dextran compositional information into an adhesive mechanical model.

The constitutive equation is readily solved for the case of a constant strain ε_0, yielding a mathematical description of adhesive stress relaxation (Eq. 2). Model

descriptors are adjusted to fit the experimental data and complete generation of the viscoelastic constitutive equations. The modeled response for each PEG:dextran formulation is plotted along with experimental data as a solid colored line (Figure 28). High Pearson's correlation (R > 0.98 in all cases) between the modeled responses and experimental data support the choice of viscoelastic theory and particularly the SLS to describe adhesive mechanics.

$$\frac{d\sigma}{dt}+\frac{1}{\tau}\sigma=[K_e+K_1]\frac{d\varepsilon}{dt}+\frac{K_e}{\tau}\varepsilon \quad \textbf{(1)}$$

$$\frac{\sigma(t)}{\varepsilon_0}=K_e+K_1e^{\frac{-t}{\tau}} \quad \textbf{(2)}$$

Equilibrium and Maxwell arm descriptors are plotted are analyzed functions of CHO:NH_2 to delineate the dependencies of steady state and dynamic adhesive mechanics on PEG:dextran composition. The SLS equilibrium stiffness is interpreted as an indicator of tissue-material reactivity and resultant adhesive bond density, while Maxwell variables reflect the available molecular mobility and stress relaxation following adhesive interaction. The rise of K_e with CHO:NH_2 implies aldehyde-mediated reactivity with tissue, although the nearly identical values of the 5 and 7 formulations (15.8 and 15.9 kPa, respectively) suggest a threshold to the adhesive bond density achievable through isolated variations of dextran aldehyde solid content (Figure 30).

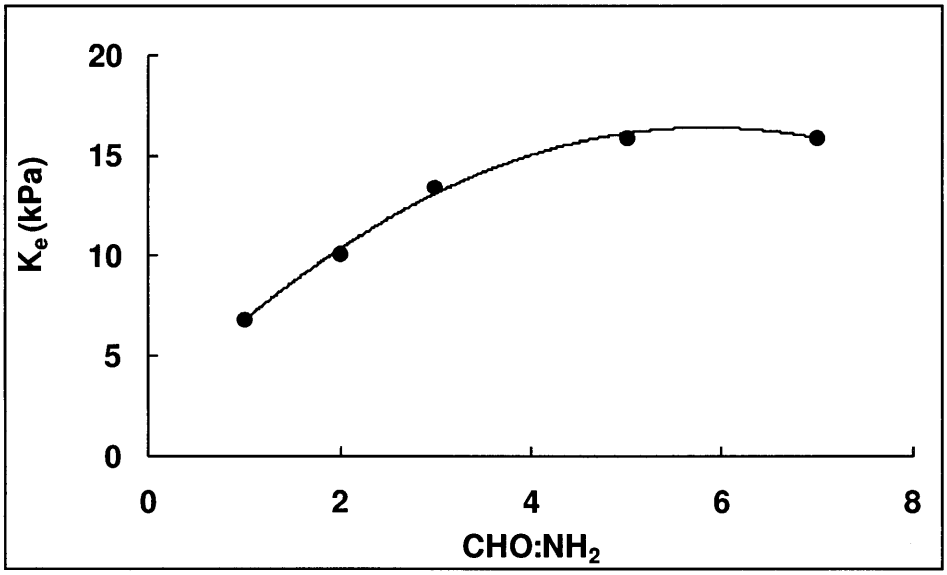

Figure 30 SLS equilibrium arm stiffness Ke quadratically varied with CHO:NH_2 across PEG:dextran variants (R = 0.99), indicating an initial increase and eventual saturation of aldehyde-mediated adhesive bond formation.

Because aldehyde variation was achieved through increase in material solid content, the rise of K_1 with CHO:NH_2 is attributed to the increased number of dextran chains undergoing relaxation both within the PEG:dextran bulk and at the tissue-material interface (Figure 31). The inflection of the quadratic τ curve within the examined CHO:NH_2 range demonstrates that adhesive relaxation mechanisms have maximally protracted kinetics at intermediate aldehyde content (Figure 32). As τ depends on η and K_1, reduced value at low CHO:NH_2 likely reflects high interfacial and network flow (low η) due to relatively sparse aldehyde bonding with tissue and within the bulk, while low τ at high CHO:NH_2 likely stems from a high aldehyde bond density and extensive molecular relaxation (elevated K_1). Theoretical reasons for these relationships are extended below, along with associated implications for and correlations to sealant efficacy.

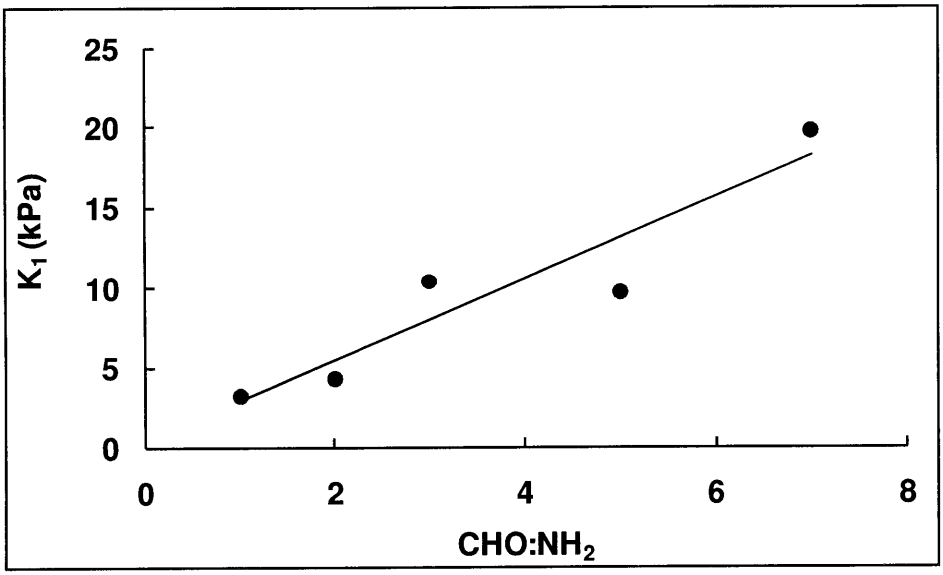

Figure 31 Maxwell arm stiffness K_1 linearly varied with CHO:NH_2 (R = 0.94), suggesting increased aldehyde content enhances the stress relaxation capacity of PEG:dextran adhesive constructs throughout the examined compositional range.

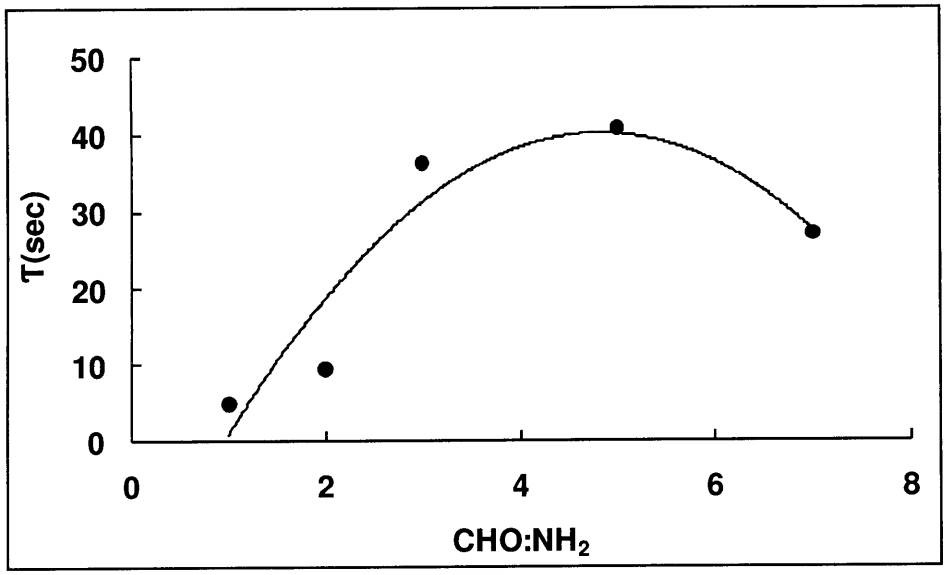

Figure 32 Maxwell arm time constant τ quadratically varied with CHO:NH_2, (R = 0.94), with a clear inflection representing at kinetic maximum within the material design space

SLS model validation

The functional SLS model is validated through correlation analyses of predicted and measured adhesive mechanics featuring PEG:dextran formulations within the examined compositional range ($CHO:NH_2$ of 1.5, 2.5, and 6). These materials are synthesized with the same polymer constituents described in Table 1, again varying only in solid content of the dextran aldehyde component. PEG:dextran formulations with $CHO:NH_2$ of 1.5, 2.5, and 6 are synthesized with 4.4, 7.4, and 17.7 percent solid content of dextran aldehyde, respectively.

Predicted adhesive stress relaxation curves for PEG:dextran variants were generated with Eq. 2 and interpolation of model element values. Modeled stress relaxations generated with these methods correlate well to experimental data (Figure 33), with a high Pearson's coefficients in all cases ($R_{1.5}$ = 0.98, $R_{2.5}$ = 0.96, R_6 = 0.98). Successful prediction of adhesive mechanics demonstrates SLS parameter continuity within the design space and the potential for strategic adjustment of PEG:dextran composition to meet various application requirements.

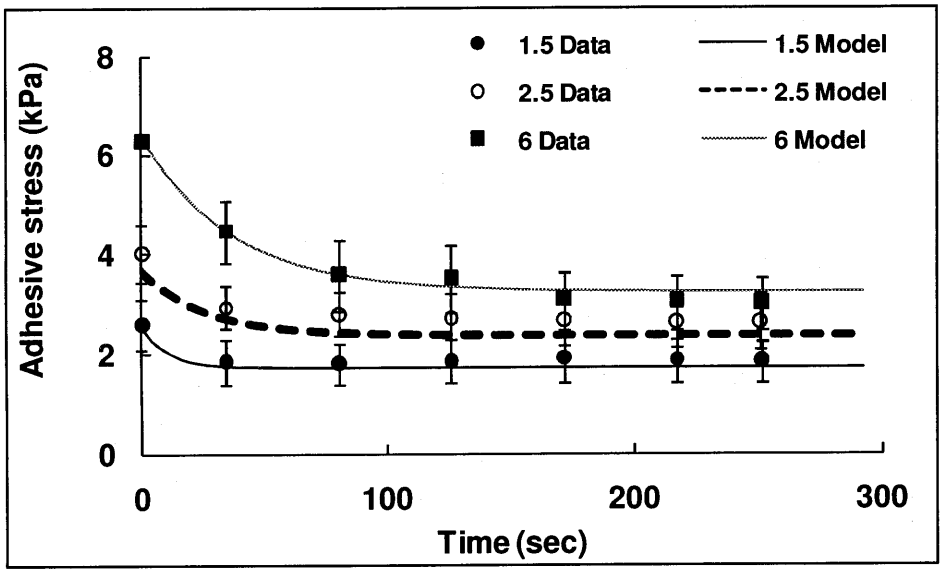

Figure 33 The viscoelastic responses of PEG:dextran adhesive test elements formed with in-range formulations ($CHO:NH_2$ = 1.5 , 2.5, and 6) were predicted based on above regressions and governing constitutive equations. The modeled responses (lines) correlated well with experimental stress relaxation data (data points) for both PEG:dextran formulations ($R_{1.5}$ = 0.98, $R_{2.5}$ = 0.96, R_6 = 0.98). Data points represent averages ± SEM (n = 4 – 5)

Correlation analyses

Correlations between PEG:dextran material properties and sealant performance metrics suggest a proportional positive influence of increased aldehyde content on both network formation and tissue-material interaction. Specifically, PEG:dextran elastic modulus and gelation time strongly correlated to both wound burst pressure and retained lumen area across the examined range of $CHO:NH_2$ ($|R| > 0.98$ in all Pearson's correlation two-way analyses). It is important to note that linear correlations generally do not persist if PEG:dextran composition is systematically altered in a fashion other than via aldehyde content. For example, increasing the solid content of constituent PEG amine will dramatically increase the elastic modulus of PEG:dextran without any significant change to adhesive performance (data not shown).

SLS variable descriptor K_e inversely correlated (R = -0.95) to the percent retention of lumen area over all PEG:dextran, FG, and CA sealants (Figure 34). K_e reflects the equilibrium mechanical state exhibited by a fully relaxed interface and is presumed proportional to the tissue-material adhesive bond density. Inverse correlation to K_e indicates that disturbance of tissue structure is more severe with increased adhesive bonding. Wound burst pressure strongly correlated to K_e with the exception of the CA samples, both reinforcing the import of adhesive bond density and suggesting a role for auxiliary factors (Figure 35). SLS modeling facilitated examination of potential secondary mechanical factors, particularly the extent (via K_1) and kinetics (via τ) of available stress relaxation. Linear correlation of burst pressure across all materials is moderately attained (R = 0.94) when analyzed against the instantaneous SLS stiffness ($K_e + K_1$) (Figure 36). Burst pressure correlation to instantaneous stiffness implicates available adhesive relaxation as an influential factor determining performance, with the capability to entropically dissipate stress improving sealant function. Performance metric correlations to SLS variables suggest that both adhesive bond density and available stress relaxation will together determine overall sealant efficacy.

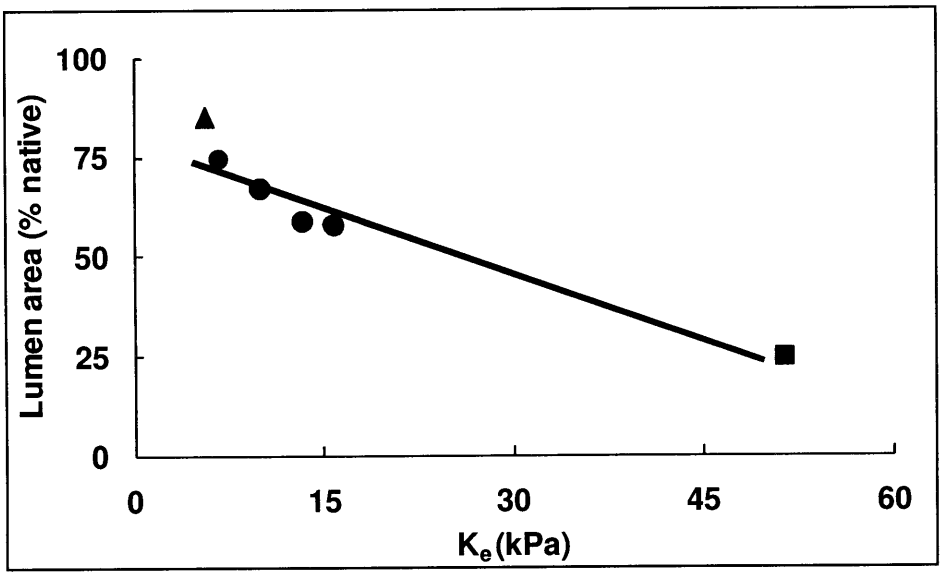

Figure 34 Performance metric correlations to SLS model descriptors revealed the influence of separable aspects of viscoelastic adhesive mechanics on burst pressure and local tissue response. Equilibrium stiffness K_e inversely correlated (R = -0.95) to retained lumen area across PEG:dextran (•), fibrin (FG, ▲), and octyl-cyanoacrylate (OC, ■) samples, indicating higher adhesive bond density compromised local tissue structure

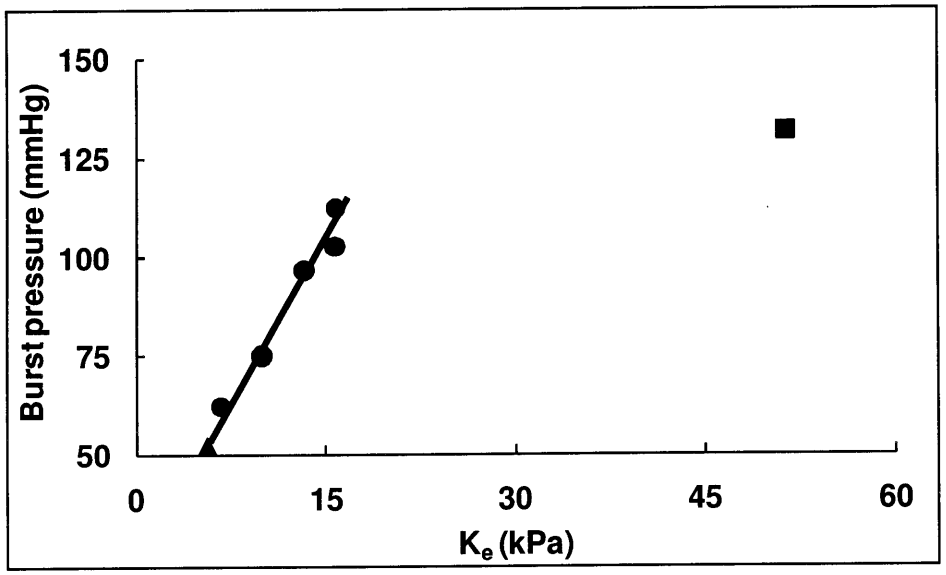

Figure 35 The burst pressure of PEG:dextran and FG repaired wounds had strong linear correlation to K_e, while the CA samples dramatically diverged from this trend.

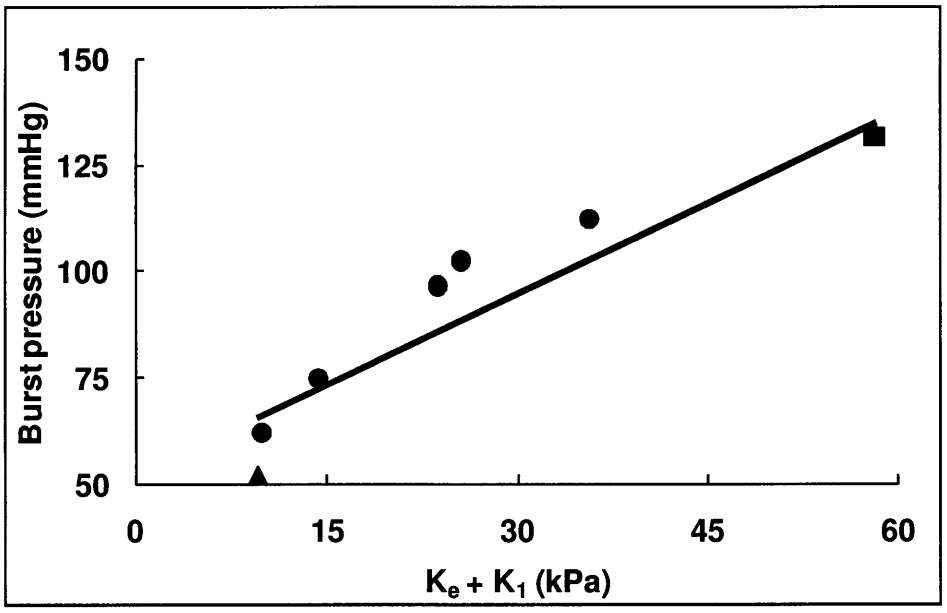

Figure 36 Burst pressure across all sealant types showed significant linear correlation (R = 0.94) to the instantaneous interfacial stiffness ($K_e + K_1$), implicating the ability to relax stress as an additional factor governing failure resistance following material application and cyclical loading.

3.2.5 Discussion

Ex vivo metrics of PEG:dextran sealant performance varied with the constituent aldehyde content and were within the range of clinically available fibrin (FG) and octyl-cyanoacrylate (CA) sealants. Solid modeling of tissue-material test element mechanics effectively described adhesive stress relaxation and distinguished viscous and elastic characteristics governing sealant performance. Correlation analyses of model variable descriptors to performance metrics of PEG:dextran, CA, and FG supported the expected influence of tissue-material reactivity on sealant functionality and tissue response, and also brought forth the benefit of maintaining a stress relaxation capacity after adhesion. PEG:dextran sealants clearly demonstrated aldehyde-mediated adhesion and a substantial capacity to relax adhesive stress in a test element configuration.

Viscoelastic adhesive mechanics imply macromolecular mobility within the tissue, material, and/or interface, and provide a mechanism for entropic dissipation of mechanical work imparted to the application site. If macromolecular mobility is limited by tissue-material crosslinking, adhesive stress will result in an increase of internal bond energies in lieu of an entropic mechanical response. The microscopic breaking of adhesive bonds will occur at a critical bond energy and macroscopically manifest as adhesive failure. Thus, given two equally crosslinked tissue-material interfaces under identical loading conditions, the more viscoelastic interface should have a greater failure resistance by virtue of bond energy minimization. The developed SLS modeling scheme

of PEG:dextran adhesion provides a computational tool for predicting viscoelastic mechanics and can facilitate the design of failure-resistant material formulations.

Saturation and eventual loss of all solid-like properties with increasing aldehyde content is expected in the PEG:dextran system. In the limit where $CHO:NH_2$ approaches infinity, the dextran aldehyde component will remain soluble and formation of a crosslinked gel is lost. Prior to the anticipated compositional threshold, aldehyde-mediated chemistry should play a key role in both PEG:dextran network formation and reaction with tissue and insomuch provide an efficient vehicle for control of bulk and adhesive properties. Strong dependencies of pertinent PEG:dextran properties on aldehyde content clearly emerged throughout this study. Furthermore, property trends indicate that the influences of aldehyde content on the kinetics and end-state of PEG:dextran network formation (indicated via gelation time and bulk stiffness) and adhesive reactivity with tissue (indicated via burst pressure, retained lumen area and SLS equilibrium arm stiffness K_e) are indeed limited and roughly characterized by a sensitivity threshold as $CHO:NH_2$ exceeds 3.

The plateaus of equilibrium arm stiffness K_e and sealant performance metrics (burst pressure, lumen deformation) with increasing $CHO:NH_2$ suggests that dextran aldehyde molecules enable gel integrity and tissue seal and are the limiting element in tissue-material interaction. Sealant apposition to tissue can only occur if the aldehyde groups react with both PEG nodes within the gel and tissue sites outside of the gel. The concentration of aldehydes therefore determines the extent of internal gel cohesion and external adhesion to tissue. At a critical $CHO:NH_2$, increasing dextran aldehyde

molecules no longer promotes additional adhesive interactions, possibly owing to steric hindrance of adhesive bond formation. If a clinical application requires more extensive modulation of the above properties, concurrent adjustments of other compositional variables within the PEG:dextran system (for example PEG solid content) will likely be required to compensate for steric effects.

Molecular engineering of PEG:dextran stress relaxation mechanisms could augment aldehyde-mediated adhesion to tissue and improve failure resistance of tissue-material interfaces. Polymer chain mobility and hence stress relaxation could be manipulated through the molecular length of constituent dextran and the grouping of aldehydes along a dextran chain. Longer chains with more distant reactive sites should possess greater molecular mobility and thus entropically dissipate greater amounts of strain energy. Such a material design strategy is distinctly different from simply increasing aldehyde content to improve adhesive strength at the expense of an unfavorable tissue response, an approach which would essentially conform to the established limitations of sealant technologies.

Traditional tissue adhesives and their associated limitations have raised the need for an alternative adhesive system with tunable bioreactivity. Herein we have identified PEG:dextran as a soft tissue adhesive which can be functionally modulated through the constituent aldehyde content. The adhesive mechanical model we utilized relates PEG:dextran chemistry to tissue-material interactions and overall performance. In this specific case the model suggests that viscoelastic adhesion can improve the efficacy of

these and other polymeric sealants. In general such a melding of empiric and modeling approaches may continue to aid in rational application- and tissue-specific material design.

3.2.6 Conclusion

The efficacy of soft tissue sealants is limited by sub-optimal extremes of bioreactivity and adhesion strength characteristic of available materials. PEG:dextran hydrogels viscoelastically adhere to tissue to a controllable extent and demonstrate great potential to address current clinical needs. Through systematic analyses of material formulations with graded levels of aldehyde content, we show that PEG:dextran adheres to intestinal tissue largely based on aldehyde-mediated reactivity with the capability to relax stress in the presence of sustained strain. A viscoelastic solid model of adhesive mechanics suitably represents the mechanical properties of tissue-material test elements formed with PEG:dextran and other traditional sealants. Incorporation of PEG:dextran compositional information into the model provides a design tool for strategic adjustment of material composition based on application requirements. Through correlation analyses between pertinent sealant performance metrics and viscoelastic model descriptors, the exploitation of stress relaxation emerges as a potential means of increasing interfacial failure resistance following adhesive applications to soft tissue.

3.2.7 Study Transition

Study 2 reveals the importance of maintaining native tissue viscoelasticity following adhesive interactions and insomuch suggests a material design principle applicable to all implants which intimately interact with soft tissue. However, aldehyde-mediated adhesion and tissue response was assessed with a single tissue type (duodenal) which represents only one of the possible target anastomotic sites for clinical sealant applications. We foresee natural soft tissue variability (biochemical, mechanical, etc.) among potential sealant targets as a complication in generalizing the proposed design strategy to other targeted tissue beds or new biomaterial systems. Target tissue mechanics will define the desired native viscoelasticity while local biochemistry may modulate susceptibility to aldehyde-mediated adhesion. To substantiate the notion of tissue-specific effects, we next analyze adhesion between PEG:dextran and a range of soft tissues (duodenal, heart, lung, liver) and seek a mechanistic basis for emergent differences.

3.3 STUDY 3 TISSUE-SPECIFIC ADHESION

Publication disclosure
The following presentation of Study 3 is based on:
Aldehyde-amine chemistry enables modulated biosealants with tissue-specific adhesion.
Artzi N, Shazly T, Baker A, Bon A, Edelman ER.
Advanced Materials 2009

3.3.1 Abstract

Bioreactive hydrogels featuring aminated star polyethylene glycol and high molecular weight dextran aldehyde polymers (PEG:dextran) possess readily tunable compositional variables that elicit control over both network formation and tissue-material interactions. Previous studies comparing PEG:dextran to traditional soft tissue sealants suggest these materials have potential to address clinical needs owing to sufficiently high adhesion strength with an acceptable tissue response. Though all candidate sealants rely on intimate tissue-material interaction for functional adhesion, target tissue properties have been largely ignored in material design. Instead, one general formulation is proposed for application to the full range of soft tissues across diverse clinical applications. Here we demonstrate that aldehyde-mediated adhesion to tissue strongly depends on target tissue type and propose a rational approach for the engineering of application-specific surgical sealants.

3.3.2 Introduction

Hydrogels consisting of aminated star polyethylene glycol and high molecular weight dextran aldehyde polymers (PEG:dextran) possess a predictable range of cohesive and adhesive properties [47, 50, 70]. The cohesive integrity of PEG:dextran is derived from imine bonds that form through a Schiff base reaction between constituent amines and aldehydes. When crosslinked on soft tissue surfaces, aldehydes not consumed in bulk network formation can participate in analogous bonds with tissue amines to attain adhesion. Aldehydes in excess of what is required for cohesion or adhesion can induce tissue toxicity. Consequently, aldehyde density is the key material design parameter for informative evaluation of both tissue-material adhesion and tissue response. Here we demonstrate that the natural variation of amine density among multiple soft tissues will have a parallel influence on tissue-material interactions and form a basis for tissue-specific material design.

We designed and evaluated a series of PEG:dextran formulations featuring low (8.8%, L-PD), medium (14.0%, M-PD), and high (20.0%, H-PD) levels of dextran aldehyde solid content. Additional design parameters, including dextran molecular weight (10 kDa), dextran oxidation state (50%), and PEG amine solid content (25%), were identical among formulations and selected to provide stable and bioreactive networks for evaluation of adhesive interactions. We demonstrate that physical and mechanical aspects of PEG:dextran adhesion are tissue-specific and can be readily adjusted through manipulation of material aldehyde content. Because adhesion is mediated through material crosslinking to local tissue amines, judicious modification of

formulation aldehyde content is a logical approach to ensure sufficient adhesion strength for a given clinical scenario.

Aldehyde-mediated adhesive design is complicated by significant biochemical variations among soft tissues. We examined the surface amine group densities in biopsy samples of rat cardiac, lung, liver, and duodenal tissue and correlated biochemistry to PEG:dextran adhesion. Mechanical and biochemical data clearly demonstrate the influence of target soft tissue type on the outcome of aldehyde-mediated interactions. The need for careful titration of material composition is reiterated by the *in vivo* tissue response to PEG:dextran, as local inflammation is also influenced by material aldehyde density. These concepts define a therapeutic window for optimal tissue-sealant interactions, bounded below by the need for adequate adhesion strength and above by the condition of biocompatibility.

3.3.3 Materials and Methods

PEG:dextran composition

The synthesis of star PEG amine and dextran aldehydes as well as PEG:dextran network formation have been previously described [14-17]. Briefly, eight-arm 10 kDa star PEG polymer with amine end groups was dissolved in water to form a 25 wt. % aqueous solution. Linear dextran (10 kDa) was oxidized with sodium periodate to yield dextran aldehyde, which was also prepared as an aqueous solution (8.8 – 20.0 wt. %). The polymeric constituents of PEG:dextran were prepared as minimally viscous aqueous solutions and consistently polymerized through injection from a dual chamber syringe equipped with a mixing tip. The present study examines the effect of aldehyde content on adhesion strength and tissue response, motivating the design and synthesis of a series of materials with isolated variation in dextran aldehyde solid content.

Subcutaneous Mouse Model

A subcutaneous implantation model of tissue response was used to evaluate material biocompatibility *in vivo*. A subcutaneous pocket was created in anesthetized C57BL/6 mice and PEG:dextran (200 µl) was injected into the pocket using a dual chamber syringe equipped with a sterile mixing tip. After 9 days, the mice were sacrificed and the skin and subcutaneous tissues were harvested. The samples were snap frozen in liquid nitrogen and stored at -80 °C until histological and zymographic analyses. All experimental protocols were approved by the MIT Animal Care and Use Committee and were in compliance with NIH guidelines for animal use. Harvested tissue was sectioned using a cryotome to create 20 µm thick sections. Hematoxylin and

eosin staining was performed using standard methods. Fibrotic response was based on morphology and measured in multiple random locations in five images from tissue samples from each mouse. Zymography was performed using quenched fluorescein-labeled gelatin and quantified using Adobe Photoshop as previously described [21].

Fluorescent PEG amine

To characterize the PEG:dextran morphology at the tissue-material interface as well as track gradual material release from the tissue surface, constituent PEG amine was labeled with fluorescein. PEG amine (2.4 g) was dissolved in 6 mL dichloromethane, followed by the addition of 0.015 g 6-(fluorescein-5-carboxyamido) hexanoic acid (Invitrogen) and 12 µL triethylamine (Sigma). The mixture was stirred at room temperature for 48 hours. The resulting solid after solvent evaporation was dissolved in 100 mL water, dialyzed and lyophilized. PEG amine solutions of 25 wt. % solid content, 0.5 % of which were fluorescently labeled, were then prepared and crosslinked with dextran aldehyde solutions in the established manner yielding fluorescent materials.

Adhesion mechanics

The adhesion mechanics following PEG:dextran application to soft tissues was measured with monotonic uniaxial tensile testing (Bose® Biodynamic Test Instrument, Minnetonka, MN). Adhesive test elements were created from a 200 µl application of PEG:dextran evenly distributed between two uniformly sized tissue biopsies (disks of 8 mm diameter, total test element thickness of 1 mm) of rat duodenum, heart, lung or liver. Tissue surfaces were gently dried prior to material application. After applying

PEG:dextran between tissue surfaces and allowing five minutes for material polymerization, adhesive test elements were displaced at a constant rate (0.05 mm/sec) and the load response was continuously recorded (200 measurements/sec). Recorded loads were normalized by test element cross-sectional area and reported as an interfacial stress response to a change in thickness.

Adhesive interface morphology

PEG:dextran morphology following adhesion to various soft tissues was assessed with quantitative microscopy. Uniform biopsies from freshly harvested rat lung, liver, heart, and duodenum provided a controlled surface area (20 mm^2) for material application. Fluorescently labeled PEG:dextran (50 µl) was applied to tissues after blot drying and allowed to fully polymerize. Tissue samples were then cryosectioned (20 µm sections) and stained with rhodamine phalloidin (Invitrogen) and DAPI (Vector Laboratories). PEG:dextran morphology at the tissue-material was quantified using image analysis techniques (Leica Microsystems, MetaMorph®) to characterize the transitory material between tissue surfaces and material bulk. *Please see appendix for additional detail (*A9 Morphological Analyses of Adhesive Interface*).*

Aldehyde affinity of soft tissue surfaces

To determine the aldehyde affinity of various soft tissues, the conjugation of aldehyde-coated fluorescent microspheres (Molecular Probes) to soft tissue surfaces was quantified. Biopsies of rat lung, liver, heart, and duodenum were prepared with equal surface area (20 mm^2) and submerged in 0.5 ml of 0.5 % f-MS solutions for 20

minutes on rocker at 37ºC. Tissue samples were thoroughly rinsed with 10 ml PBS three times. Tissue specimens were then processed and analyzed to quantify the percent surface coverage by f-MS (Leica Microsystems, MetaMorph®). *Please see appendix for additional detail (*A10 Fluorescent Microspheres*)*

Material retention

To track material loss following PEG:dextran adhesion to various soft tissues, fluorescently labeled materials were applied to lung, liver, heart and duodenum biopsies (4 mm disks). Identical volumes (200 µl) of PEG:dextran (14 % dextran aldehyde variant, L-PD) were applied to tissue surfaces and allowed to polymerize for five minutes. Samples were then submerged in PBS at 37 ºC for four hours. The fluorescent signal (485 nm excitation and 538 nm emission) accruing in the media was periodically monitored throughout the suspension period to assess the kinetics of material dissociation from the tissue.

3.3.4 Results

***In vivo* tissue response**

The *in vivo* tissue response to subcutaneous implants was used to evaluate the biocompatibility of PEG:dextran materials and particularly the influence of aldehyde content on tissue response. PEG:dextran variants (L-PD, M-PD, and H-PD) were implanted into a subcutaneous pocket in mice which were then survived for nine days. Inflammation as manifest by thicker fibrous capsule rose with aldehyde content (Figure 37). Inflammatory cell-mediated proteolysis affects wound repair as matrix metalloproteases cleave the extracellular matrix weakening the tissue and surgical anastomoses. The gelatinase activity in the tissues, measured using analytical fluorescent microscopy and *in situ* zymography, also increased with material aldehyde content (Figure 38). This trend in proteolytic activity is likely a result of the increased pro-inflammatory mediators and activation of polymorphonuclear leukocytes generated by the reactive aldehyde groups.

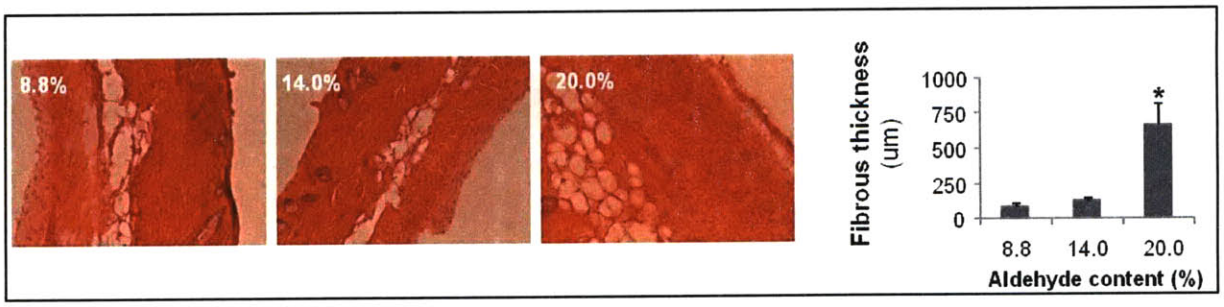

Figure 37 Tissue reactivity in-vivo was assessed for subcutaneous implants of materials having low (8.8 wt. %), medium (14.0 wt. %) or high (20.0 wt. %) dextran aldehyde solid content. Histomorphometric analysis reveals increased fibrotic capsule thickness and inflammatory cell presence in materials with high aldehyde content. (* $p < 0.05$ compared with 14.0% solid content).

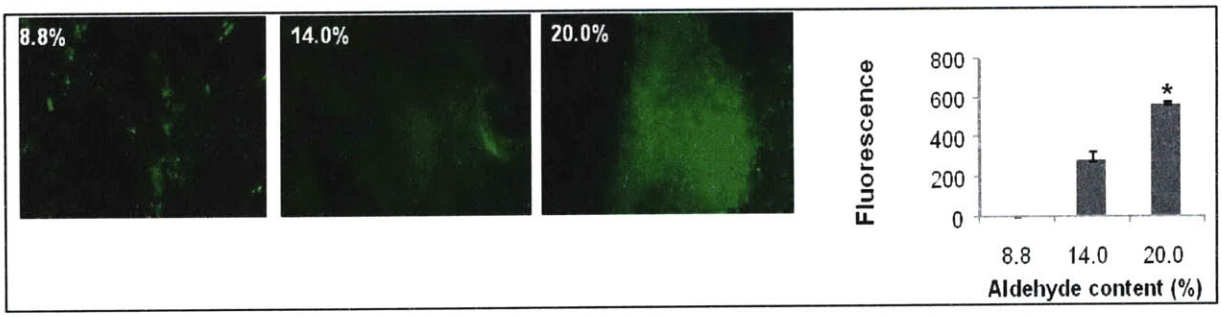

Figure 38 Tissue reactivity in-vivo was assessed for subcutaneous implants of materials having low (8.8 wt. %), medium (14.0 wt. %) or high (20.0 wt. %) dextran aldehyde solid content. Gelatinase zymographic activity was increased with material aldehyde levels. (* $p < 0.05$ compared with 14.0% solid content).

Adhesion mechanics

Adhesion mechanics were measured *ex vivo* with soft tissues harvested from rats (adult Sprague-Dawley, Charles River Laboratories, MA) immediately after animal sacrifice (under university IACUC protocol and federal guidelines for animal care). Adhesive test elements were constructed with biopsy specimens of uniform thickness (1 mm) from heart, lung, liver, and duodenal tissues to facilitate uniaxial mechanical testing of tissue-material interfaces. The stress response of adhesive test elements over a range of applied displacement varied with material aldehyde content and tissue type (Figure 39).

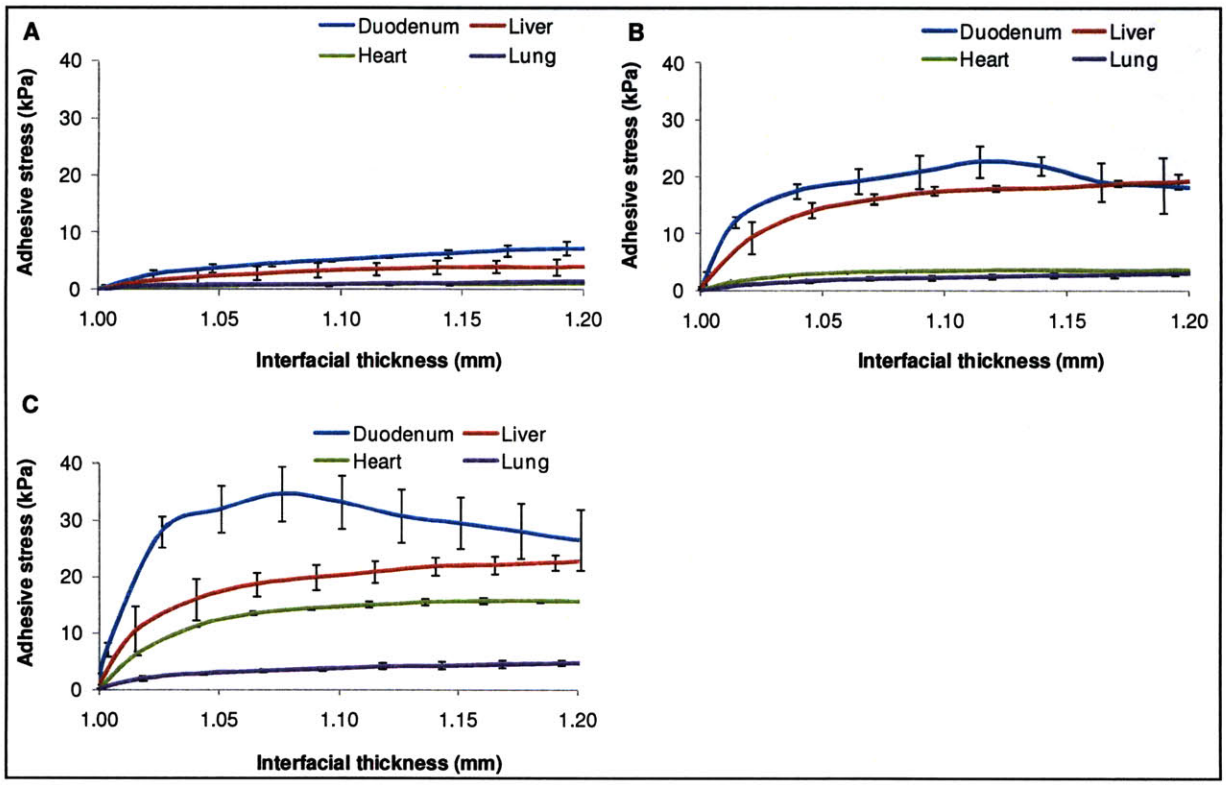

Figure 39 The adhesion of PEG:dextran-based adhesives depends on tissue type (heart, lung, liver, or duodenal rat biopsies) and constituent chemistry, evaluated at low (A, 8.8 wt. %), medium (B, 14.0 wt. %) or high (C, 20.0 wt. %) concentrations of dextran aldehyde solid content.

Interfacial moduli were calculated from the initial stress response ($1 <$ interfacial thickness < 1.05) to allow for succinct comparison of adhesive mechanics (Figure 40). The modulus of H-PD adhesion to duodenal test elements (724 ± 86 kPa) was significantly greater ($p < 0.001$) than lung (72 ± 7 kPa), while heart and liver moduli were comparatively intermediate (296 ± 60, 431 ± 15 kPa, respectively). The extent to which aldehyde content altered adhesive stiffness is markedly tissue-specific. Cardiac tissue test elements exhibited the greatest relative increase in interfacial stiffness when comparing L-PD and H-PD variants (1785 %), while lung tissue had a much weaker dependence (283 %). Overall, these data support the notion that both tissue type and

material chemistry influence aldehyde-mediated adhesive interactions, providing a functional basis for tissue-specific sealant design.

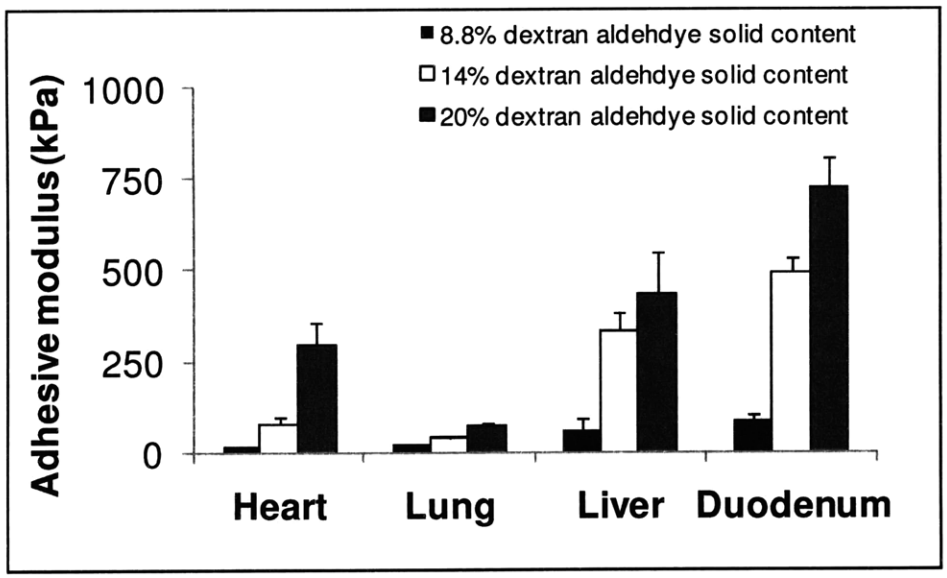

Figure 40 The moduli of the adhesive test elements increased with aldehyde content dependant on tissue type.

Adhesive interface morphology

The interfacial regions between PEG:dextran and excised rat cardiac, lung, liver and duodenal tissues were physically analyzed with fluorescent microscopy. Three distinct domains were evident upon material adherence, including the target tissue, bulk material, and an adhesive regime interposed between the two (Figure 41). The adhesive regime depicts the intermediate material structure resulting from concurrent dextran aldehyde reactivity with PEG and tissue amines. The morphology of the adhesive regime varied with tissue type, appearing fibrillar and discontinuous on cardiac and lung tissues, and more continuous and intact over liver and duodenum. Quantitative microscopic evaluation of the adhesive regimes based on fluorescent material intensity

provides normalized metrics of area per unit interfacial length (adhesive regime size) and the material concentration (adhesive regime density). Significant differences in the resultant PEG:dextran morphology were measured following tissue-material adhesion (Figure 42). While the adhesive regime above duodenal tissue was minimal in size (0.24 ± 0.11) and comparatively dense (1.27 ± 0.17), interactions with heart, lung, and liver yielded more expansive and disperse adhesive interfaces. Comparisons between adhesive morphology and mechanics confirmed common physical intuition, as both adhesive regime metrics strongly correlate to interfacial moduli ($|R| = 0.95$, $p < 0.05$, L-PD variant) across tissue types, indicating that small and dense material transitions between tissue and bulk yield stiff adhesive interactions.

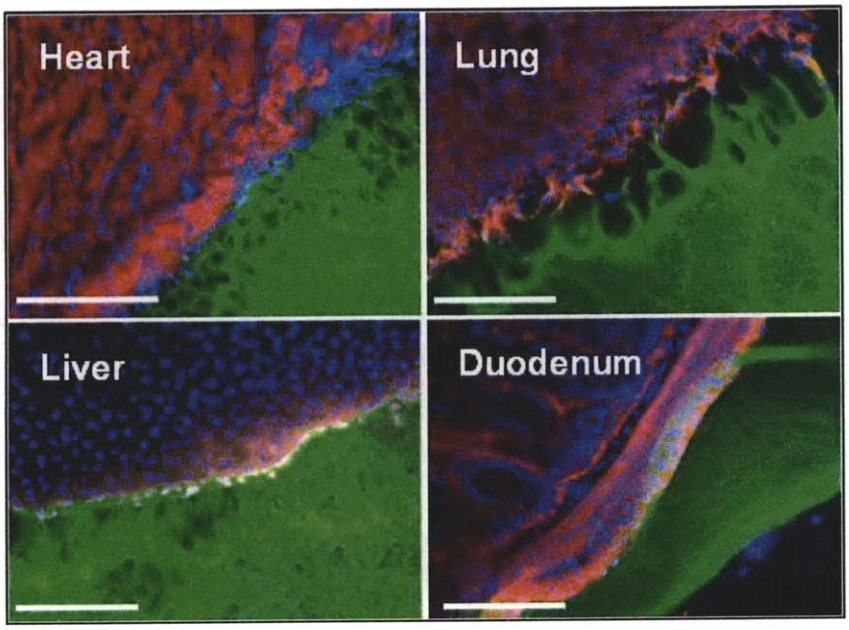

Figure 41 The interface between PEG:dextran (green) and various soft tissues, highlighted with rhodamine phalloidin (actin, red) and DAPI (cell nuclei, blue), varies with tissue.

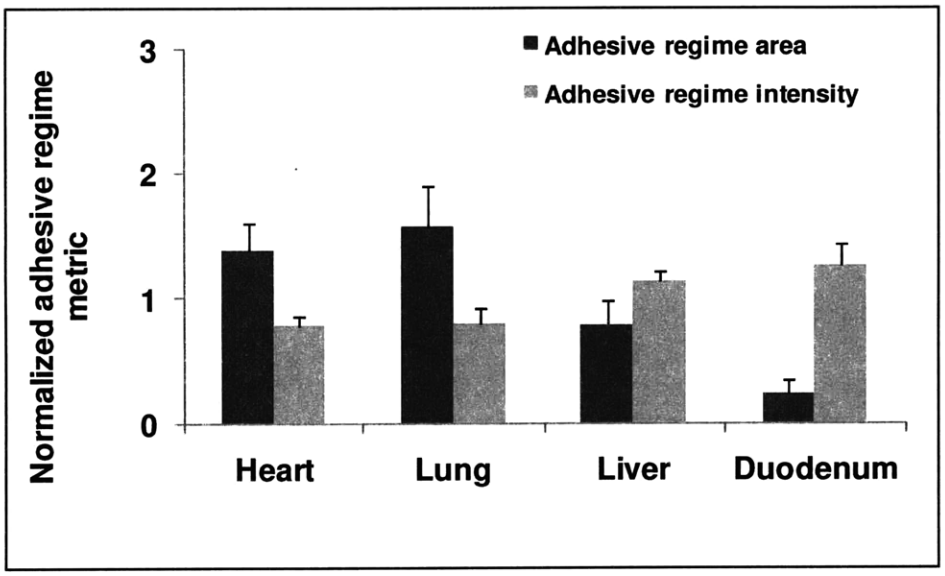

Figure 42 Interfaces with PEG:dextran with excised soft tissues exhibit a range of adhesive regime area (size normalized to interfacial length) and density (fluorescence intensity), indicating that adhesion is modulated by tissue type.

Aldehyde affinity of soft tissue surfaces

The conjugation of aldehyde-coated fluorescent microspheres (f-MS) to soft tissues was used to probe tissue surface chemistry and provide a mechanistic basis for the demonstrated variability in adhesive interactions. Tissue biopsies of controlled surface area were excised from rat heart, lung, liver and duodenum and allowed to react with f-MS through gentle mixing in an aqueous solution. Following suspension, the fluorescent intensity at the surface of the tissue samples was quantified to generate an aldehyde conjugation metric reflecting the percent of tissue surface coverage by immobilized f-MS (Figure 43). The conjugation metric is indicative of the aldehyde affinity of soft tissues and provides a fairly direct measure of the targeted biochemistry for PEG:dextran adhesion. Soft tissues display a range of f-MS conjugation metrics, with duodenal tissue possessing the greatest apparent aldehyde affinity. Comparison of tissue conjugation

metrics to adhesive mechanical data parenthetically supports aldehyde-mediated adhesion, as interfacial moduli strongly correlate ($R = 0.92$, $p < 0.05$) to aldehyde affinity across tested tissue types and material variants. The aldehyde content of materials and aldehyde affinity of tissue seemingly present a mechanism by which to design and select materials based on clinical applications. *Please see appendix for additional detail (A10 Fluorescent Microspheres).*

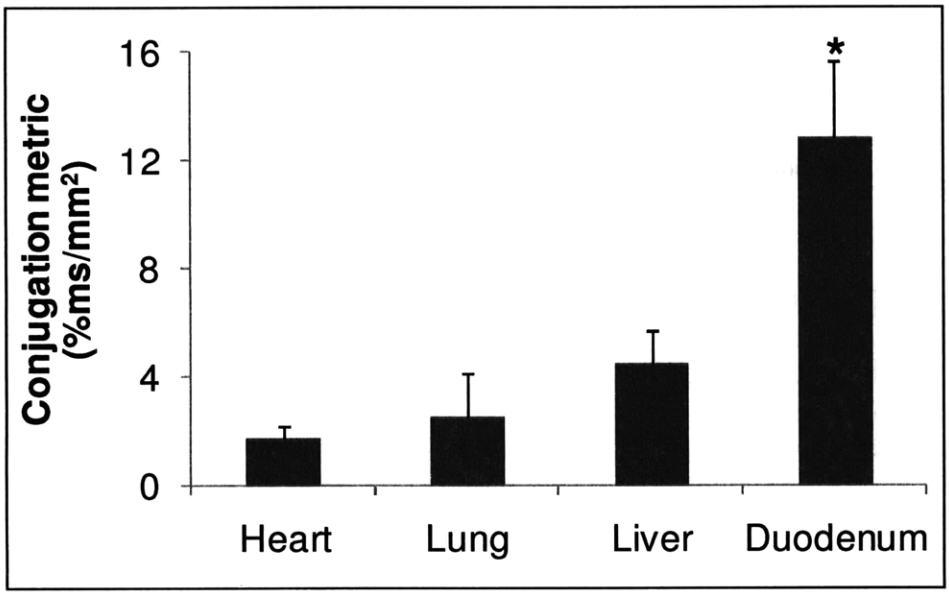

Figure 43 The relative aldehyde reactivity of heart, lung, liver and duodenal rat tissue were assessed though tissue sample conjugation of fluorescent aldehyde-coated microspheres. Aldehyde reactivity was lowest in the lung and heart, greater in the liver and highest in the duodenum (* $p < 0.05$ compared with all other tissues).

Material retention

The extent of tissue-material interaction should largely determine the tissue retention of an adhesive material. Fluorescent PEG:dextran materials were applied to tissue biopsies and submerged in media under defined conditions. The presence of released fluorescent signal was monitored as the media was periodically changed. This signal is

a surrogate for the effective material loss from a tissue surface and varied based on underlying tissue type. Relatively rapidly fluorescent accumulation occurred when PEG:dextran was applied to heart and lung tissue, while hepatic and duodenal specimens exhibited protracted release kinetics (Figure 44). PEG amine content lost to the media evidentially depends on the material continuity at the tissue surface, as significant correlations of cumulative material loss to adhesive regime size and intensity ($|R| > 0.90$, $p < 0.05$) were found across tissue types.

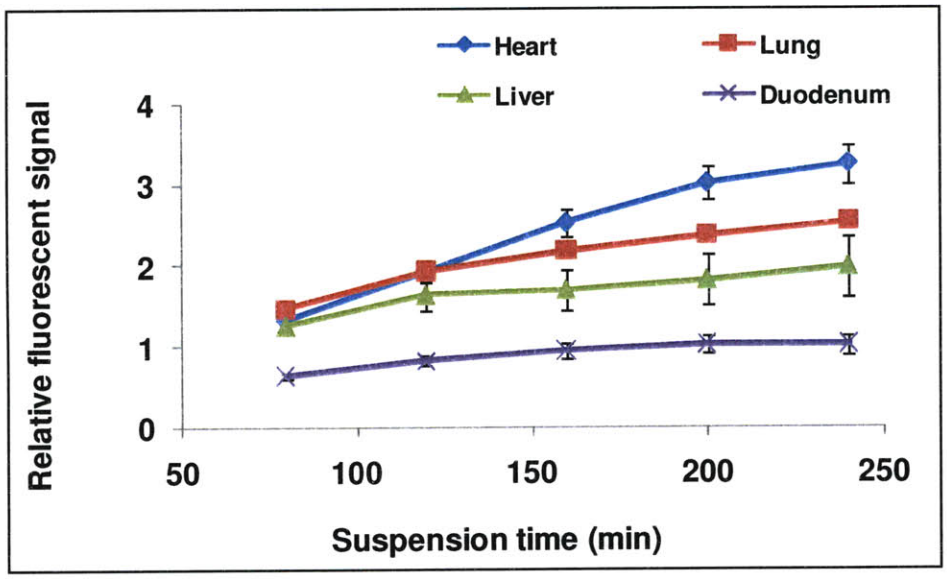

Figure 44 Differential adhesive retention was seen when applied to different tissues. Adhesive is most stable when applied to the duodenum while those applied to the liver, lung and heart degrade faster and at an increasing rate.

3.3.5 Discussion

Soft tissues provide a range of biological functions within diverse environments. These readily observable differences suggest that natural biochemical variability also likely exists among soft tissue surfaces. In this work we demonstrate that the apparent amine content on tissue surfaces indeed depends strongly on tissue type. Duodenal, cardiac, hepatic, and pulmonary tissue, all of which are potential targets for clinical sealants, span an approximate six-fold range in surface amine content. We sought to determine the feasibility of designing tissue-specific sealants which draw on this biochemical variance to improve upon the performance of currently used materials.

The clinical need to control tissue-sealant interaction is evident, as available materials fail to strike an optimal balance between sufficient adhesion strength and limiting tissue response. The bioadhesive hydrogel PEG:dextran primarily interacts with soft tissues via material aldehyde-tissue amine bond formation, and thus is an ideal probe of tissue-specific adhesion in a series of tissues with different target group densities (amine groups). Variations in tissue type and PEG:dextran aldehyde content were both seen to modulate the mechanical stiffness of adhesive constructs *ex vivo*, as indicated by the defined adhesive moduli. Tissue type also influenced the physical integrity of adhesive interfaces and material retention time subsequent to PEG:dextran application to biopsy specimens. When viewed in combination, mechanical and physical data suggest tissue chemistry regulates the strength and duration of PEG:dextran bioadhesion.

Much like adhesive interactions, PEG:dextran biocompatibility is also aldehyde-mediated. Material formulations with high aldehyde content induced the most severe tissue response according to multiple markers of inflammation. The tissue response was assessed in a subcutaneous model which offers no information on a tissue-specific inflammatory response. Although this can be viewed as a limitation of the present study, we believe that inflammation is a largely consistent biological process throughout the body, implying that excess aldehyde will reduce PEG:dextran biocompatibility in all soft tissue beds.

The data generated presented herein gives credence to tissue-specific adhesion and can guide the development of aldehyde-mediated clinical sealants. For example, where tissues are less responsive to changes in PEG:dextran aldehyde content, as in the case of lung, aldehydes might simply be provided at some minimal level with an anticipated limitation in adhesion strength and implant duration. In the other tissues, where aldehyde affinity is higher and resultant adhesion more responsive to material chemistry, one may consider designing compositions for extended duration and desired adhesion strength to meet application requirements. The notion of tissue-specific adhesion has momentum for clinical sealant development, but additional work is needed go beyond providing guidelines and actually optimize PEG:dextran or other material formulations to maximize therapeutic benefit with acceptable tissue response.

3.3.6 Conclusion

Aldehyde-presenting PEG:dextran materials exhibit tissue-specific adhesive properties. However, the benefit of increased adhesion of materials with greater aldehyde content must be balanced by adverse biologic responses to excess free aldehydes. Substantial difference in soft tissue aldehyde affinity shifts the balance between adhesion and inflammation for each tissue and suggests that a class of materials could be optimized for specific needs. Though tissue surface chemistry is an often ignored it is a critical determinant of tissue-material interaction and must be considered in future attempts at adhesive optimizations. Unlike cyanoacrylate and fibrin glue, PEG:dextran based materials have flexible design parameters that enable their mediation for specific application. Quantification and consideration of tissue properties must be a part in the design of any adhesive material to advance material selection for the full range of target tissues and clinical needs. The performance of existing and future adhesive materials should be examined with regard to tissue specificity.

3.3.7 Study Transition

As underlying theme of this work is the functional benefit of approximating soft tissue composition with a hydrogel-based adhesive system. The biocompatibility conferred by highly swellable materials is well documented in other systems and also observed in PEG:dextran, particularly the less bioreactive material formulations. However, we fully expect some reduction in functional potential as a consequence of material swell. As material swell induces a volumetric expansion at the tissue-material interface, a loss of adhered material density may compromise adhesive strength and failure resistance of PEG:dextran sealants. We next assess the significance of a swell-induced property loss in PEG:dextran, and seek material design solutions to enhance the sealant functional potential throughout the course of inevitable swell *in-situ*.

3.4 STUDY 4 THE EFFECTS OF MATERIAL SWELL ON ADHESION

Publication disclosure
The following presentation of Study 4 is based on:
Doping with DOPA: functional enhancement of hydrogel-based adhesive sealants.
Shazly T, Baker A, Naber J, Bon A, Edelman ER.
Under Review: Biomaterials 2009

3.4.1 Abstract

Soft tissue sealants are routinely used in surgical procedures despite limitations of insufficient adhesion or excessive local inflammation. In this study, we apply an emergent biomimetic strategy to modulate the wet adhesion of a candidate hydrogel-based sealant and assess the coupled effect on material biocompatibility. Marine mussels provide a natural model for sealant design as they adhere to various surfaces under considerable hydrodynamic forces. A major component of marine mussel adhesion plaques is the modified amino acid 3, 4-dihydroxy-l-phenylalanine (DOPA). We applied DOPA conjugation to functionally enhance a two-component hydrogel sealant composed of aminated star polyethylene glycol and linear dextran aldehyde polymers (PEG:dextran). Covalent incorporation of 0.3 wt. % DOPA into the PEG:dextran network significantly improved adhesive interfacial integrity and bursting strength of repaired duodenal wounds following hydration. Furthermore, functional DOPA levels did not drastically exacerbate the *in vivo* tissue response to subcutaneous PEG:dextran implantations as measured by local formation of a fibrous layer, inflammation and stimulation of matrix metalloprotease activity. Taken together, these data support DOPA conjugation as a promising approach to augment hydrogel-based sealant performance without compromising biocompatibility.

3.4.2 Introduction

The bioadhesive properties of soft tissue sealants provide a range of potential therapeutic opportunities [6, 8, 17]. Sealant adhesion results from in-situ polymerization initiated by tissue constituents such as trace water and calcium ions in cyanoacrylate derivatives and fibrin glues, respectively [17, 71]. Sealants form external adhesive bonds with tissue elements and internal cohesive bonds with self to control tissue-material interfacial and bulk material properties, often in a linked manner. Cyanoacrylate-based materials are relatively stiff and bind avidly to tissue, while more compliant fibrin glues exhibit comparatively limited adhesion [7, 14, 56]. Although the operative chemistries vary between traditional materials, individual sealants make use of the same type of chemical reaction to create both adhesive and cohesive bonds, thus promoting continuity between the interstices of the material bulk and the tissue-material interface. For all materials, the extent and nature of adhesive crosslinking, bulk properties, the biological response, and degradation kinetics cumulatively define sealant performance [20].

Despite a sustained developmental effort spanning over 50 years, no available material meets the full range of clinical needs [8, 18]. Sealant performance is generally bounded by deficiencies stemming from low adhesion strength or excessive tissue inflammation and likely reflects inadequate reactive chemistry on the one hand and the lack of directed tissue-material interactions on the other [13]. To address these issues, a two-component hydrogel composed of amine-functionalized star polyethylene glycol and dextran aldehyde polymers (PEG:dextran) was proposed as an aldehyde-mediated

adhesive with tunable functional properties [45, 46, 70]. PEG:dextran hydrogels are crosslinked by imine bonds between constituent amines and aldehydes. An analogous chemistry governs the primary PEG:dextran adhesive mechanism wherein free hydrogel aldehyde groups bind to amine groups on the tissue surface. We have previously demonstrated that rational adjustment of formulation reactive group concentrations can control of both adhesive and bulk material properties in the PEG:dextran system .

Persistent sealant adhesion to tissues under physiologic loading implies that overly stiff materials will generate local stress concentrations at the tissue-material interface. Excessive interfacial stress can destroy underlying tissue architecture and compromise material integrity [70, 72]. Thus, an ideal sealant would match tissue compliance to minimize interfacial stress and limit the risk of adhesive failure. In this respect, hydrogels are an attractive material class for sealant development as their mechanics after swell are generally comparable to native soft tissue [58]. The characteristically high water content of hydrogels also confers excellent biocompatibility, providing further impetus for their use as implantable biomaterials [73-75].

While hydrogel swell is beneficial to interfacial mechanics and biocompatibility, bulk material expansion may reduce sealant functionality. Here we demonstrate that the adhesive interface between PEG:dextran and duodenal tissue is physically altered and functionally compromised as a result of material hydration *ex vivo*. We adopt a biomimetic design strategy to mitigate swell-induced functional loss, particularly the conjugation 3,4-dihydroxy-l-phenylalanine (DOPA) to the PEG:dextran network. DOPA

has been recognized as a key amino acid governing the remarkable wet adhesion capabilities exhibited by marine animals, and has been successfully used as a tissue-reactive element in other material systems [76-79].

When incorporated into the PEG:dextran network, DOPA counterbalances swell-induced property loss as indicated by the burst pressure of repaired intestinal wounds in an *ex vivo* model of sealant performance. DOPA conjugation also minimizes the swell-induced reduction of PEG:dextran integrity near the tissue-material interface, with observable modulation of network continuity in 0.3 wt. % modifications. Significant correlation ($R = 0.92$, $p < 0.05$) between retained adhesive network integrity and *ex vivo* burst pressure after swell reiterates the importance of intrinsic material response to hydration. The *in vivo* tissue response to a series of modified PEG:dextran implants demonstrates that material biocompatibility is largely maintained at functionally effective DOPA levels, although higher concentrations induce significantly greater inflammation. Incorporating DOPA into the PEG:dextran bulk is a promising design strategy to safely enhance soft tissue sealant performance, and is likely applicable to other hydrogel-based adhesives.

3.4.3 Materials and Methods

Material synthesis

The syntheses of star PEG amine and linear dextran aldehyde polymers along with PEG:dextran copolymerization have been previously described [45, 46]. Briefly, eight-arm, 10 kDa star PEG polymer with amine end groups was dissolved in water to form a 25 wt. % aqueous solution. Linear dextran (10 kDa) was oxidized with sodium periodate to produce dextran aldehyde polymer (50% oxidation of glucose rings, two aldehyde groups per oxidized glucose ring), which was prepared as an 8.8 wt. % aqueous solution. Polymeric constituents spontaneously react to form a hydrogel following a volumetrically-balanced injection from a dual-chamber syringe equipped with a 12-step mixing tip. The PEG:dextran network crosslinks are derived from reaction between the constituent aldehyde and amine groups through a Schiff base intermediate.

Variations of both PEG:dextran network constituents were used in this work, specifically fluorescein-labeled PEG amine (FITC-PEG) and DOPA-modified dextran aldehyde. In order to synthesize FITC-PEG, star PEG amine (2.4 g) was dissolved in dichloromethane (6 mL), followed by the addition of 15 mg 6-(fluorescein-5-carboxyamido) hexanoic acid, succinimidyl ester (Invitrogen) and 12 µL triethylamine (Sigma). The mixture was continuously stirred at room temperature for 48 hours. The resulting solid after solvent evaporation was dissolved in 100 mL water, dialyzed against 4 L of water (Spectra/Por Biotech Cellulose Ester dialysis membranes, MWCO 500, Spectrum Laboratories) and lyophilized for 48 hours (-46ºC, 3×10^{-3} mbar). FITC-PEG

solutions of 25 wt. % solid content, 0.5% of which were fluorescently labeled, were used for co-polymerization with dextran aldehyde solutions.

A series of modified polymers was created by mixing various masses of DOPA (Sigma) with dextran aldehyde solutions (20 mL) for 3 hours at 60ºC. After mixing, homogeneous solutions were dialyzed for 24 hours against 4 L of water (as above). Solutions were snap frozen in liquid nitrogen and lyophilized (as above). Dehydrated solid was recovered and reconstituted in water to yield DOPA-modified dextran aldehyde polymer solutions.

Material characterization: DOPA conjugation to dextran aldehyde

Hydrogen NMR was used to determine the extent of DOPA conjugation to dextran aldehyde. A series of homogeneous DOPA and dextran aldehyde solutions were prepared in D_2O as described above (without solution dialysis) with initial free DOPA concentrations of up to 12 wt. %. Pure DOPA and dextran aldehyde solutions were also prepared for comparative analyses. NMR spectra were recorded (Bruker Avance 400 MHz instrument) and chemical shifts were reported in ppm relative to the deuterated solvent.

Functional mechanical testing: *ex vivo* bust pressure

Adult Sprague-Dawley rats (250 – 300 g, Charles River Laboratories, MA) were sacrificed by carbon dioxide asphyxiation under university IACUC protocol and federal guidelines for animal care. The duodenum was excised and immersed in 10 ml Krebs-

Henseleit buffer at room temperature. Longitudinal duodenal segments were cut and inserted into a mechanical testing apparatus capable of controlled luminal perfusion (Bose® Biodynamic Test Instrument, Minnetonka, MN). A wound was introduced by full-thickness puncturing of the intestinal wall with an 18 gauge needle. Wounds were then repaired with 200 µl application of PEG:dextran to the outer intestinal surface. A five minute sealant curing time was allowed, after which intestinal samples were submerged in PBS for up to one hour. The burst pressure of repaired intestinal wounds was measured through gradual increase of lumen pressure developed through restriction of flow (50 ml/min) distal to the sample lumen. Failure of the wound repair site resulted in an immediate loss of luminal pressure and visible PBS leakage at the tissue-material interface. The maximum luminal pressure prior to interface failure indicates the wound burst pressure [70].

Interfacial integrity

The interfacial integrity of PEG:dextran adhered to excised rat duodenal tissue (harvested as above) was quantitatively assessed after sample hydration treatments of up to one hour. Material formulations (200 µl) featuring FITC-PEG were applied to the serosal surface and allowed to polymerize for five minutes prior to sample hydration. Following submersion in PBS for the designated swell times, samples were snap frozen in liquid nitrogen, cryosected (20 µm thick sections), and stained with DAPI mounting medium (Vector Laboratories) in accordance with standard protocols. Sections were imaged with a fluorescent microscope (Leica) at 200x magnification with optical filters amenable to FITC-PEG and DAPI emission/absorption spectra. Image analyses

software (MetaMorph) was used to overlay corresponding images and depict the interfacial region between PEG:dextran and duodenal tissue. The linescan software feature was used to quantify the fluorescent signal from FITC-PEG in the first 500 μm extending normally from the serosal surface. The average fluorescent signal from 3-5 linescans per image reflects PEG:dextran integrity at the adhesive interface.

Biocompatibility: *in vivo* tissue response

The biocompatibility of PEG:dextran adhesives was evaluated by the local tissue response to subcutaneous implants in mice. Briefly, a pocket was created in the dorsal subcutaneous space of anesthetized C57BL/6 mice and 200 μl of material was injected into the pocket using a syringe with a sterilized mixing tip. After nine days, the mice were sacrificed and the skin and subcutaneous tissues at the implantation site were harvested. Tissue samples were frozen in liquid nitrogen and stored at -80ºC until histological analyses. All experimental protocols were approved by the MIT Animal Care and Use Committee.

Harvested tissues were cryosected into 20 um sections and stained with hematoxylin and eosin using standard methods. Light microscopy at 100x magnification was used to assess the local fibrotic response in three randomly selected locations on each tissue section and quantified by the fibrotic layer thickness (Adobe Photoshop). Zymography was performed using quenched fluorescein-labeled gelatin and fluorescence intensity was quantified and normalized to indicate relative enzymatic activity (MetaMorph) [80]. Immunohistochemical staining for macrophages was

performed as previously described [81]. Briefly, sections were blocked in 10% goat serum for 40 minutes and incubated overnight with a primary antibody for Mac-3 (Biolegend). The samples were then washed three times with PBS and incubated with an anti-rat antibody labeled with alexafluor-594 dye (Invitrogen). After two hours of incubation, the samples were washed extensively and coverslipped in DAPI-containing mounting media (Vector Laboratories). The fluorescent intensity from alexafluor-594 dye was quantified and normalized to provide a metric of macrophage activity (MetaMorph).

3.4.4 Results

Material characterization

Hydrogen NMR was used to capture the signature spectra of dextran aldehyde (Figure 45), DOPA (Figure 46), and a series of DOPA-dextran aldehyde conjugates. A diagnostic signal for the imine proton present in the conjugate form (8.3 ppm) was integrated against the three aromatic protons of DOPA to determine the extent of conjugation [82]. In a system exhibiting complete DOPA conjugation, a ratio of 3:1 between the integrals of the aromatic DOPA and imine bond peaks would be expected and was found (Figure 47). Conversely, when conjugation is not complete and DOPA exists in both free and conjugated forms, the integrals of the imine and aromatic peaks reflect the relative amount of conjugation in the material system. The reaction efficiency nonlinearly depended on reaction conditions when initial DOPA concentrations ranged from 0.1 to 12 wt. %, with only 10.3 % conjugation in the most concentrated solution (Figure 48). Four conjugates of dextran aldehyde polymers with initial DOPA contents ranging from 0 to 6 wt. % were synthesized for evaluation in the remainder of this work (Table 15).

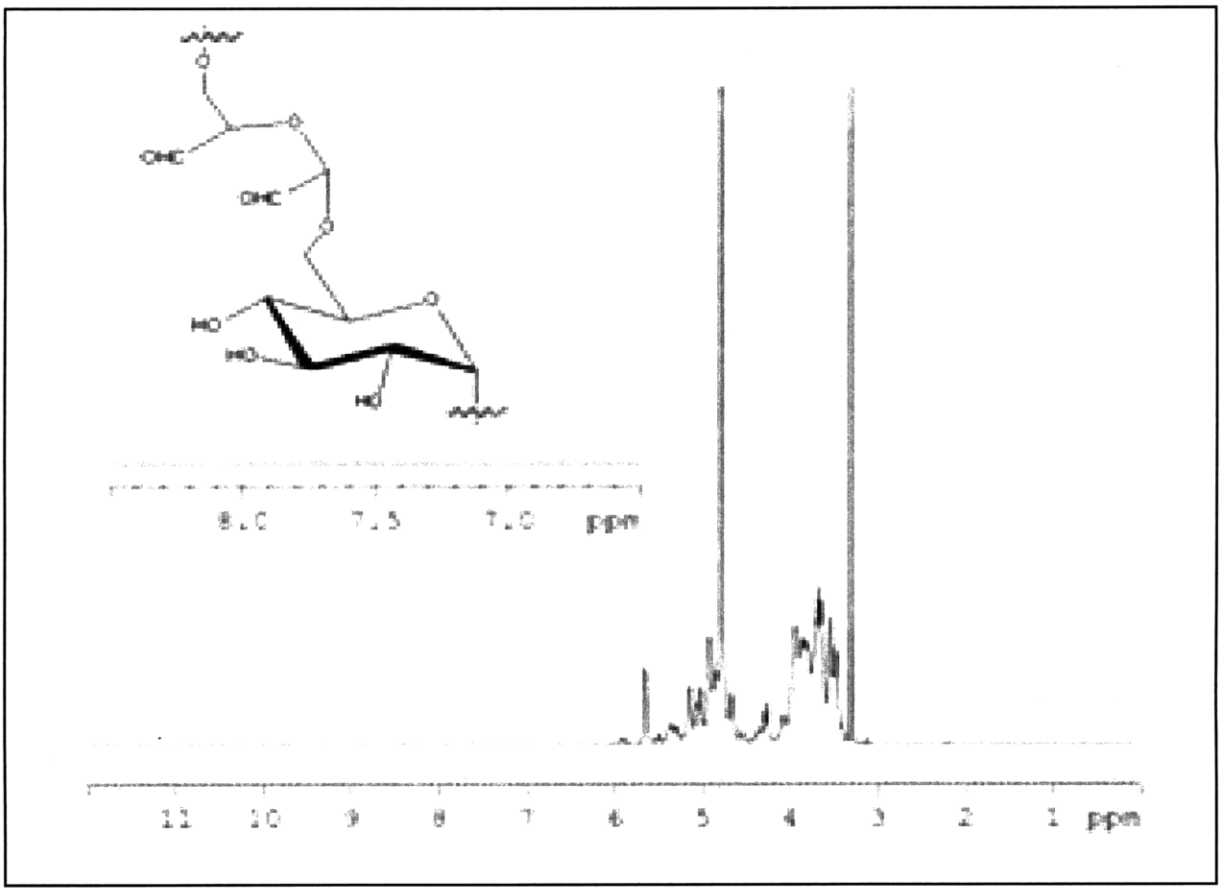

Figure 45 NMR spectra of dextran aldehyde, with inset showing molecular structure and ppm region-of-interest for determination of imine bond density.

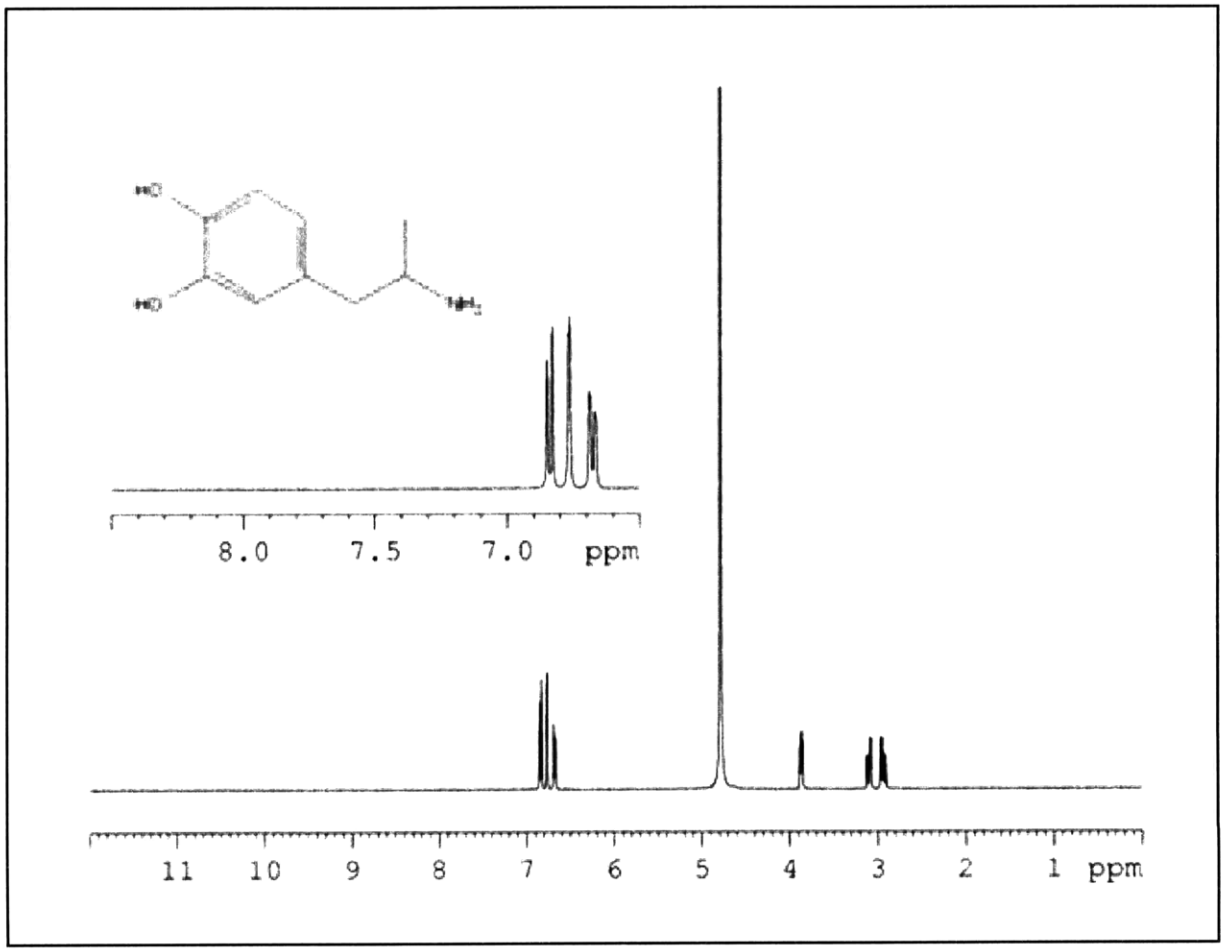

Figure 46 NMR spectra of DOPA, with inset showing molecular structure and ppm region-of-interest for determination of imine bond density.

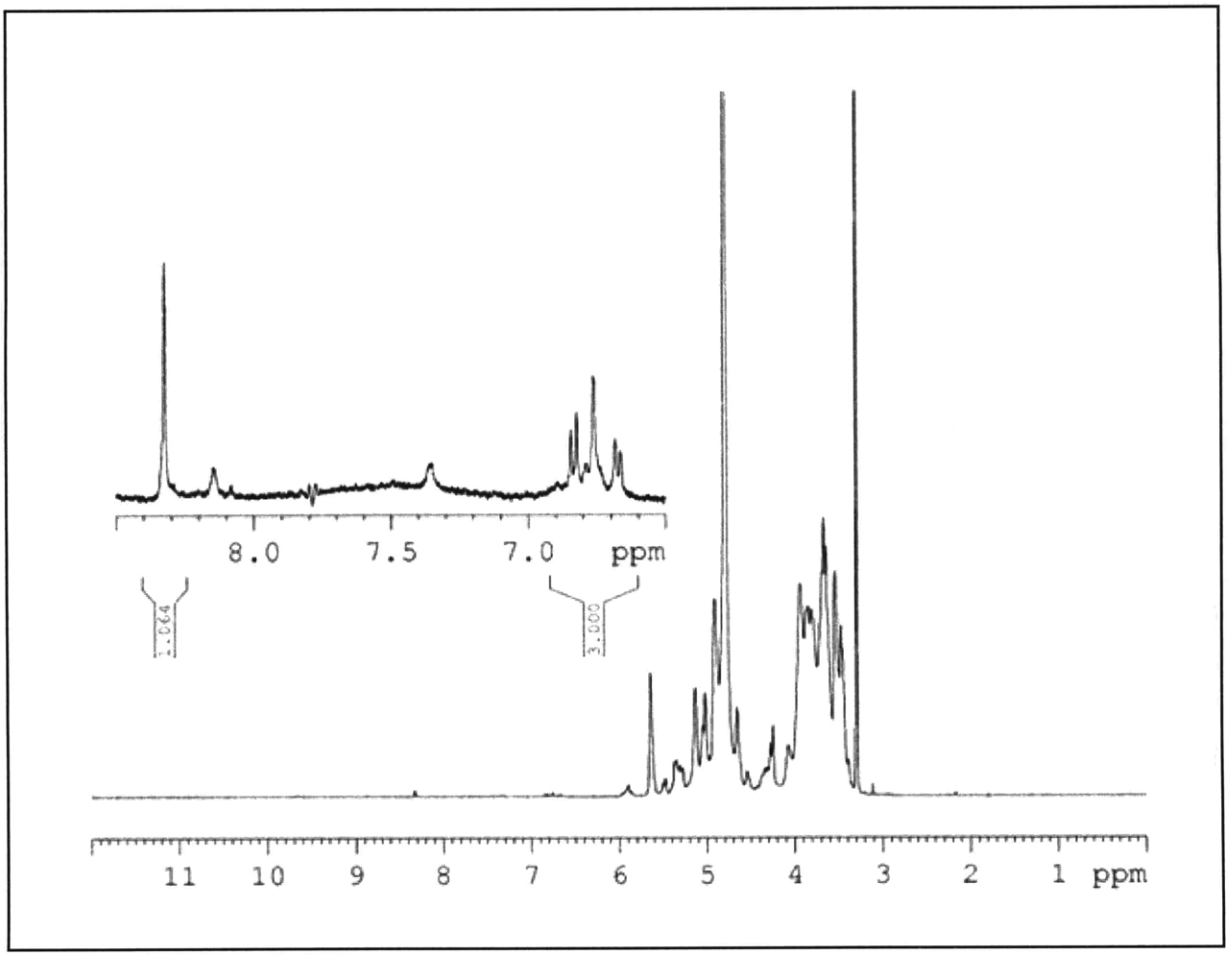

Figure 47 NMR spectra of 0.3 wt. % conjugation of DOPA to dextran aldehyde dextran aldehyde, with inset showing the ppm region-of-interest for determination of imine bond density. Following conjugation, the triplet peaks (6.6 to 6.9 ppm) indicate total DOPA content, while the imine peak (8.3 ppm) was diagnostic of conjugated DOPA.

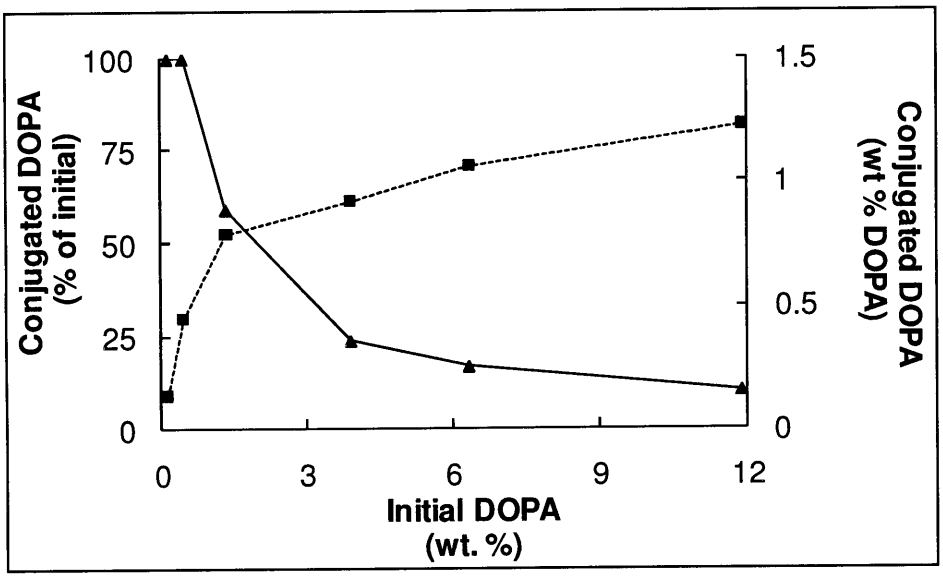

Figure 48 The ratio between the integrals of the triplet and imine peaks was used to calculate the extent of conjugation following reaction, with a 3:1 ratio indicating complete conjugation. The % of initial DOPA (▲) and the wt. % of conjugated DOPA in the modified polymers (■) are presented as a function of initial DOPA concentration in solution to indicate the variation of reaction efficiency and product.

Table 15 Compositional description of the DOPA modified dextran aldehyde polymers. Constituent dextran aldehyde properties (molecular weight, oxidation state, and solid content) were constant across material variants, while initial DOPA content ranged from 0 to 6 wt. %. The resultant extent of conjugated DOPA was determined by hydrogen NMR.

Dextran aldehyde			DOPA conjugation		Reaction efficiency
Molecular weight (kDa)	Oxidation state (%)	Solid content (wt. %)	Initial DOPA content (wt. %)	Conjugated DOPA (wt. %)	Conjugated DOPA (% of initial)
10	50	8.8	0	0	-
10	50	8.8	0.3	0.3	100
10	50	8.8	2.0	0.8	40
10	50	8.8	6.0	1.1	18

Burst pressure of repaired duodenal wounds

The *ex vivo* burst pressure of repaired puncture wounds following swell signifies the potential of adhesive sealants to mitigate tissue dehiscence or leakage in multiple clinical scenarios. Intestinal samples were wounded, repaired with PEG:dextran variants, and submerged in PBS for up to one hour. The failure resistance of wounds

repaired with unmodified PEG:dextran monotonically diminished with swell, exhibiting a 39 ± 18% reduction in burst pressure following one hour hydration (Figure 49). The swell-response of modified PEG:dextran was markedly different, as the measured burst pressure of the 0.3% DOPA conjugate varied between 66 ± 6.7 and 77 ± 9.7 mmHg with no discernable dependence on swell time. Higher DOPA concentrations also stabilized initial wound burst pressure throughout hydration, although the diminished overall performance of 0.8 and 1.1% conjugates compared to unmodified PEG:dextran points to a loss of functional sealant potential with excessive doping. The reduction of PEG:dextran failure resistance at higher DOPA concentrations may reflect an interference with bulk network formation, a notion further supported by a substantial protraction of material gelation times for these formulations (data not shown).

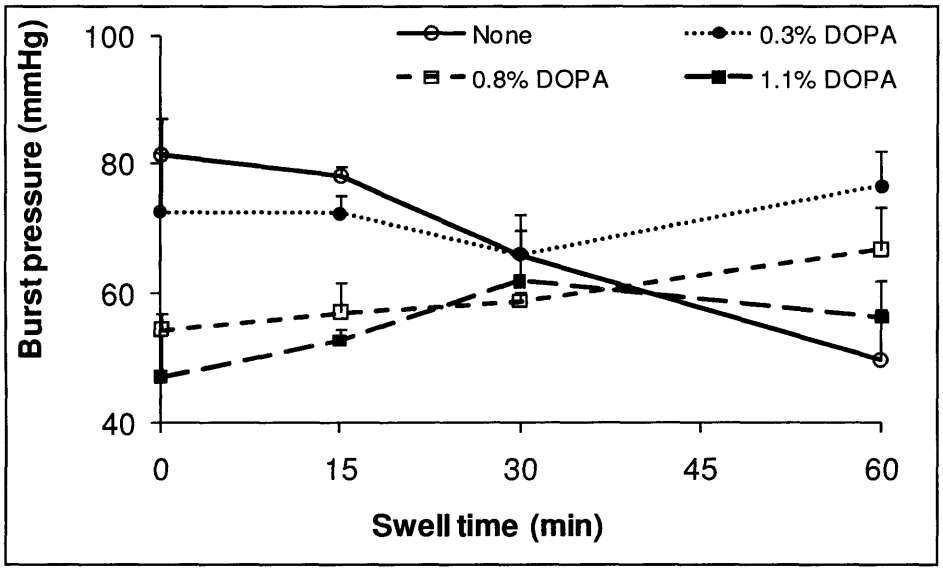

Figure 49 The ex-vivo burst pressure of repaired rat duodenal wounds as a function of sample swell time. Puncture wounds were repaired with PEG:dextran formulations featuring 0 % (○), 0.3 % (●), 0.8 % (□), or 1.1 % (■) DOPA and then submerged in PBS. Following the designated swell time, sample lumens were perfused with PBS (50 mL/min) and gradually pressurized. The pressure at which the wound site failed was recorded as the burst pressure. Error bars represent 1 standard error of measurement (n = 4).

Interfacial integrity

The integrity of adhesive interfaces between PEG:dextran variants and excised duodenal tissue was assessed as a function of swell time. Integrity was quantified via the fluorescent intensity emitted from PEG:dextran featuring FITC-PEG, providing a direct correlate to average material density at the adhesive interface. The differential responses of the unmodified PEG:dextran and the 0.3% DOPA conjugate portray a reduction of swell-induced disturbance in the modified network (Figure 50). Quantification of PEG:dextran intensity in the interfacial vicinity indicates both a swell-induced loss of unmodified network integrity and the significant mitigation of this loss with 0.3% DOPA incorporation (Figure 51). Following one hour swell treatments, the measured network integrity correlates well ($R = 0.92$, $p < 0.05$) with the burst pressure of repaired wounds across PEG:dextran variants, highlighting the influence of tissue-material continuity on sealant performance (Figure 52).

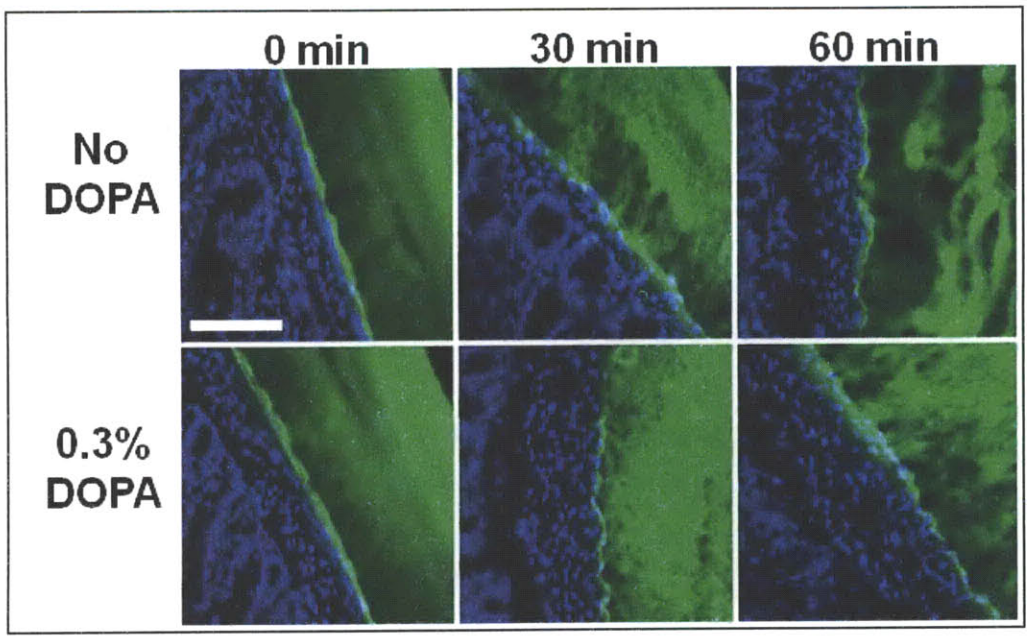

Figure 50 The interfacial integrity between duodenal tissue (cell nuclei stained blue with DAPI) and FITC-labeled PEG:dextran variants (green) varied as a function of swell time. The interfacial integrity of unmodified PEG:dextran (upper panels) visibly diminished with swell, while the 0.3% DOPA variant (bottom panels) remained comparatively stable. Scale bar = 1000 μm and applies to all images.

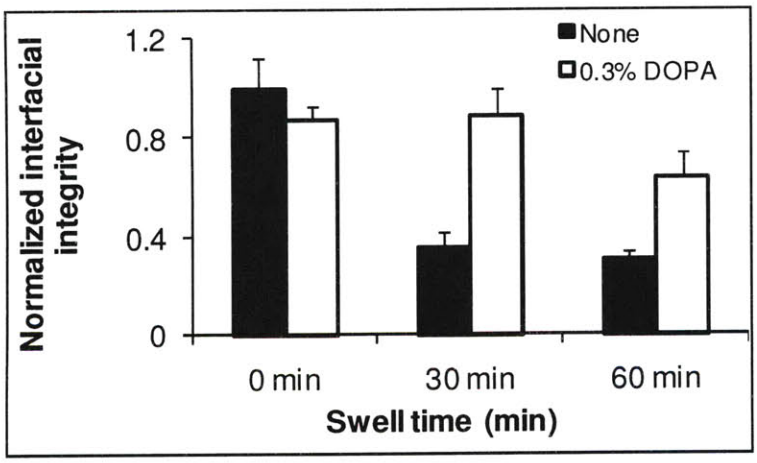

Figure 51 The material integrity extending normally from the tissue surface (500 μm) was assessed with analytical microscopy and presented as a function of swell time (B). Error bars represent 1 standard error of measurement (n = 4). * indicates $p < 0.05$ determined by ANOVA with post-hoc analysis when compared to 0 minute swell time for each material.

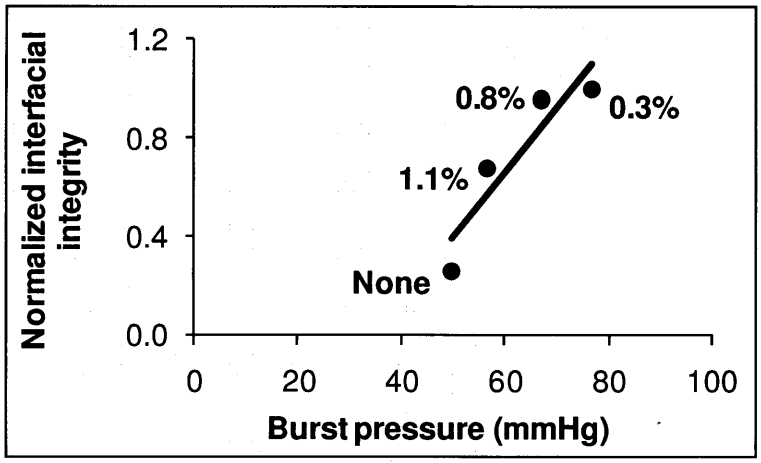

Figure 52 Linear correlation (R = 0.92, p < 0.05) between sample burst pressure and interfacial integrity after swell suggests that local loss of material reduces sealant functional potential (data point descriptors reflect DOPA content).

Material biocompatibility

The efficacy of strongly adherent surgical sealants is often limited by associated tissue response. The biocompatibility of PEG:dextran variants was examined through subcutaneous material implantations in mice. Three indicators of the tissue inflammation were assessed based on microscopic analyses of stained sections, including the fibrotic layer thickness, enzymatic activity, and macrophage density. PEG:dextran implants elicited a fibrotic response to an extent obviously dependent on material DOPA content (Figure 53). The fibrous layer thickness incited by unmodified PEG:dextran implantations was minimal (90 ± 40 μm), suggesting that the established biocompatibility of material constituents (PEG and dextran) is largely maintained in this adhesive system. DOPA conjugation up to 0.8% was associated with a slight increase in fibrosis, with thicknesses of 280 ± 40 μm and 190 ± 60 μm in the less concentrated PEG:dextran variants. The tissue response to 1.1% DOPA implants was an order of magnitude more severe than to unmodified PEG:dextran (fibrotic thickness of 890 ± 70 μm), demonstrating hydrogel biocompatibility is compromised with extreme network modification (Figure 54).

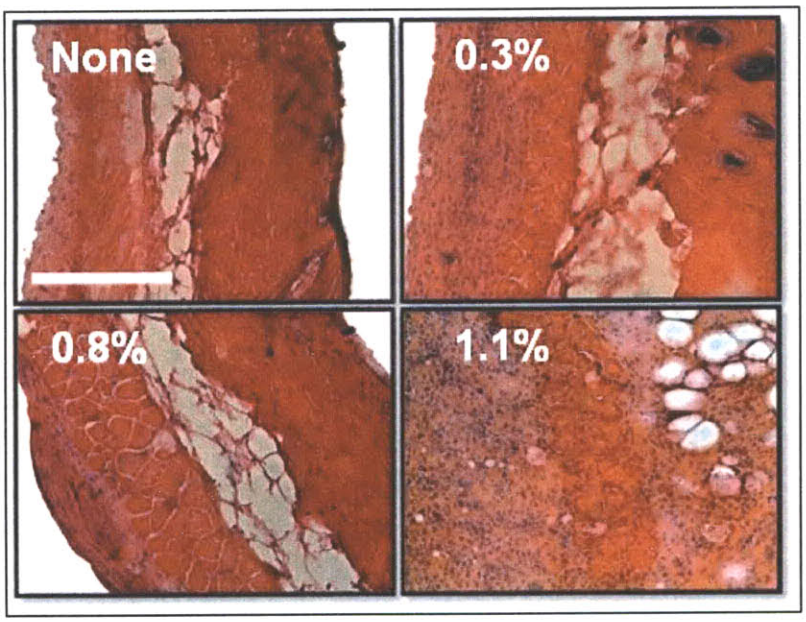

Figure 53 Tissue fibrous layer thickness local to PEG:dextran variants increases with DOPA content. Mice were implanted with material (200 µl) subcutaneously and tissues were harvested after nine days. Hematoxylin and eosin stained sections of tissue demonstrate increased cellular infiltration and formation of fibrous tissue surrounding the implanted material. Scale bar = 500 µm and applies to all images.

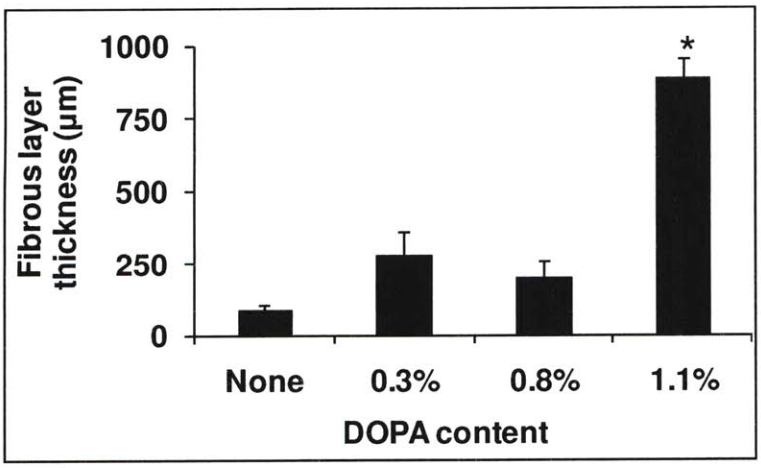

Figure 54 Fibrous layer thickness was measured and found to be significantly increased in 1.1% DOPA content materials. Error bars represent 1 standard error of measurement (n = 4 to 5). * indicates $p < 0.05$ determined by ANOVA with post-hoc analysis when compared to unmodified PEG:dextran.

Inflammatory cell-mediated proteolysis impedes wound repair via matrix metalloprotease (MMP) cleavage of extracellular matrix proteins. MMP activity is often elevated during surgery and particularly problematic at surgical anastomoses because of the potential to destabilize wound sites and facilitate tissue dehiscence [83, 84]. The gelatinase activity in local tissues following PEG:dextran implantations was measured using in-situ zymography (Figure 55). The fluorescent intensity indicative of gelatinase activity monotonically increased in response to formulation DOPA content, suggesting a stimulation of pro-inflammatory mediators and polymorphonuclear leukocytes by bioreactive DOPA (Figure 56).

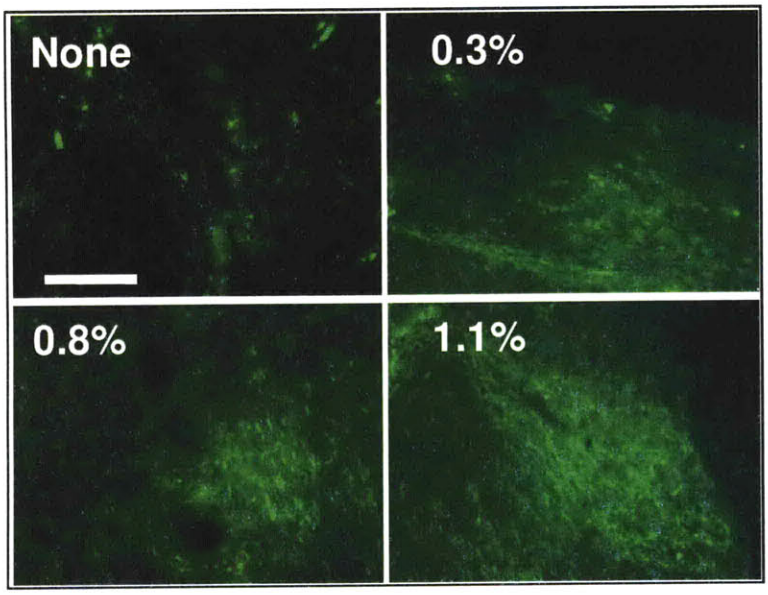

Figure 55 Analysis of gelatinase activity in subcutaneous tissue following implantation of PEG:dextran variants. In-situ zymography with an internally quenched FITC-labeled gelatin substrate indicated. Scale bar = 1000 μm and applies to all images.

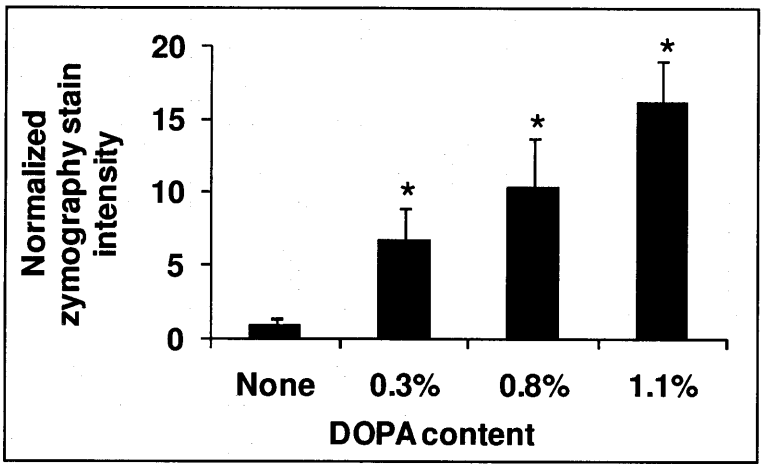

Figure 56 Increased DOPA content stimulated tissue gelatinase activity (B). Error bars represent 1 standard error of measurement (n = 4 to 5). * indicates $p < 0.05$ determined by ANOVA with post-hoc analysis when compared to unmodified PEG:dextran .

Macrophages migrate to implantation sites and serve numerous functions associated with tissue inflammation, including the regulation of fibroblast activity, secretion of MMPs, and phagocytosis of material debris [85, 86]. Fluorescent mac-3 labeling demonstrated that macrophages were present at various densities following the implantation of PEG:dextran materials (Figure 57). The density of macrophages in local tissues was low and statistically indistinguishable until the highest DOPA concentration was used (Figure 58). Macrophage density was approximately six-fold greater in tissues subjected to 1.1% DOPA implantations compared to unmodified PEG:dextran, which again suggests that excessive DOPA content will substantially reduce material biocompatibility.

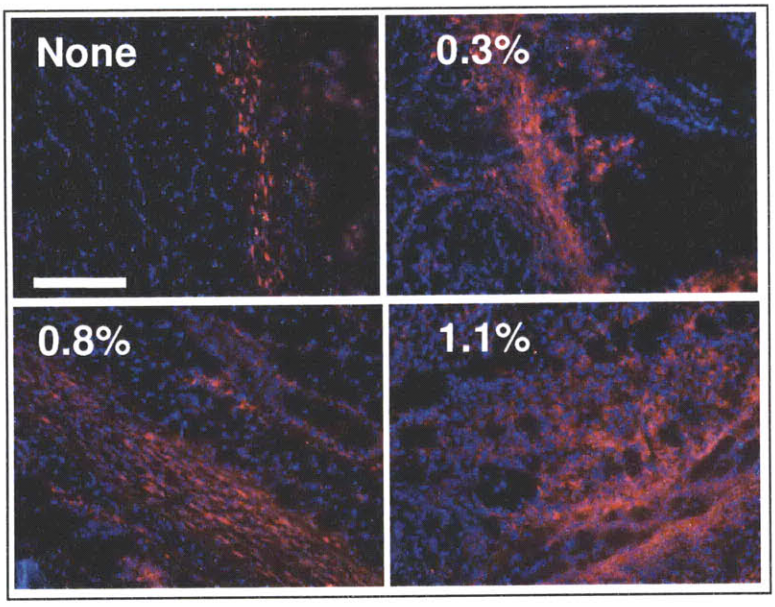

Figure 57 Macrophage infiltration (red by immunofluorescent staining for Mac-3) varied among subcutaneous implantations of PEG:dextran materials. Scale bar = 1000 μm and applies to all images.

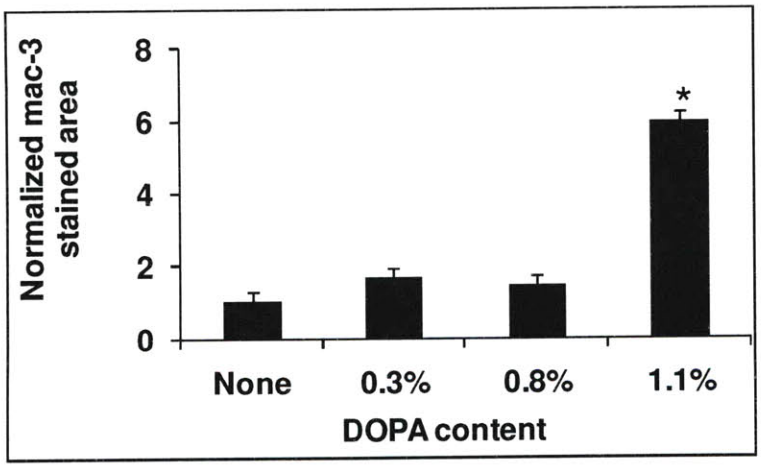

Figure 58 Macrophage infiltration was quantified with analytical microscopy and found to be increased in 1.1% DOPA content materials. Error bars represent 1 standard error of measurement (n = 4 to 5). * indicates $p < 0.05$ determined by ANOVA with post-hoc analysis when compared to unmodified PEG:dextran.

3.4.5 Discussion

Soft tissue sealants are utilized in numerous clinical procedures and consequently exposed to various physiological surroundings. The in-situ environment and material properties of the employed sealant will together dictate tissue-material interactions and determine overall clinical efficacy. The local hydration state and material hydrophilicity constitute a tissue-material property pair that affects the rate and extent to which biological fluids will permeate sealants and influence adhesive interactions. For example, sealants will rapidly encounter fluids when used to attain hemostasis in cases of severe bleeding. In other clinical scenarios, such as anastomotic augmentation following gastrointestinal resection, sealant exposure to tissue exudates may occur more gradually. Regardless of hydration kinetics, intrinsic material properties alone define the *in vivo* equilibrium swell state, as hydrophilic or hydrophobic sealants will ultimately incorporate more or less biological fluid into the material network, respectively. To accurately predict the performance of swellable sealants, the effects of hydration on tissue-material adhesive interactions must be considered.

Hydrogel-based sealants could potentially suffer swell-induced reduction in clinical efficacy by various mechanisms, including a passive interfacial dissociation due to material expansion. Soft tissues are relatively stable with regard to water content, but applied sealants will expand continually until they too reach an equilibrium swell state. Sealant volume expansion could physically disturb the tissue-material interface and diminish adhesive failure resistance under physiological loading. Here, we demonstrate that reduction of PEG:dextran integrity at the adhesive interface is a consequence of

swell and correlates with loss of sealant functional properties *ex vivo*. Although hydrogels are a biocompatible material class for sealant development, extreme swell will likely reduce *in vivo* functional performance. Analogous phenomena are expected to limit highly hydrophilic biomaterials across a range of clinical applications, motivating the pursuit for techniques of hydrogel property enhancement under swollen conditions.

Nature often inspires engineering solutions to dilemmas of biomaterial design. In this work we adopted a biomimetic approach to bulk PEG:dextran modification that was previously used in other material systems. Reports on the effects of both surface and bulk DOPA-based modifications have collectively demonstrated modulated interaction with both organic and inorganic surfaces [78, 87-89]. Prior studies have found that polyDOPA films can be applied through simple dip-coating and promote adherence to surfaces of metals, ceramics, polymers, and various cell lines [89]. The observed functional potential of DOPA is supported by the role of this amino acid in vigorous and water-resistant adhesion of marine animals. Multiple variants of the adhesive foot protein 3 in *Mytilus californianus* (Mcfp-3) have been implicated in marine mussel adhesion, with all proteins containing DOPA-rich domains [90]. The presently examined DOPA conjugate to dextran aldehyde further recapitulates mussel adhesive plaques in which adhesive proteins are embedded within polysaccharide matrices to facilitate flexibility and failure resistance at the point of contact with underlying substrates [91].

Our study found that limited DOPA content within PEG:dextran significantly improved sealant functional performance after swell without sacrificing hydrogel

biocompatibility. However, higher levels of DOPA content were detrimental to both sealant function and biocompatibility. The local fibrotic response and macrophage invasion were severely elevated following implantation of 1.1% DOPA conjugates as compared to less concentrated material formulations. *In situ* zymographic analysis demonstrated a monotonic increase in protease activity with DOPA content. The 1.1% DOPA variant incited an ~ 15-fold escalation in enzymatic activity as compared to unmodified PEG:dextran. The need to tailor DOPA content in PEG:dextran is manifest by the local tissue response in subcutaneous implant models and should direct future material design. Furthermore, the functional enhancement provided by DOPA is best realized at low concentrations. Excessive DOPA content likely interferes with network polymerization, providing further incentive to limit the extent of chemical modification in PEG:dextran.

The mechanisms by which DOPA additive modulates the adhesive properties of PEG:dextran and other material systems remain unclear, but some possibilities are suggested by this work. Prior to swell treatments, low DOPA levels did not substantially alter the metrics of PEG:dextran functional performance. Differential properties between unmodified PEG:dextran and the 0.3% DOPA-PEG:dextran conjugate did however emerge after swell and could conceivably stem from two basic mechanisms; either direct modulation of the PEG:dextran network swell response and/or DOPA-mediated adhesion to tissue surfaces in the presence of water. The former possibility was explored through multiple comparative measurements of the elastic moduli of the unmodified PEG:dextran and the DOPA conjugate, pre- and post-swell. After one-hour

swell treatment, unmodified PEG:dextran underwent an approximately 85% reduction in surface stiffness, while the conjugate was softened by only 50% (please see appendix for experimental details, A11 Nanoindentation Experiment). Additional measurements of material swell ratio and bulk elastic modulus as a function of hydration time further suggest that DOPA is modulating the performance of PEG:dextran by limiting network response to hydration, ultimately demonstrating that stable material properties better maintain initial sealant performance (please see appendix for experimental details, A12 Swell Response of DOPA Conjugates).

Reducing the material swell response after adhesion could facilitate better maintenance of initial interfacial stability and may explain the relatively enhanced functional performance of DOPA-PEG:dextran conjugates. Such phenomena fit nicely within the context of this thesis work as DOPA can optimize material cohesion by virtue of potentially mitigating the reduction of material strength in aqueous media. In further keeping with the focus on imine-based tissue-material interactions, DOPA may affect material bioadhesion as this molecule represents a terminal node in the PEG:dextran network and consequently alters available bioreactive node densities. Alternatively, DOPA may form clustered hydrogen bonds to tissue entities via the hydroxlyated ring as suggested by previous studies [79].

Biomaterials must be evaluated at physiologically-relevant states to understand their true clinical potential. The environments in which soft tissue sealants are employed differ as a consequence of their application in surgical procedures, with a range of pH,

mechanical forces, and target tissue chemistries encountered in routine use [20]. However, common among all sealant applications is the eventual exposure of adhesive interfaces to biological fluids. Hydrogels are appealing platforms for development of implants which intimately interact with soft tissues because of their composition and associated biocompatibility; yet high material swell magnifies the influences of hydration on tissue-material interactions. DOPA-based hydrogel network modification can effectively combat a clinically-relevant functional loss related to swell as exemplified in PEG:dextran sealants. DOPA conjugation has been implemented both at material surfaces and throughout the bulk in multiple material systems, with the presently demonstrated preservation of biocompatibility and enhancement of function implying a universal significance for the design of hydrogel-based biomaterial implants.

3.4.6 Conclusion

It is recognized that the local physiological environment can modulate biomaterial implants to an extent which diminishes their therapeutic potential. In-situ swell of a hydrogel-based soft tissue sealant represents a biologically-induced dynamic which may compromise interfacial integrity and clinical efficacy. We demonstrate that PEG:dextran sealants suffer a swell-induced reduction of material density at the adhesive interface with a correlated loss of function in an *ex vivo* model. Conjugation of DOPA to PEG:dextran enhances the post-swell sealant performance, an effect congruent with the established role of this amino acid in the wet adhesion of both marine animals and other synthetic materials. Functionally effective levels of DOPA within PEG:dextran did not substantially alter material biocompatibility as indicated by the subcutaneous tissue response to a series of material formulations. In general, DOPA-based modification provides a means to safely enhance wet adhesive properties and as such is a powerful approach to sealant design.

4. Experimental Difficulties, Future Work and Thesis Conclusion

4.1 Experimental Difficulties

Scientific research is often iterative, sometimes circular, and on fine occasion yields interpretable results. Up to this point this thesis is a presentation of only the latter, but describing the evolution of reported techniques may assist future researchers. In particular, the methods employed for adhesion strength testing, *in vitro* cellular studies, image analyses, and histology were initially impeded by the following technical difficulties.

Adhesion strength testing: Two varieties of tissue-material elements were constructed for mechanical testing of adhesion in this work. The test elements described in **Study 1** were advantageous in the sense that minimal material and tissue were used for each experimental run and sample fixation within the mechanical testing grips was relatively simple. Prior to arriving at the described method, it was difficult to secure duodenal samples in standard tensile grips without damaging the tissue. Threading the duodenal lumen with a solid, flexible tube proved crucial for test element stability, and is likely applicable to other testing configurations. This methodology was sufficient to differentiate between the ultimate adhesive strength of a range of materials, but was not conducive to mechanical modeling primarily because of the nature of contact between opposed tissue samples (point contact). The test elements utilized throughout the remainder of this work (**Studies 2 and 3**) involved excising larger sections of duodenal as well as other soft tissues with dermal punches. These samples

were appropriate to stress analysis and mechanical modeling because of the well-defined contact geometries following adhesive application (circular cross-sections). A technical difficulty that had to be overcome with this arrangement was ensuring that the contact area was as intended and not only relegated to the circumference of test elements. This was achieved by modifying the tubular fittings over which the samples were attached such that they were solid (no hollow bore) to prevent tissue collapse toward the center during testing.

***In vitro* cellular studies:** The cellular assays presented in **Study 1** were conducted after exposure of cultures to either material degradation products or small volumes of bulk materials. Other work (not shown) was also conducted which involved the direct exposure of cells in culture to larger volumes of materials. When performing these experiments, the number of cells that could be assayed subsequent to material exposure was greatly limited; a majority of the cells were actually beneath/within the material and not readily extracted for analysis. Furthermore, using large volumes of material interfered with the employed assays to an extent which could not be simply accounted for with standard curves. To address these concerns, we utilized cell culture inserts such that cells could share media with substantial material bulk without being largely covered or engulfed. Although no *in vitro* data featuring the cell culture inserts is presented in this thesis, this approach was successful in reducing material interference with assays and preserving cell densities for analysis. We recommend that future studies of hydrogel/cell co-cultures are conducted with cell culture inserts which allow media sharing without direct contact.

Image analyses: Both **Study 3** and **Study 4** included quantitative microscopic analyses of the interfacial region between adhered material and soft tissue. In **Study 3**, the adhesive regime was defined as the area of disturbed material network juxtaposed to the tissue surface, and was normalized by the interfacial length. Despite the normalization, there is still a degree of judgment required to identify *disturbed material network*. The methodology employed in **Study 4** makes use of the linescan feature of MetaMorph® and removes the element of judgment from the experiment; in this approach, average bulk integrity across a predetermined distance normal to the interface was quantified with no regard to apparent network state. Although both methods yielded repeatable data with acceptable levels of error, the linescan feature is both faster to execute and removes an obvious source of source of error.

Histology: A variety of histological techniques were employed throughout this work, and along the way some adjustments to standard procedures for analyzing intact tissue-material interfaces were devised. Firstly, prior to snap-freezing duodenal samples, it is very helpful to fill the lumen with tissue freezing medium to preserve the tubular morphology. Early attempts without filling the lumen result in duodenal collapse upon freezing and destruction of the tissue-material interface. The issue of tissue staining also required a slight modification to standard techniques, as the recommended times for slide submersion in either xylene or ethanol were too extreme to prevent hydrogel dissolution. For H&E stains, the usual triplicate submersions in these particular solutions were replaced by a single submersion with no loss of tissue stain and apparent

retention of material. We expect that future endeavors to stain tissue-hydrogel interfaces will require similar modifications. Finally, when cryosectioning rat duodenum, there was no tangible advantage to producing sections thinner than 20 μm; the established benefits for analyses of arterial tissue did not seem to apply in this scenario.

4.2 FUTURE WORK

The experimental data and design concepts resulting from this work provide both motivation and guidance for the continued development of PEG:dextran as a clinical adhesive. As restated throughout this thesis, an underlying goal was to promote such advancement but do so in a manner that is readily extendable to other material systems. We demonstrated that PEG:dextran is an advantageous probe of tissue-material interactions, and believe further experimentation can continue to yield general findings which are germane to a wider range of biomaterials.

For example, the incentive to design viscoelastic adhesives is readily discernible (**Study 2**), but the optimal method for controlling tissue-material mechanics has not been identified. In our work, we varied PEG:dextran bioreactive chemistry (and consequently adhesive mechanics) through the solid content of the constituent dextran polymer. A similar effect could be achieved by increasing the extent of dextran oxidation, which may better preserve molecular mobility (as opposed to increasing solid content) since network density would remain essentially constant. Alternatively, using varied lengths of constituent polymers may also influence chain mobility after tissue-material interfacial formation and likewise promote viscoelastic adhesion. Further experimentation design to impart increased adhesive viscoelasticity at fixed reactive chemistry may be a viable approach to improve PEG:dextran (or other) sealant functional performance without reducing biocompatibility.

We successfully established that biochemical variability among soft tissues creates potential for tailored sealants with enhanced performance (**Study 3**). However, we did not propose optimal PEG:dextran formulations for the examined tissues, which would require a broader study of the considerable compositional design space represented by this material system (up to six independent variables). Furthermore, we did not rate the *in vivo* functional efficacy of adhesive materials at realistic implantation sites (only subcutaneous implantations were performed). Such experimentation entails comparatively advanced animal models and surgical techniques, but would provide a more meaningful assessment of differential material performance and tissue response.

DOPA incorporation within PEG:dextran favorably modulated adhesion subsequent to interfacial hydration, specifically at lower concentrations (**Study 4**). Comparatively higher DOPA content within PEG:dextran both incited a negative tissue response and reduced the sealant functional potential as assessed in an *ex vivo* model. These data suggest that DOPA conjugation is a promising design strategy, but as with the tissue-specificity study, fall short of providing optimal material formulations for specific applications. Two immediate experimental paths emerge at the conclusion of this work: elucidating the mechanistic basis for PEG:dextran property modulation by DOPA and examining material performance at additional DOPA concentrations (only three formulations tested).

4.3 THESIS CONCLUSION

A growing understanding of the complexities and consequences of tissue-material interactions has facilitated a steady progression of biomaterial technologies. We have become increasingly aware that both the tissue response to a material and vice versa must be considered for efficacious biomaterial design. Clinical sealants provide an informative platform to study tissue-material interactions due to a functional dependence of these implants on sustained reaction with tissue. Through analyses of adhesive mechanics, native tissue properties, material properties, and tissue response, we have extracted multiple design principles for creating biocompatible yet strongly adherent soft tissue sealants. Concepts resulting from this work include the use of aldehyde-amine chemistry to direct hydrogel adhesion to soft tissues, the functional benefits of maintaining native tissue viscoelasticity with adhesive interactions, the potential for design of tissue-specific sealants, and the use of biomimetic amino acid conjugation to promote hydrogel adhesion after swell. The findings of this work reveal aspects of tissue-material interactions which extend beyond the engineering of clinical sealants with prospective relevance to a broader range of biomaterial implants.

5. References

1. Williams, D.F., *On the mechanisms of biocompatibility.* Biomaterials, 2008. **29**(20): p. 2941-53.
2. Shard, A.G. and P.E. Tomlins, *Biocompatibility and the efficacy of medical implants.* Regen Med, 2006. **1**(6): p. 789-800.
3. Lewandowska-Szumiel, M. and J. Komender, *Interaction between tissues and implantable materials.* Front Med Biol Eng, 2000. **10**(2): p. 79-82.
4. Fagrell, D., A. Berggren, and E. Tarpila, *Capsular contracture around saline-filled fine textured and smooth mammary implants: a prospective 7.5-year follow-up.* Plast Reconstr Surg, 2001. **108**(7): p. 2108-12; discussion 2113.
5. Aboushwareb, T., et al., *A keratin biomaterial gel hemostat derived from human hair: Evaluation in a rabbit model of lethal liver injury.* J Biomed Mater Res B Appl Biomater, 2008.
6. Buchta, C., et al., *Biochemical characterization of autologous fibrin sealants produced by CryoSeal and Vivostat in comparison to the homologous fibrin sealant product Tissucol/Tisseel.* Biomaterials, 2005. **26**(31): p. 6233-41.
7. MacGillivray, T.E., *Fibrin sealants and glues.* J Card Surg, 2003. **18**(6): p. 480-5.
8. Jackson, M.R., *Tissue sealants: current status, future potential.* Nat Med, 1996. **2**(6): p. 637-8.
9. Evans, L.A. and A.F. Morey, *Current applications of fibrin sealant in urologic surgery.* Int Braz J Urol, 2006. **32**(2): p. 131-41.
10. Albala, D.M. and J.H. Lawson, *Recent clinical and investigational applications of fibrin sealant in selected surgical specialties.* J Am Coll Surg, 2006. **202**(4): p. 685-97.
11. Motta, A., et al., *Fibroin hydrogels for biomedical applications: preparation, characterization and in vitro cell culture studies.* J Biomater Sci Polym Ed, 2004. **15**(7): p. 851-64.
12. Nivasu, M.V., T.T. Reddy, and T. Shekharam, *In situ polymerizable polyethyleneglycol containing polyesterpolyol acrylates for tissue sealant applications.* Biomaterials, 2004. **25**: p. 3283.
13. Forseth, M., K. O'Grady, and D.M. Toriumi, *The current status of cyanoacrylate and fibrin tissue adhesives.* J Long Term Eff Med Implants, 1992. **2**(4): p. 221-33.
14. Lamsa, T., et al., *Tissue adhesives and the pancreas: biocompatibility and adhesive properties of 6 preparations.* Pancreas, 2008. **36**(3): p. 261-6.
15. Singer, A.J. and H.C. Thode, Jr., *A review of the literature on octylcyanoacrylate tissue adhesive.* Am J Surg, 2004. **187**(2): p. 238-48.
16. Canonico, S., *The use of human fibrin glue in the surgical operations.* Acta Biomed, 2003. **74 Suppl 2**: p. 21-5.
17. Silver, F.H., M.C. Wang, and G.D. Pins, *Preparation and use of fibrin glue in surgery.* Biomaterials, 1995. **16**(12): p. 891-903.
18. Ciapetti, G., et al., *Cytotoxicity testing of cyanoacrylates using direct contact assay on cell cultures.* Biomaterials, 1994. **15**(1): p. 63-7.
19. Kaplan, M. and K. Baysal, *In vitro toxicity test of ethyl 2-cyanoacrylate, a tissue adhesive used in cardiovascular surgery, by fibroblast cell culture method.* Heart Surg Forum, 2005. **8**(3): p. E169-72.
20. Sierra D., S.R., *Surgical Adhesives and Sealants.* 1996, Lancaster: Technomic Publishing AG.
21. van der Ham, A.C., et al., *Transient protection of incomplete colonic anastomoses with fibrin sealant: an experimental study in the rat.* J Surg Res, 1993. **55**(3): p. 256-60.
22. Gold, J.S. and R.P. Dematteo, *Combined surgical and molecular therapy: the gastrointestinal stromal tumor model.* Ann Surg, 2006. **244**(2): p. 176-84.
23. Bailey, A.A., et al., *Diagnosis and outcome of small bowel tumors found by capsule endoscopy: a three-center Australian experience.* Am J Gastroenterol, 2006. **101**(10): p. 2237-43.
24. Multimedia Images, A.D.A.M. *Small Bowel Resection.* 2009 [cited; Available from: www.nmh.org/.../graphics/images/en/7171.jpg.
25. Demetriades, D., et al., *Penetrating colon injuries requiring resection: diversion or primary anastomosis? An AAST prospective multicenter study.* J Trauma, 2001. **50**(5): p. 765-75.
26. Ivatury, R.R., et al., *Complex duodenal injuries.* Surg Clin North Am, 1996. **76**(4): p. 797-812.
27. Margenthaler, J.A., et al., *Risk factors for adverse outcomes following surgery for small bowel obstruction.* Ann Surg, 2006. **243**(4): p. 456-64.
28. *The digestive system*, in *NIH Publication No. 06-5101*, National Institute of Diabetes and Digestive and Kidney Diseases.
29. *Histoogical display of Ulcer, Radiology Department of the University of Connecticut Health Center*, in http://www.uchc.edu/, University of Connecticut Health Center
30. Serra-Mitjans, M., J. Belda-Sanchis, and R. Rami-Porta, *Surgical sealant for preventing air leaks after pulmonary resections in patients with lung cancer.* Cochrane Database Syst Rev, 2005(3): p. CD003051.

31. Lim, E. and P. Goldstraw, *Surgical sealants for air leaks after pulmonary surgery.* Eur J Cardiothorac Surg, 2007. **32**(3): p. 552-3.
32. Tovar, M.C., et al., *Comparative study of air coagulation, fibrin sealant, and suture in experimental liver injury.* Eur J Surg, 1998. **164**(1): p. 57-63.
33. Fink, D., et al., *Application of biological glue in repair of intracardiac structural defects.* Ann Thorac Surg, 2004. **77**(2): p. 506-11.
34. Ratner, H., Schoen, Lemons, *Biomaterials Science.* second ed, ed. E.A. Press. 2004, London: Elsevier Academic Press.
35. Silverstein, L.H., G.M. Kurtzman, and P.C. Shatz, *Suturing for optimal soft-tissue management.* J Oral Implantol, 2009. **35**(2): p. 82-90.
36. Vogt, P.M., et al., *[Bases and methods of suturing.].* Chirurg, 2009. **80**(5): p. 437-47.
37. McAlister, V., P.J. O'Dwyer, and N.J. O'Higgins, *Effect of fibrin sealant on the healing colonic anastomosis.* Br J Surg, 1991. **78**(7): p. 889.
38. Rami, R. and M. Mateu, *Surgical sealant for preventing air leaks after pulmonary resections in patients with lung cancer.* Cochrane Database Syst Rev, 2001(4): p. CD003051.
39. Byrne, D.J., et al., *Adverse influence of fibrin sealant on the healing of high-risk sutured colonic anastomoses.* J R Coll Surg Edinb, 1992. **37**(6): p. 394-8.
40. van der Ham, A.C., et al., *Healing of ischemic colonic anastomosis: fibrin sealant does not improve wound healing.* Dis Colon Rectum, 1992. **35**(9): p. 884-91.
41. Leggat, P.A., D.R. Smith, and U. Kedjarune, *Surgical applications of cyanoacrylate adhesives: a review of toxicity.* ANZ J Surg, 2007. **77**(4): p. 209-13.
42. Ray, G., *Wound complications associated with the use of bovine serum albumin-glutaraldehyde surgical adhesive in pediatric patients.* Neurosurgery, 2008. **63**(4): p. E820; author reply E820.
43. Singh, R.P., V. Maheshwari, and A.K. Verma, *Evaluation of gelatin/resorcinol/aldehyde as a hemostatic agent and tissue adhesive: an experimental study in rat.* Int Surg, 2008. **93**(1): p. 25-31.
44. Kunihara, T., et al., *Recommendation for appropriate use of GRF glue in the operation for acute aortic dissection.* Ann Thorac Cardiovasc Surg, 2008. **14**(2): p. 88-95.
45. Bhatia, S.K., et al., *Polysaccharide-based tissue adhesives for sealing corneal incisions.* Curr Eye Res, 2007. **32**(12): p. 1045-50.
46. Bhatia, S.K., et al., *Interactions of polysaccharide-based tissue adhesives with clinically relevant fibroblast and macrophage cell lines.* Biotechnol Lett, 2007. **29**(11): p. 1645-9.
47. Artzi, N., et al., *Characterization of Star Adhesive Sealants Based On PEG/Dextran Hydrogels.* Macromol Biosci, 2009.
48. Sokolsky-Papkov, M., A.J. Domb, and J. Golenser, *Impact of aldehyde content on amphotericin B-dextran imine conjugate toxicity.* Biomacromolecules, 2006. **7**(5): p. 1529-35.
49. Draye, J.P., et al., *In vitro and in vivo biocompatibility of dextran dialdehyde cross-linked gelatin hydrogel films.* Biomaterials, 1998. **19**(18): p. 1677-87.
50. Shazly, T., *Property Determinants of Dextran:Polyethylene Glycol Adhesive Sealants*, in *Materials Science and Engineering.* 2005, Massachusetts Institute of technology: Cambridge. p. 100.
51. Liu, S., M. Kapoor, and A. Leask, *Rac1 expression by fibroblasts is required for tissue repair in vivo.* Am J Pathol, 2009. **174**(5): p. 1847-56.
52. Ishii, M., et al., *Local VEGF administration enhances healing of colonic anastomoses in a rabbit model.* Eur Surg Res, 2009. **42**(4): p. 249-57.
53. Manso, A.M., et al., *Cardiac fibroblasts require focal adhesion kinase for normal proliferation and migration.* Am J Physiol Heart Circ Physiol, 2009. **296**(3): p. H627-38.
54. Edelman, E.R., et al., *Basic fibroblast growth factor enhances the coupling of intimal hyperplasia and proliferation of vasa vasorum in injured rat arteries.* J Clin Invest, 1992. **89**(2): p. 465-73.
55. Wippermann, J., et al., *Long-term effects in distal coronary anastomoses using different adhesives in a porcine off-pump model.* J Thorac Cardiovasc Surg, 2006. **132**(2): p. 325-31.
56. Ellman, P.I., et al., *Evaluation of an absorbable cyanoacrylate adhesive as a suture line sealant.* J Surg Res, 2005. **125**(2): p. 161-7.
57. Siedentop, K.H., et al., *Safety and efficacy of currently available fibrin tissue adhesives.* Am J Otolaryngol, 2001. **22**(4): p. 230-5.
58. Bader, R.A., *Synthesis and viscoelastic characterization of novel hydrogels generated via photopolymerization of 1,2-epoxy-5-hexene modified poly(vinyl alcohol) for use in tissue replacement.* Acta Biomater, 2008.
59. Ciarletta, P., P. Dario, and S. Micera, *Pseudo-hyperelastic model of tendon hysteresis from adaptive recruitment of collagen type I fibrils.* Biomaterials, 2008. **29**(6): p. 764-70.
60. Fung, Y.C., *Biomechanics: Mechanical Properties of Living Tissues.* 2nd ed. 1993: Springer-Verlag New York, Inc.
61. Zhang, W., H.Y. Chen, and G.S. Kassab, *A rate-insensitive linear viscoelastic model for soft tissues.* Biomaterials, 2007. **28**(24): p. 3579-86.

62. Velada, J.L., et al., *Reproducibility of the mechanical properties of Vivostat system patient-derived fibrin sealant.* Biomaterials, 2002. **23**(10): p. 2249-54.
63. Alexandre, E., et al., *Hydrogel networks of poly(ethylene oxide) star-molecules supported by expanded polytetrafluoroethylene membranes: characterization, biocompatibility evaluation and glucose diffusion characteristics.* Macromol Biosci, 2004. **4**(7): p. 639-48.
64. Groll, J., et al., *A novel star PEG-derived surface coating for specific cell adhesion.* J Biomed Mater Res A, 2005. **74**(4): p. 607-17.
65. Sofia, S.J., V.V. Premnath, and E.W. Merrill, *Poly(ethylene oxide) Grafted to Silicon Surfaces: Grafting Density and Protein Adsorption.* Macromolecules, 1998. **31**(15): p. 5059-70.
66. Irvine, D.J., et al., *Comparison of tethered star and linear poly(ethylene oxide) for control of biomaterials surface properties.* J Biomed Mater Res, 1998. **40**(3): p. 498-509.
67. Moller, S., et al., *Dextran and hyaluronan methacrylate based hydrogels as matrices for soft tissue reconstruction.* Biomol Eng, 2007. **24**(5): p. 496-504.
68. Lee, J.M., S.A. Haberer, and D.R. Boughner, *The bovine pericardial xenograft: I. Effect of fixation in aldehydes without constraint on the tensile viscoelastic properties of bovine pericardium.* J Biomed Mater Res, 1989. **23**(5): p. 457-75.
69. Ward, I.M., *The Mechanical Properties of Solid Polymers.* 2nd ed. 2004, West Sussex: John Wiley and Sons, Ltd.
70. Shazly, T.M., et al., *Viscoelastic adhesive mechanics of aldehyde-mediated soft tissue sealants.* Biomaterials, 2008. **29**(35): p. 4584-91.
71. Samuel, N.T., et al., *Comprehensive characterization of the effect of tissue storage conditions on tissue-adhesive interaction.* J Biomater Sci Polym Ed, 2008. **19**(11): p. 1455-68.
72. Hilborn, J. and L.M. Bjursten, *A new and evolving paradigm for biocompatibility.* J Tissue Eng Regen Med, 2007. **1**(2): p. 110-9.
73. Peppas, N.A. and J.J. Sahlin, *Hydrogels as mucoadhesive and bioadhesive materials: a review.* Biomaterials, 1996. **17**(16): p. 1553-61.
74. Suggs, L.J., et al., *In vitro cytotoxicity and in vivo biocompatibility of poly(propylene fumarate-co-ethylene glycol) hydrogels.* J Biomed Mater Res, 1999. **46**(1): p. 22-32.
75. Liu, Y. and M.B. Chan-Park, *Hydrogel based on interpenetrating polymer networks of dextran and gelatin for vascular tissue engineering.* Biomaterials, 2009. **30**(2): p. 196-207.
76. Burke, S.A., et al., *Thermal gelation and tissue adhesion of biomimetic hydrogels.* Biomed Mater, 2007. **2**(4): p. 203-10.
77. Hwang, D.S., S.B. Sim, and H.J. Cha, *Cell adhesion biomaterial based on mussel adhesive protein fused with RGD peptide.* Biomaterials, 2007. **28**(28): p. 4039-46.
78. Lee, B.P., J.L. Dalsin, and P.B. Messersmith, *Synthesis and gelation of DOPA-modified poly(ethylene glycol) hydrogels.* Biomacromolecules, 2002. **3**(5): p. 1038-47.
79. Waite, J.H., *Reverse engineering of bioadhesion in marine mussels.* Ann N Y Acad Sci, 1999. **875**: p. 301-9.
80. Gawlak, M., et al., *High resolution in situ zymography reveals matrix metalloproteinase activity at glutamatergic synapses.* Neuroscience, 2009. **158**(1): p. 167-76.
81. Baker, A.B., et al., *Heparanase alters arterial structure, mechanics, and repair following endovascular stenting in mice.* Circ Res, 2009. **104**(3): p. 380-7.
82. E. Pretsch, P.B., C. Affolter, *Structure determination of organic compounds.* 3rd ed. 2000, Berlin: Springer-Verlag.
83. Pasternak, B., et al., *Doxycycline-coated sutures improve mechanical strength of intestinal anastomoses.* Int J Colorectal Dis, 2008. **23**(3): p. 271-6.
84. Nugent, H.M., et al., *Adventitial endothelial implants reduce matrix metalloproteinase-2 expression and increase luminal diameter in porcine arteriovenous grafts.* J Vasc Surg, 2007. **46**(3): p. 548-556.
85. Glaros, T., M. Larsen, and L. Li, *Macrophages and fibroblasts during inflammation, tissue damage and organ injury.* Front Biosci, 2009. **14**: p. 3988-93.
86. Shima, I., et al., *Expression of matrix metalloproteinases in wound healing after glaucoma filtration surgery in rabbits.* Ophthalmic Res, 2007. **39**(6): p. 315-24.
87. Dalsin, J.L., et al., *Mussel adhesive protein mimetic polymers for the preparation of nonfouling surfaces.* J Am Chem Soc, 2003. **125**(14): p. 4253-8.
88. Statz, A.R., et al., *New peptidomimetic polymers for antifouling surfaces.* J Am Chem Soc, 2005. **127**(22): p. 7972-3.
89. Lee, H., et al., *Mussel-inspired surface chemistry for multifunctional coatings.* Science, 2007. **318**(5849): p. 426-30.
90. Lin, Q., et al., *Adhesion mechanisms of the mussel foot proteins mfp-1 and mfp-3.* Proc Natl Acad Sci U S A, 2007. **104**(10): p. 3782-6.
91. Silverman, H.G. and F.F. Roberto, *Understanding marine mussel adhesion.* Mar Biotechnol (NY), 2007. **9**(6): p. 661-81.

92. Constantinides, G., et al., *Probing mechanical properties of fully hydrated gels and biological tissues.* J Biomech, 2008. **41**(15): p. 3285-9.

6. Appendix

A1 Swelling and Degradation

The following procedure was followed to study hydrogel swelling and degradation via gravimetric analyses:

1. Prepare dual chamber syringes with various dextran aldehyde and aminated PEG components, with CHO:NH_2 ranging from approximately 1-10 (Table 1).
2. Cast PEG:dextran materials in disk-shaped molds (8 mm diameter, 3 mm thick). Prepare disk samples in triplicate.
3. Extract PEG:dextran samples from molds. Measure sample dimensions with digital calipers.
4. Weigh samples with a digital scale; denoted as dry mass.
5. Suspend each disk in an aqueous medium (100 ml MilliQ™ water, 250 ml glass beaker).
6. Weigh and measure sample dimensions at predetermined time points.
7. Record and analyze gravimetric data with Excel and Minitab softwares.

A2 UNIAXIAL TENSILE TESTING

The following procedure was used to measure the elastic moduli of PEG:dextran materials:

1. Prepare dual chamber syringe with specific dextran aldehyde and aminated PEG (Table 2)
2. Cast materials with a dual chamber syringe and a 12-step mixing tip into dog-bone molds, with extension region dimensions of: length = 10 mm, width = 8 mm, and thickness = 6 mm.
3. Flatten top and bottom of sample with glass cover slips.
4. Allow sample to cure for 1 minute. Gently remove cover slips.
5. While sample is in the mold, add 1 ml of 1X phosphate buffered saline (PBS) to top side. Allow PBS to absorb for 30 seconds.
6. Repeat step 5 with sample bottom side.
7. Carefully remove sample from mold.
8. Repeat steps 5 and 6 with sample out of mold.
9. Apply a displacement rate-controlled uniaxial extension to the sample with Electroforce® mechanical tester and the following parameters:
    a. Ramp displacement profile (monotonically increasing, constant rate)
    b. 1.2 mm total displacement
    c. Displacement rate of 0.05 mm/sec
10. Capture force/displacement data throughout entire 1.2 mm extension.
    a. Transfer data to Excel file.

b. Record and analyze uniaxial tensile data with Excel and Minitab softwares.

A3 ADHESION STRENGTH TESTING I

The following procedure was used to measure the adhesion strength of PEG:dextran materials to excised intestinal tissue:

1. Prepare dual chamber syringe with the specific dextran aldehyde and aminated PEG solutions (Table 3).
2. Sacrifice rats using carbon dioxide asphyxiation under appropriate protocol for animal care.
3. Directly following sacrifice, harvest small intestine. Remove all waste products from intestinal lumen.
4. Store harvested tissue in Krebs-Henseleit buffer at room temperature throughout duration of experiment (10 hours).
5. Cut 25 mm longitudinal sections of small intestine.
6. Thread two small intestine sections with silicon tubes (2.4 mm o.d., 25 mm length).
7. Bend silicon tubes with threaded intestines, bringing sample ends together.
8. Secure one sample (in bent configuration) in each vice grip of mechanical tester. The bent configuration promotes sample stability throughout mechanical test (Figure 12).
9. Using dual chamber syringe, polymerize 0.25 ml total volume of a test material onto bottom intestinal sample.
10. Immediately bring samples together such that intestinal samples are in contact through the material, and a zero or near zero load is detected by the load cell. Allow 1 minute for material to cure and achieve adherence with tissue surfaces.
11. Apply a constant rate displacement of 0.05 mm/sec over 4 mm total displacement.

12. Capture force/displacement data. Record and analyze adhesion strength data with Excel and Minitab softwares.

A4 CYTOTOXICITY STUDIES

The following procedure was used to quantify the cytotoxic effect of PEG:dextran degradation products on vSMC:

1. Obtain two cryovials of second passage vSMC from storage. Use standard cell culture protocol to plate each vial onto a P10 culture plate.
2. Prepare the 8 selected PEG:dextran material formulations (Table 4). Use a silicon mold to cast a disk (8 mm diameter, 3 mm thick) of each material variation.
3. Suspend each disk in a scintillation vial in 20 ml Dubelco's modified eagle medium (DMEM, 1X glucose) to promote material degradation. Keep at room temperature.
4. Immediately following start of material suspension, sterilize vials (and contents) with 4 hours exposure to UV light under culture hood.
5. After cell cultures reach confluence, passage onto ten 12-well plates (1:5 passage expansion).
6. Incubate wells until approximately 50% confluent. At this point, conduct cell counting on well one of five selected plates.
7. At 50% confluence, replace the media in each of the wells with a 1:1 mixture of media and material suspension supernatant (1 ml of each, 2 ml total volume per well). In this co-culture, material degradation products have developed over a 7 day period, and the degradation supernatant is termed the early degradation products.
8. Incubate the co-culture for 24 hours.
9. Following 24 hour incubation period, conduct cell counting and cytotoxicity assays.

10. Repeat the above steps (1-9) again with the same materials following a 21 day material degradation period. The degradation supernatant is now termed the late degradation products.
11. Record and analyze cytotoxicity data with Excel software.

Cytotoxicity assay culture treatments

1. DMEM control – Cells cultured initially in normal media, but at 50% confluence media was replaced with 50% media + 50% DMEM (for final 24 hour incubation).
2. Fully lysed – Cells cultured in normal media for the entire duration of the experiment. Lysis buffer applied to culture prior to cytotoxicity assay in order to form the basis for a data transform into a relative cytotoxicity.
3. Material samples – Cells cultured in normal media until 50% confluent, at which point the normal media is replaced with (50% normal media + 50% degraded sample supernatant) for 24 hour co-culture incubation.

A5 PROLIFERATION STUDIES

The following procedure was used to quantify the effect of polymerized PEG:dextran materials on fibroblast proliferation:

1. Culture 3T3 cells to approximately 50% confluence in 12-well plates.
2. Aspirate media from each well plate.
3. Add 0.25 ml (single drop from 12-step mixing tip) of a given PEG:dextran formulation PEG:dextran to each well plate (Table 5). Follow the same material sterilization procedure as with the cytotoxicity assay above.
4. Add 1 ml media to each well plate
5. Incubate (cells + materials) for 24 hours.
6. Following co-culture, conduct proliferation assay on all well plates.
7. Record and analyze proliferation data with Excel software.

Proliferation assay culture treatments

1. Media control – Cells cultured in normal media throughout duration of the experiment. No PEG:dextran materials were applied to culture prior to the conduction of the proliferation assay.

2. Material control – Proliferation assays were conducted on wells with PEG:dextran materials but without any cells. The chemical effect of each material on the assay reagents was examined with these controls, and was taken into account in the interpretation of cell proliferative measurements.

3. Material samples – Cells were grown in 12-well plates in accordance with normal culture protocol until approximately 50% confluent. At this point, 0.25 ml of PEG:dextran was polymerized on the cell layer, and the cells + material were co-cultured for 24 hours.

A6 Burst Pressure Testing

Experimental setup for burst pressure testing

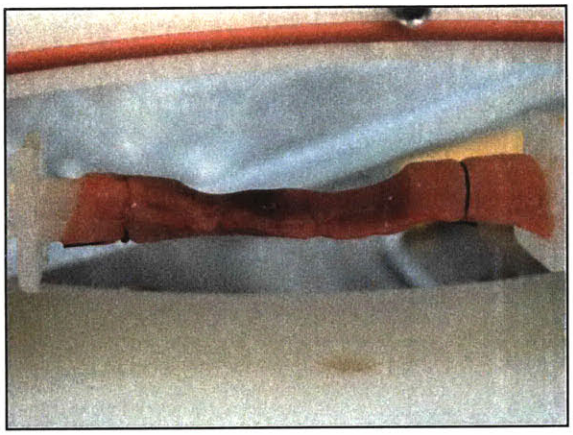

Figure 59 Duodenal tissue placement within testing apparatus for luminal perfusion. The wound at the center of the tissue is repaired with various adhesive materials.

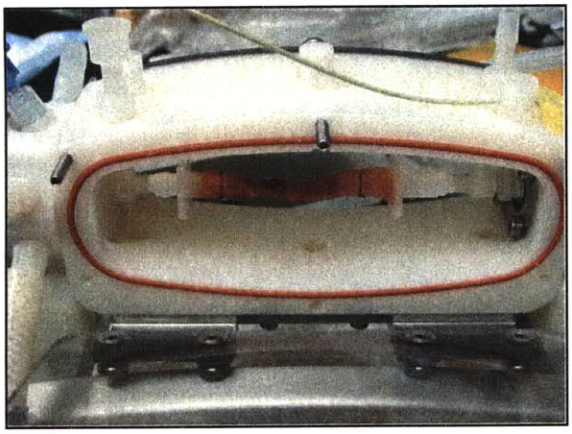

Figure 60 Repaired duodenal tissue is housed in a chamber throughout perfusion.

A7 Lumen Area Determination

Histological images for determination of duodenal lumen area

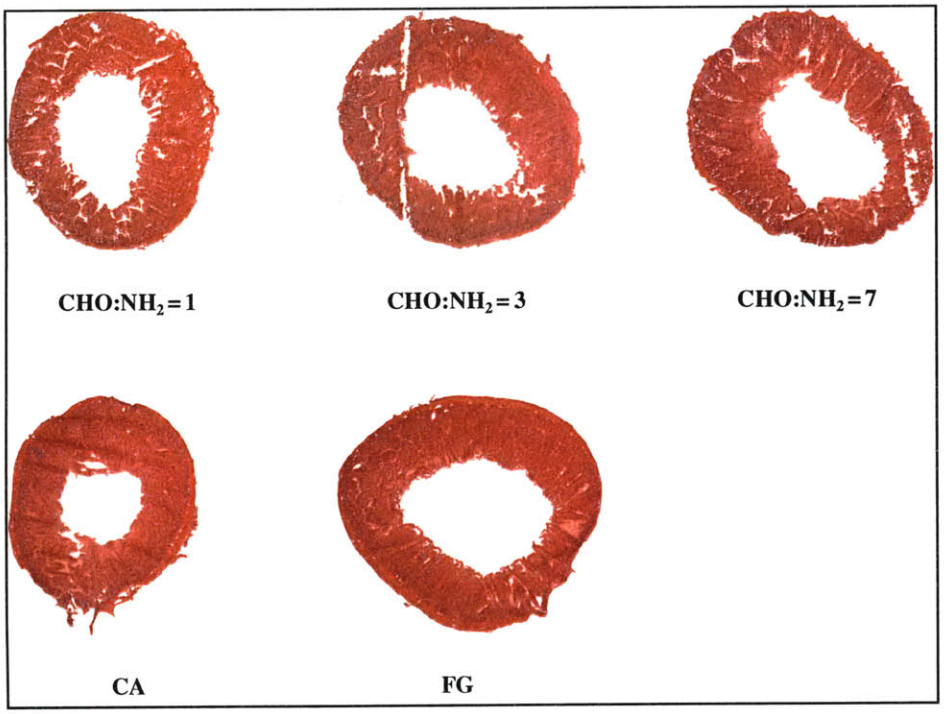

Figure 61 Duodenal cross-sections prepared through cryosectioning and staining of duodenal samples. Tissue sections were analyzed to assess the extent of morphological disturbance (luminal compression) resulting from sealant application and dynamic loading.

A8 Adhesion Strength Testing II

Sample setup for testing of adhesive mechanics

The initial adheion strength testing setup(3.1.3 Materials and Methods) was replaced by the arrangement shown below. The tissue-material-tissue interface provided by the pictured arrangement was amenable to stress analyses because of the well defined adhesive contact area.

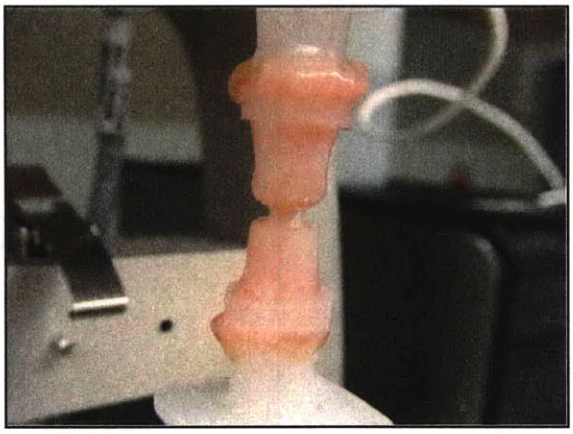

Figure 62 Tissue-material-tissue interface for adhesive mechanical testing

A9 Morphological Analyses of Adhesive Interface

Iniital definition of adhesive regime

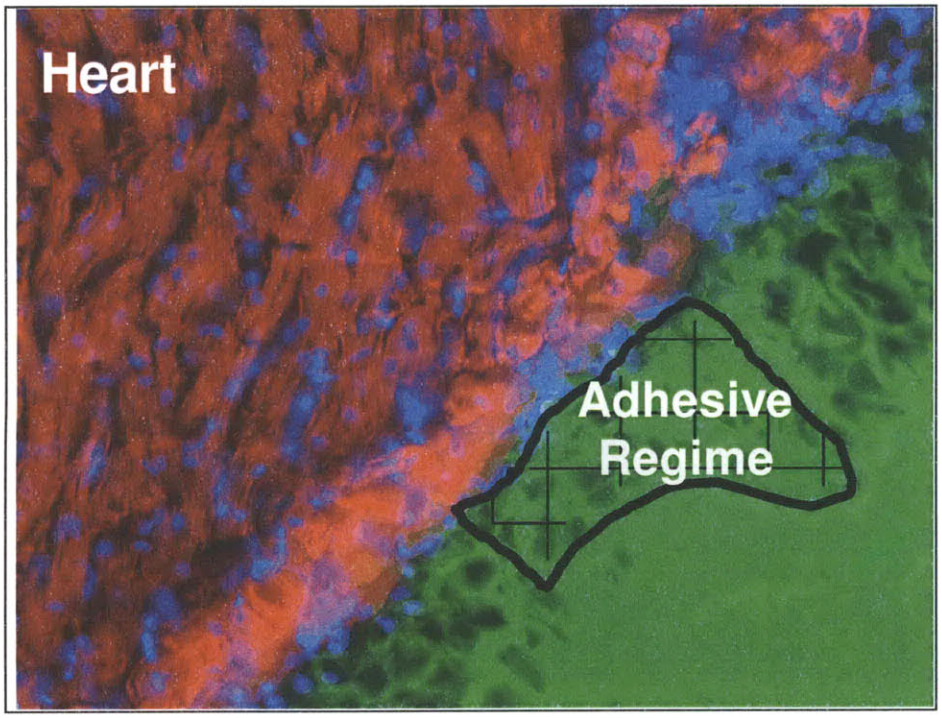

Figure 63 The adhesive regime is defined as the region of material discontinuity extending into the material from the tissue-material interface.

A10 Fluorescent Microspheres

Fluorescent microspheres on the surface of soft tissues

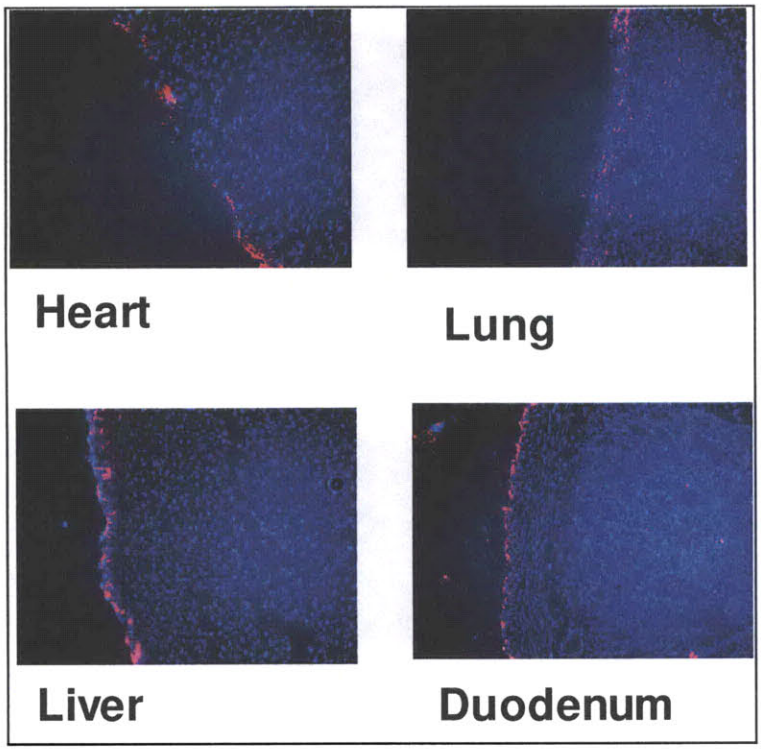

Figure 64 Aldehyde-coated microspheres adhere to the surfaces of soft tissues. Microspheres are fluorescently labeled and appear pink, while cell nuclei are stained with DAPI and appear blue.

A11 NANOINDENTATION EXPERIMENT

The following experiment was performed in the Nanaolab at MIT under the guidance of Dr. Krystyn Van Vliet and with a great deal of assistance from Alan Schwartzman and Z. Ilke Kalcioglu.

Experimental goals

DOPA conjugation enhances the sealant function of PEG:dextran after interfacial exposure to aqueous medium. Here we measure the surface mechanics of the unmodified PEG:dextran and 0.3% DOPA conjugate before and after swell treatments. The metric used to analyze the materials is the elastic modulus from an *adhesion test* on the MicroMaterials nanoindentation system [92]. Comparative analyses will suggest if the observed functional enhancement is a result of intrinsic hydrogel modification (increasing network stiffness, particularly at the surface) or is due to modulated adhesion in an aqueous environment. If the moduli of unmodified and conjugate samples are the same in both swell states, this data would indicate that the observed enhancement of wet adhesion with conjugation is reflective of augmented tissue-material interactions. Alternatively, discrepancies in mechanical data may indicate that DOPA-modulates intrinsic material properties to confer enhanced sealant performance.

Experimental Approach

Two discs (8 mm diameter, 3 mm thickness) of each sample type (unmodified PEG:dextran and DOPA conjugate) were prepared. Prior to testing, each disc was

either maintained as prepared (no swell treatment) or submersed for one hour in PBS (swell treatment). In total, four samples were analyzed:

1. Unmodified PEG:dextran, no swell treatment
2. Unmodified PEG:dextran, swell treatment
3. Conjugate, no swell treatment
4. Conjugate, swell treatment

The parameters used for the nanoindentation adhesion test were:

*1 mm radius spherical tip – a large and relatively blunt tip was selected for interaction with this soft material.

Max load	0.2 mN
Max depth	11734 nm
Initial load	0.001 mN
Limit stop	0.01mN
Load rate	0.04 mN/sec
Dwell	10 sec
Unload rate	0.04mN/sec

The sample loading profile is depicted below (Figure 65):

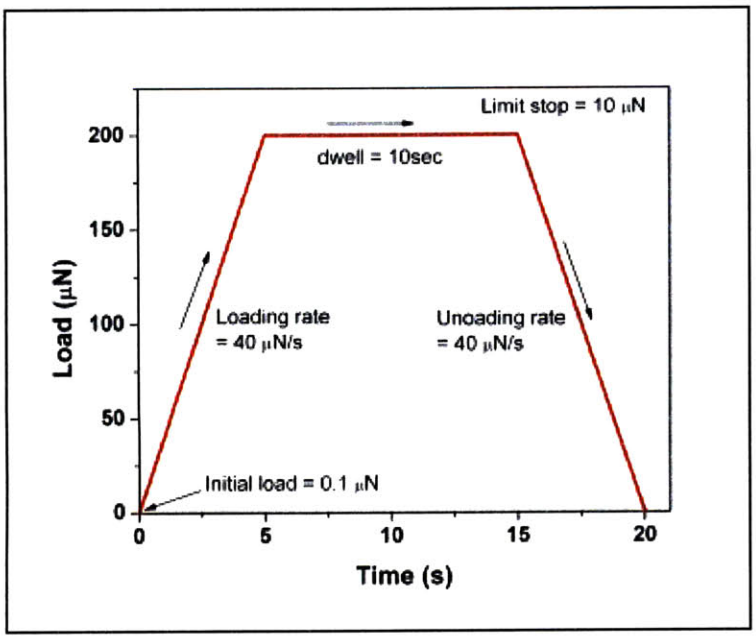

Figure 65 Sample loading profile for adhesion test on MicroMaterials System

Experimental Data

Nanoindentation adhesion tests of each material/treatment show significant repeatability, as evidenced by both the degree of curve overlap (Figure 66-Figure 69) and the tabulated averages and standard deviations of the calculated elastic moduli (Table 16). Two analytical methods were used to analyze the nanoindentation data and generate the moduli values. The Oliver-Pharr method is integrated into the MicroMaterials software package and was readily extracted from the experimental data. The JKR method was performed on an Excel sheet based on the following theoretical equation derived to account for adhesion between the material and the tip:

$$E_{JKR} = \sqrt{\frac{S^3(1-\nu_s^2)^2}{6R} \cdot \left[\left(\frac{2}{3\sqrt{1+\frac{P}{F_{po}}}}+1\right)^3 \frac{1}{P+2F_{po}+2F_{po}\sqrt{\left(1+\frac{P}{F_{po}}\right)}}\right]}$$

The JKR method explicitly considers the increase in area under strain due to adhesion, and as a result always produces lower values for the elastic modulus which typically are closure to values attained by alternate methods (bulk material testing). The largest standard deviation among all moduli was only 14 % of the mean value (Conjugate, No Swell, Oliver-Pharr method), which can be at least partially attributed to sample dehydration throughout testing.

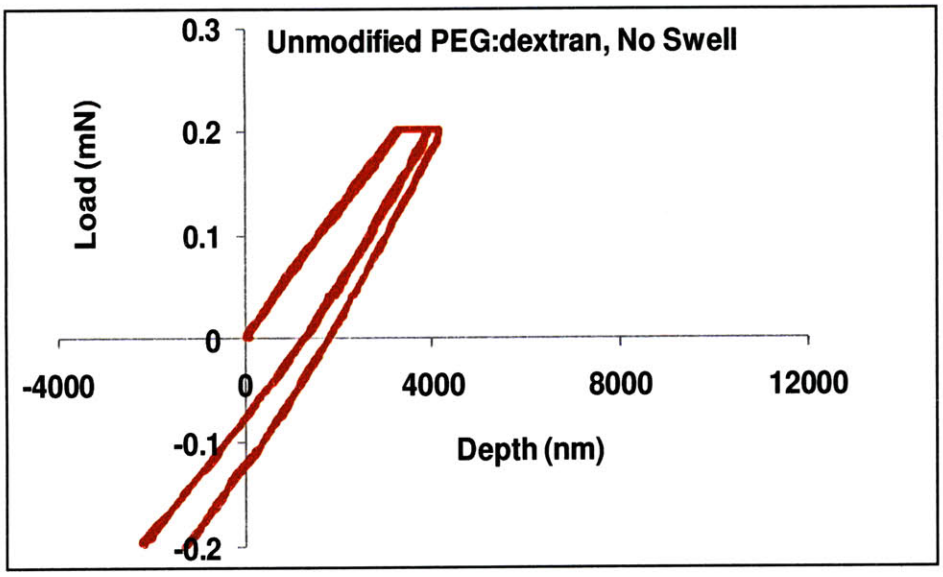

Figure 66 Adhesion test curves of unmodified PEG:dextran without swell treatment.

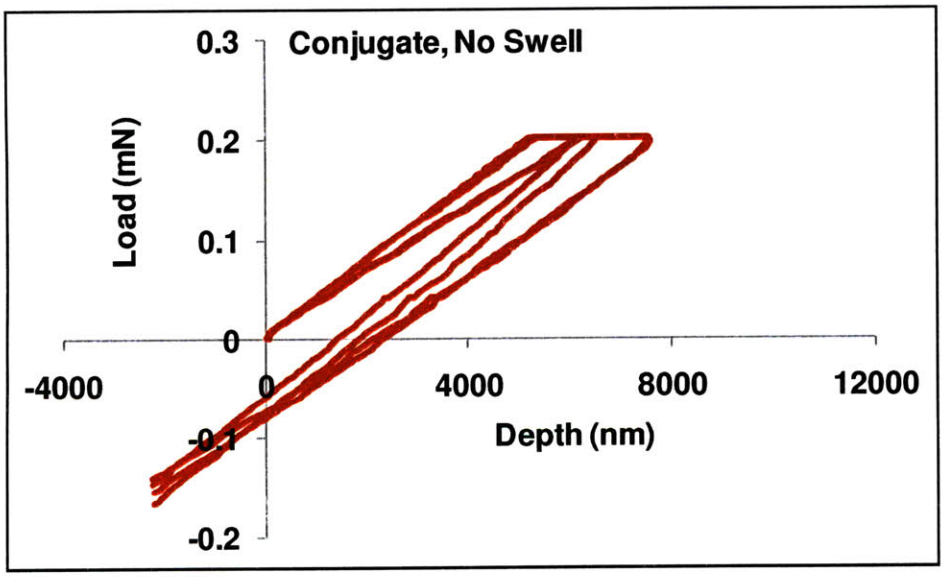

Figure 67 Adhesion test curves of DOPA-modified PEG:dextran without swell treatment.

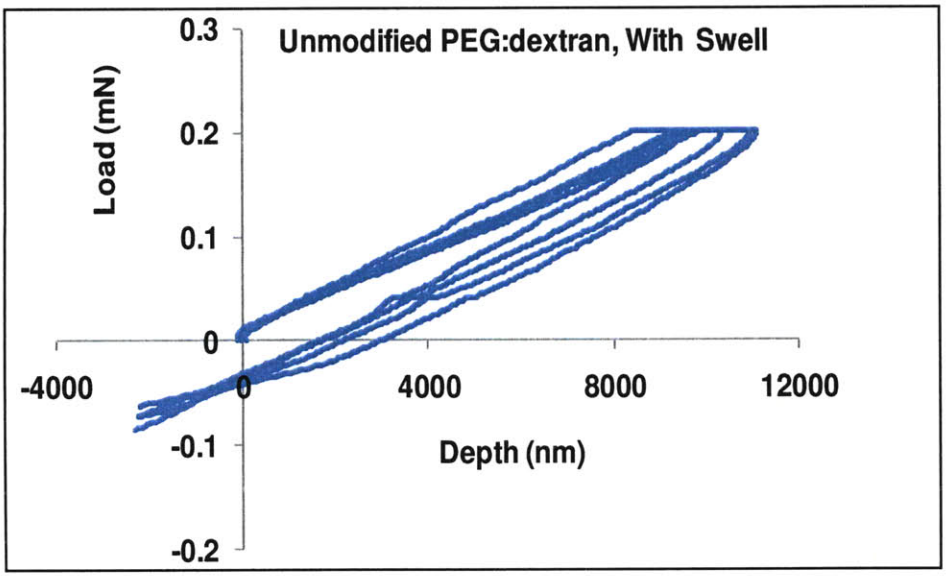

Figure 68 Adhesion test curves of unmodified PEG:dextran with swell treatment.

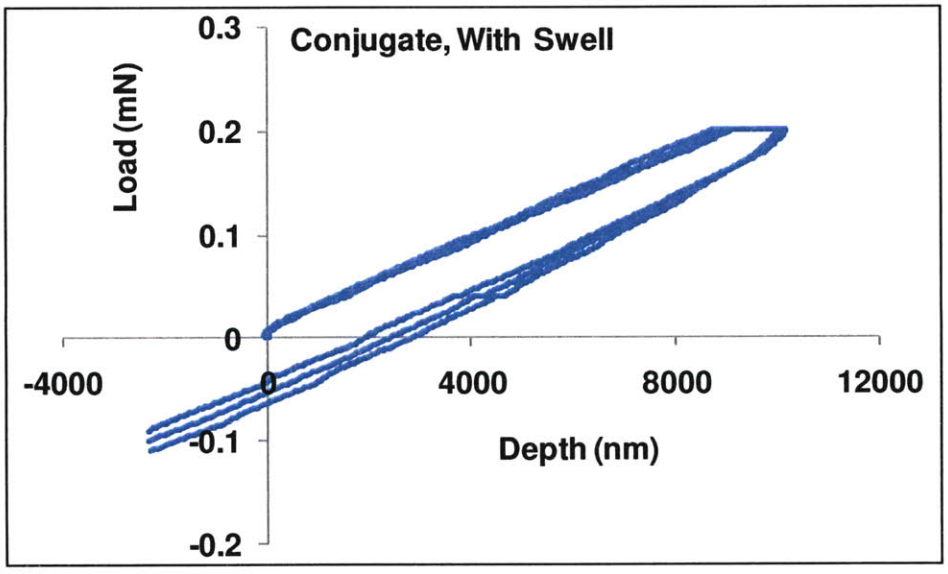

Figure 69 Adhesion test curves of DOPA-modified PEG:dextran with swell treatment.

Table 16 Calculated elastic moduli based on adhesion test

Elastic Moduli (kPa)	Unmodified PEG:dextran		Conjugate	
	Oliver-Pharr	JKR	Oliver-Pharr	JKR
No Swell				
Avg	641	406	251	154
St Dev	12	26	34	17
With Swell				
Avg	133	60	140	72
St Dev	13	7	4	6

The following constants (along with the average S for each sample) were used to calculate E_{JKR}:

v	0.5
R[nm]	1000000
P[nN]	200000
Fpo[nN]	150000

Sample Comparisons

As expected for a material which exhibits substantial adhesion, nanoindentation data best agreed with uniaxial tensile testing data when analyzed with the JKR method (E_{JKR} of 406 vs. $E_{Uniaxial}$ of 161 kPa). The data acquired for unmodified PEG:dextran without swell yielded an E_{JKR} that is more than double the value measured by uniaxial tensile testing. A possible reason for this discrepancy is an underestimation of adhesive tip-material interactions, as the material under study is designed to be particularly sticky. Nevertheless, the E_{JKR} is the metric is used rather than the $E_{OliverPharr}$ to compare between material/treatment variants.

The conducted experiments were designed to provide insight as to what extent the amino acid conjugate modulated material properties in two swell states (one hour swell vs. no swell). When comparing the unmodified PEG:dextran and conjugate samples in the no swell state, we observed a 62% reduction ($p < 0.05$) in material moduli as a result of DOPA incorporation in the network. This implies that the conjugate interferes with network formation and results in less crosslinking, as suspected from prior experimentation. When either the conjugate or unmodified materials were subjected to swell treatment prior to testing, there was a substantial reduction in E_{JKR}. However, in the case of the unmodified material, the property reduction with hydration was much more extreme (406 to 60 kPa) as compared to the conjugate (154 to 72 kPa). Interestingly, the conjugate and unmodified materials had largely similar moduli (60 vs. 72 kPa) when analyzed in the swell state although the conjugate appears to have less initial crosslinking.

A12 Swell Response of DOPA Conjugates

The swelling behavior of the DOPA-PEG:dextran variants examined in Study 4 was assessed in terms of dynamic swelling ratio (q_d) and bulk elastic modulus (experimental methods described in Study 1). The purpose of these additional experiments was to provide insight into the trends in material ex-vivo performance (burst pressure) observed throughout the course of swell treatment.

A substantial difference between unmodified PEG:dextran q_d and the conjugates q_d was observed as a function of swell time, with the conjugates swelling to an essentially equal and significantly lesser ($p < 0.05$) extent as compared to the unmodified PEG:dextran (Figure 70). However, no correlation between q_d and burst pressure was found among the PEG:dextran variants throughout the observed swell time, suggesting q_d alone is not predictive of material performance in hydrated conditions.

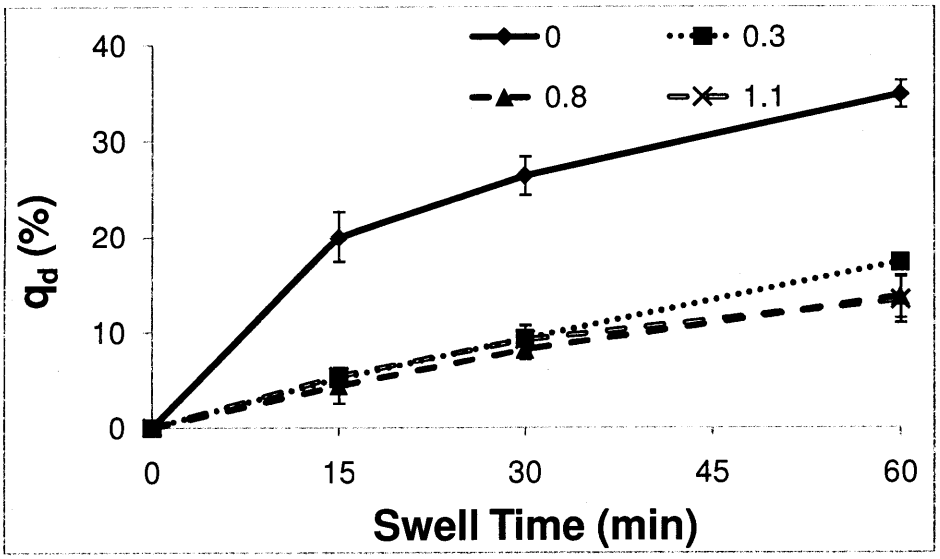

Figure 70 The swell ratio (qd) of PEG:detxran-DOPA variants over the course of 1 hour submersion in PBS. The legend number denotes the wt. % of DOPA in the material formulation.

The bulk elastic modulus (E) of PEG:dextran conjugates was also measured as a function of swell time (Figure 72). The unmodified PEG:dextran experienced the most substantial change (loss) of E with swell, while the DOPA conjugates were comparatively stable. Once again, correlation between the elastic modulus and burst pressure of hydrated materials was not found.

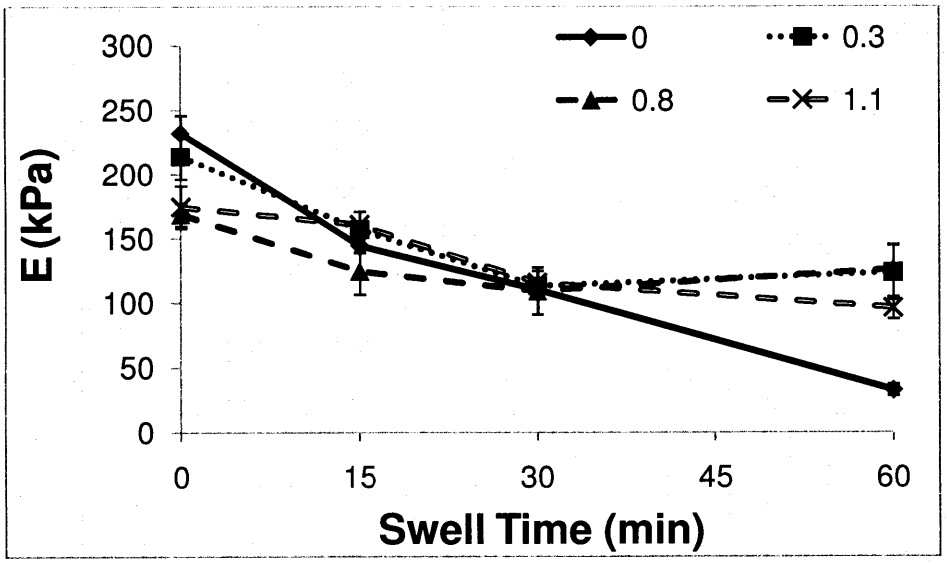

Figure 71 The elastic modulus (E) of PEG:detxran-DOPA variants over the course of 1 hour submersion in PBS. The legend number denotes the wt. % of DOPA in the material formulation.

Strong linear correlation was found in a subset of the E and burst pressure data, namely between the initial values prior to swell treatment (Figure 72). This relationship likely emerges in the PEG:dextran system because network cohesive and functional adhesive properties are based on analogous aldehyde-amine interactions, featuring material-present amines in the former and tissue-present amines in the latter. Additional correlations were found between the changes in burst pressure and modulus (Figure 73) and the changes in burst pressure and swell ratio (Figure 74) over the entire swell

treatment. These latter correlations demonstrate that stable material properties facilitate maintenance of initial performance throughout material swell.

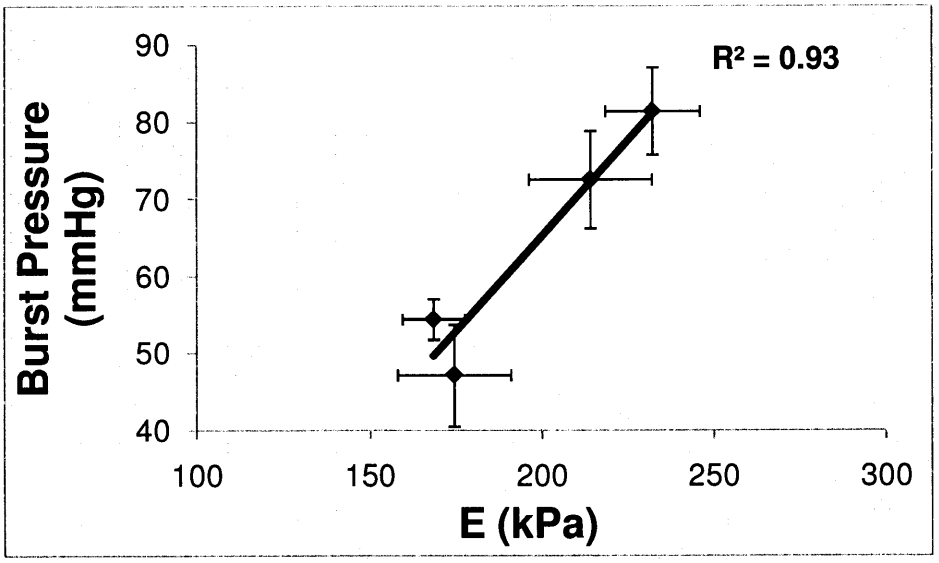

Figure 72 Linear correlation between ex-vivo burst pressure and elastic modulus of PEG:dextran-DOPA variants prior to swell treatment.

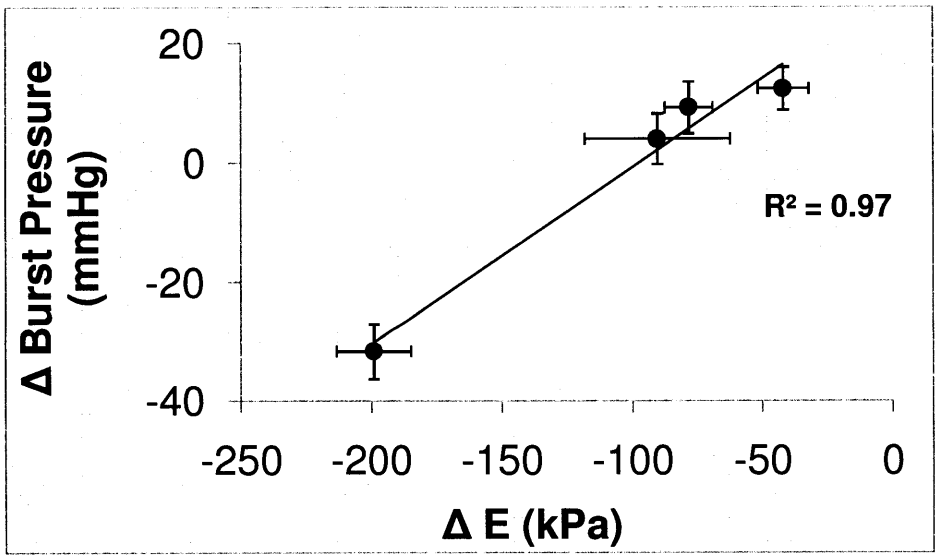

Figure 73 Strong linear correlation exists between the changes in burst pressure and modulus of PEG:dextran-DOPA variants after a 1 hour swell treatment.

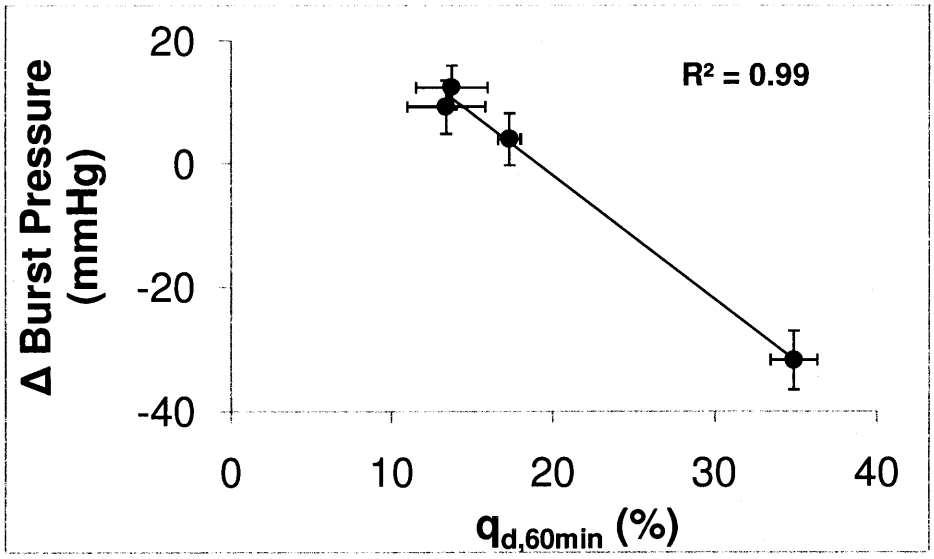

Figure 74 Strong linear correlation exists between the changes in burst pressure and swell ratio of PEG:dextran-DOPA variants after a 1 hour swell treatment.